Review

Review of the Modelling of Corrosion Processes and Lifetime Prediction for HLW/SF Containers—Part 1: Process Models

Fraser King [1,*], Miroslav Kolàř [2], Scott Briggs [3], Mehran Behazin [3], Peter Keech [3] and Nikitas Diomidis [4]

1   Integrity Corrosion Consulting Ltd., Nanaimo, BC V9T 1K2, Canada
2   LS Computing Ltd., Elkford, BC V0B 1H0, Canada
3   Nuclear Waste Management Organization, Toronto, ON M4T 2S3, Canada
4   Nagra, CH-5430 Wettingen, Switzerland
*   Correspondence: fraser.king@shaw.ca

Abstract: The disposal of high-level radioactive waste (HLW) and spent nuclear fuel (SF) presents a unique challenge for the prediction of the long-term performance of corrodible structures since HLW/SF containers are expected, in some cases, to have lifetimes of one million years or longer. Various empirical and deterministic models have been developed over the past 45 years for making predictions of long-term corrosion behaviour, including models for uniform and localised corrosion, environmentally assisted cracking, microbiologically influenced corrosion, and radiation-induced corrosion. More recently, fracture-mechanics-based approaches have been developed to account for joint mechanical–corrosion degradation modes. Regardless of whether empirical or deterministic models are used, it is essential to be able to demonstrate a thorough mechanistic understanding of the corrosion processes involved. In addition to process models focused on specific corrosion mechanisms, there is also a need for performance-assessment models as part of the overall demonstration of the safety of a deep geological repository. Performance-assessment models are discussed in Part 2 of this review.

Keywords: high-level waste; spent fuel; container; canister; modelling; lifetime prediction

1. Introduction

The container is an important component of the multi-barrier system for the disposal of high-level waste (HLW) or spent fuel (SF) in a deep geological repository (DGR). Containers will undergo time-dependent degradation due to corrosion, with long-term performance also dependent on the properties and performance of the other engineered barriers, particularly the clay- or cement-based buffer material surrounding the container. For example, the long-term performance of copper containers depends greatly on the maintenance of diffusive mass-transport conditions in the bentonite buffer material [1], as does the behaviour of carbon steel containers passivated by the presence of cementitious backfill [2].

Studies of the corrosion behaviour of container materials for the disposal of HLW/SF began as early as the 1970s [3]. Modelling has been an integral part of these studies right from the outset, either as a means for understanding the underlying mechanisms or for making predictions about the long-term performance of containers in the DGR. The earliest modelling studies were conducted in Sweden [3,4] and the United Kingdom [5,6], in both cases for active container materials (copper and carbon steel, respectively). The first attempt at predicting the lifetimes of a passive container material subject to localised corrosion involved long-term predictions of the crevice corrosion of Ti Grade 2 in the Canadian program [7,8]. Significant advances in the modelling and long-term prediction of localised corrosion processes were made in the Yuca Mountain program in the United States, particularly in the area of crevice corrosion of Ni-based alloys [9]. Modelling activities have been important components of the Japanese program as well, primarily for carbon steel

containers [10,11], and also for Ti alloys [10,12,13]. Throughout this time, the modelling of corrosion processes for copper has continued, with progressive refinement of the predictions as the understanding of the underlying corrosion mechanisms has improved [1,14–18]. More recent developments in the area of container corrosion modelling include the formal consideration of joint mechanical–corrosion degradation modes [19,20] and the widespread application of reactive transport models for predicting the consequences of microbial activity on container corrosion [21].

The progress made in developing long-term predictive models for HLW/SF containers has been accompanied, however, by a shift towards the use of "corrosion allowance" container material (copper and carbon steel) and a move away from "corrosion-resistant" materials (Ti and Ni alloys). This shift was, in part, a response to review and regulatory comments on early attempts to predict the long-term localised corrosion behaviour of passive materials [22,23]. This move away from the consideration of passive materials has been reversed somewhat of late, with the Belgian program based on the use of a carbon steel container passivated by the presence of a cementitious buffer material (the Belgian Supercontainer concept [2] and the Czech program investigating the use of a dual-wall design with a carbon steel shell and an inner stainless-steel vessel. In the Belgian concept, passivation of the carbon steel reduces the susceptibility to localised corrosion and stress-corrosion cracking (SCC), so that lifetime prediction is based on the rate of uniform corrosion only. In the Czech concept, the outer carbon steel barrier provides a sufficiently long lifetime that the inner stainless-steel container is no longer susceptible to localised corrosion or SCC because the environment will be cool and anoxic by the time it becomes exposed to the near-field environment.

This progressive development of corrosion and container-lifetime prediction models for these and other repository programs and container designs is reviewed here. This review is an update of the earlier review of King [24]. The focus is on the corrosion behaviour and the prediction of container lifetimes; the corrosion of containers for the interim storage or disposal of ILW or the assessment of postclosure gas production are not considered. The discussion is also limited to the corrosion behaviour of the four main classes of alloy proposed for HLW/SF containers, namely carbon steel and cast iron, copper, Ti alloys, and Ni alloys. Although the properties of ceramics, both as bulk materials and as coatings, and of metallic coatings have also been investigated, the modelling methodologies for these materials and container concepts are not considered to be as mature as those for the conventional alloy groups and, therefore, are also not considered here (with the exception of copper coatings).

The review has been divided into two parts; a consideration of "process" models in Part 1 and models developed for inclusion in the performance assessment of HW/SF containers in Part 2 [25]. Process models are defined here as those that relate to a specific corrosion process and which are generally either mechanistically or empirically based, for example, reactive transport models for the uniform corrosion of copper or steel or the use of extreme value statistical analysis to model empirical pit-depth data. Performance-assessment models are those designed to make predictions of the consequences of one or more corrosion processes on a larger physical and temporal scale than process models, such as the prediction of the distribution of the lifetimes of containers in the DGR. Unlike process models, performance-assessment models are difficult or impossible to validate against experimental observations, and for this reason, various approaches are used to build confidence in the predictions, such as the use of natural and archaeological analogues or the results from large-scale in situ experiments. In some cases, the distinction between process and performance-assessment models is unclear, and detailed mechanistically based process models can be used for making container-lifetime predictions as, for example, in the case of the probabilistic canister breaching model (PCBM) for carbon steel containers [26].

Process models are generally either mechanistically or empirically based and there is debate about the relative merits of determinism and empiricism [27–29]. Deterministic (or mechanistic) models are those based on a mathematical representation of the underlying

physical laws and processes involved in the corrosion process, such as mass transport or charge transfer. Empirical models are those based on some form of statistical or arithmetical analysis of experimental observations, often permitting extrapolation into the future. As will be seen, the majority of process models described here are deterministic in nature, and we will return to this discussion of determinism vs. empiricism at the end of the review.

Lastly, a word about terminology. Within the scope of this review, the terms container, canister, overpack, and waste package are used interchangeably, and we make no distinction between the various terms. For consistency, we will use the term container when the discussion is of a general or generic nature. When referring to a specific national program, however, the term adopted by the particular implementing agency will be used. For example, the term canister will be used when referring to models developed by SKB, Posiva, and Nagra, and the term waste package will be used to refer to the Alloy 22 container for the Yucca Mountain program.

2. Background

As background to the discussion of the various process and performance-assessment models, it is necessary to understand the nature of the repository environment and how it evolves over time. Various aspects of the repository design will impact the near-field environment, including the type of host rock, whether the repository is located in the saturated or unsaturated zone, and the type of buffer and backfill used around the container, if any. The nature of the environment is an important consideration when selecting the container design and material of construction, and examples from various national waste-management programs are described. Lastly, the expected evolution of the corrosion behaviour of the container is considered and the implication for the development of predictive models is discussed.

2.1. Nature of the Near-Field Environment and How It Evolves over Time

Table 1 summarises some of the key environmental factors for a number of national waste-management programs. These, and other, environmental factors will determine the selection of the container material and the container design, as well as the long-term performance.

- Host rock—in addition to determining, in part, the nature of the groundwater at repository depth, the nature of the host rock also determines the relative importance of the engineered and natural barriers in the overall safety assessment. For low-permeability sedimentary host rock (clay, shale, and limestone), the container is a relatively minor contributor to overall safety since the transport of radionuclides through the geosphere is slow. In contrast, fractured crystalline rocks do not provide the same degree of radionuclide retardation and the use of long-lived containers, supported by robust long-term corrosion predictions, is common;
- Repository location—in all but one national program, the repository is to be located in the saturated zone 300–1000 m beneath the water table. Groundwaters at this depth are invariably anoxic, so the only available O_2 is trapped in the repository sealing materials at closure. The one exception is the proposed DGR at Yucca Mountain, Nevada which is located in the vadose (unsaturated) zone located 300–400 m below the surface (Following submission of the construction license application by the U.S. Department of Energy in 2008, the Yucca Mountain Program was suspended and has essentially ceased. However, based on the Nuclear Waste Policy Act (amended in 1987), the HLW/SF repository at Yucca Mountain, Nevada is still the only designated HLW/SF repository site in the U.S.). Although the supply of atmospheric O_2 to the repository might be restricted, it is prudent to assume that the disposal drifts are essentially aerated at all times. This, in turn, impacts the choice of container material, the nature of the likely corrosion processes, and the nature of the predictive models that are required;

- Buffer—the choice of buffer material immediately around the container (and, to some degree, that of the backfill material in the tunnels) affects the near-field chemical environment at the container surface, as well as the extent of microbial activity (both bentonite and cementitious backfill suppress near-field microbial activity). Bentonite buffer also limits the rate of supply of reactants to the container surface. In contrast, the absence of backfill will make microbial activity more likely, as well as allow advective transport of species to and away from the container;

- Container temperature—the maximum container temperature in most national programs is limited by the design of the repository to ≤100 °C in order to prevent damage to the backfill material. For the high-temperature operating mode (HTOM) repository layout at Yucca Mountain, the elevated near-field temperature was deliberately designed to prevent aqueous corrosion processes during the initial period of highest radiogenic activity. Even in DGRs in the saturated zone, there will be an initial period of unsaturated conditions around the container which must be accounted for in the lifetime prediction;

- γ-radiation dose rate—the maximum γ-dose rate depends on a number of factors, including the nature of the waste, the container loading, and the duration of interim storage, as well as the container design. Although the expected γ-dose rates are small in comparison to in-reactor dose rates, many national programs assess the extent of radiation-induced corrosion (RIC), both experimentally and through the use of predictive models;

- Groundwater chemistry—the salinity of the groundwater (characterised in Table 1 by the associated Cl^- ion concentration) varies from site to site and often, for a given site, with depth. While useful as a broad indicator of the "corrosiveness" of a given location, the container is not in contact with the groundwater itself if a bentonite or cementitious backfill is used. Instead, the container is contacted by the porewater, the composition of which may be quite different from that of the groundwater. A prime example of the modification of the near-field environment by the backfill is the highly alkaline porewater in cement backfill which imparts passivity to the carbon steel overpack of the Belgian Supercontainer and impacts not only the nature of the resulting corrosion processes but also the types of models used to predict the long-term behaviour;

- Microbial activity—as noted above, the use of bentonite or cement backfill precludes near-field microbial activity. Thus, predictive models are based on the possibility of remote microbial activity and the subsequent transport of aggressive metabolic byproducts to the container surface. For un-backfilled repository designs, microbial activity is possible at the container surface, which comes with the challenge of predicting the extent of microbiologically influenced corrosion (MIC) underneath a biofilm;

- Mechanical loads—although the current review does not address purely mechanical failure modes, the nature (tensile, compressive, and shear) and magnitude of the residual and applied stresses on the container affect certain joint mechanical–corrosion degradation mechanisms.

Table 1. Characteristics of various national nuclear waste disposal programs.

Country	Waste Type	Host Rock	Repository Location [a]	Buffer [b]	Max. Container Temperature (°C)	Max. γ-Radiation Dose Rate (Gy/h)	Groundwater [Cl−] (mg/L)	Notes
Belgium	HLW (SF) *	Boom clay	Saturated	Cementitious	<100	25	27	
Canada	SF	Granite Shale/limestone	Saturated	Bentonite	100	3	34,300 200,000	1
China	HLW	Granite	Saturated	Bentonite	<100	-	1155	
Czechia	SF	Granite	Saturated	Bentonite	<100	0.5	TBD	2
Finland	SF	Granite	Saturated	Bentonite	<100	0.17–0.34	16,000	
France	HLW (SF) *	Clay	Saturated	None (HLW)	<100	<10	2000	
Germany	HLW/SF	Salt	Saturated	Crushed salt	200	<1	300,000	3
Japan	HLW	Generic	Saturated	Bentonite	100	0.03	TBD	4
Spain	SF	Granite, Clay	Saturated	Bentonite	100	–	6550	5
Sweden	SF	Granite	Saturated	Bentonite	<100	0.2	6900	

Table 1. *Cont.*

Country	Waste Type	Host Rock	Repository Location [a]	Buffer [b]	Max. Container Temperature (°C)	Max. γ-Radiation Dose Rate (Gy/h)	Groundwater [Cl⁻] (mg/L)	Notes
Switzerland	HLW/SF	Opalinus clay	Saturated	Bentonite	150	0.1–0.2	3450	
Taiwan	SF	Crystalline	Saturated	Bentonite	<100	<1	50	6
UK	HLW (SF) *	Generic	Saturated	TBD	100?	0.03–0.3	TBD	7
USA	SF/HLW	Tuff	Unsaturated	None	200–220	<1	7	8

[a] Refers to whether the proposed repository location is below the water table in the saturated zone or above the water table in the unsaturated, or vadose, zone. [b] Refers to the material in contact with the container. The same or other materials may be used as backfill elsewhere in the repository. * In some countries, SF may or may not be directly disposed of as a waste. Notes include: [1] Canada has investigated both granitic and sedimentary host rocks. The Cl⁻ concentrations given are the maximum for each type of host rock. [2] No specific site has yet been identified. Site selection is planned for 2025. [3] A broad site-selection process was launched in 2022. The characteristics listed here are for the earlier salt repository program. [4] The Japanese program has considered various generic host rock types and associated groundwaters and awaits a volunteer host community. [5] Spain has considered both clay and granite host rock formations. The groundwater [Cl⁻] given is that for granite host rock. [6] No specific site has been identified in Taiwan. The characteristics listed here are for a reference area used for R&D purposes only. [7] No specific location has been identified to host an HLW (and SF if it is deemed to be a waste) repository in the UK. Three generic types of host rock have been defined (a lower-strength sedimentary rock, a higher-strength rock, and an evaporite) and indicative groundwater compositions defined. [8] The [Cl⁻] concentration refers to that of J-13 well water, but the seepage water dripping onto the hot-drip shields and waste packages will be evaporated to dryness, potentially resulting in highly concentrated electrolytes.

2.2. Container Materials and Designs

Table 2 summarises the reference container materials for each of the national programs listed in Table 1, along with alternative materials that are either currently being, or have historically been, considered. The compositions of some of these alloys are given in Table 3.

Table 2. Reference and other candidate container materials in various national nuclear waste programs.

Country	Waste Type	Reference Container Material(s)	Alternative Container Materials Considered
Belgium	HLW (SF) *	Carbon steel	AISI 316L hMo
Canada	SF	Copper	Carbon steel, Ti alloys
China	HLW	Carbon steel	Ti alloys, copper
Czechia	SF	Carbon steel outer, stainless steel inner	Copper, Ti alloys
Finland	SF	Copper, cast iron structural support	-
France	HLW (SF) *	Carbon steel	Undefined passive alloy, ceramics
Germany	HLW/SF	Carbon steel, Hastelloy C-4, Ti 99.8-Pd, pure copper	Inconel 625, Incoloy 825, Cu10Ni, Cu30Ni, cast steel, cast iron
Japan	HLW	Carbon steel	Ti alloys, copper
Spain	HLW/SF	Carbon steel	AISI 316L, Hastelloy C-22, oxygen-free copper
Sweden	SF	Copper, cast iron structural support	Ti alloy, ceramics
Switzerland	HLW/SF	Carbon steel	Copper
Taiwan	SF	Copper, cast iron structural support	-
UK	HLW (SF) *	-	Carbon steel, copper, Ti alloys, Ni-Cr-Fe alloys
USA	SF/HLW	Alloy 22, Ti-7 drip shield	Carbon steel, various Cu and Ni-Cr-Mo alloys

* In some countries, SF may or may not be disposed of directly as a waste.

Table 3. Composition of candidate container materials (in wt.% unless otherwise stated).

Copper alloys	Cu	P	S	H	O	
Oxygen-free high-conductivity OFHC	>99.99	<0.0003	-	-	<0.0005	
Oxygen-free phosphorus deoxidised low residual P	99.90	0.004–0.012	-	-	-	
Oxygen-free with phosphorus OFP	>99.99	0.003–0.01	<0.0012	<0.00006	Tens of ppm max.	

Ferrous alloys	Fe	Mn	Si	Cu	C	Other
Carbon steel	Balance	<1.65	<0.60	<0.60	<2	Cr, Ni, Mo, Ni, W, Zr (trace)
Low-carbon steel	Balance	<1.65	<0.60	<0.60	0.05–0.15	Cr, Ni, Mo, Ni, W, Zr (trace)
Mild steel	Balance	<1.65	<0.60	<0.60	0.16–0.29	Cr, Ni, Mo, Ni, W, Zr (trace)
Nodular cast iron	>90		<4	<0.05	<6	

Table 3. *Cont.*

Ni alloys	Ni	Cr	Fe	Mo	C	Si	Other
Alloy 825	36.0–46.0	19.5–23.5	24–40	2.5–3.5	0.05	0.5	1.5–3.0 Cu, 0.2 Al, 0.03 S
Alloy 22	56.0	22.0	3.0	13.0	0.015	0.08	3.0 W

Ti alloys	Ti	O	Pd				
Grade 2	Balance	0.12					
Grade 7	Balance	0.12	0.15				
Grade 16	Balance	0.12	0.05				

2.3. Evolution of the Corrosion Behaviour and the Implications for Lifetime Prediction

The combination of the near-field environmental conditions and the selected container material will determine the expected corrosion behaviour during the postclosure period. These corrosion mechanisms are summarised in Table 4.

Table 4. Corrosion processes for reference container materials in various national nuclear waste programs.

Country	Reference Container Material(s)	Corrosion Processes Considered [a]
Belgium	Carbon steel	**Uniform corrosion**, SCC, localised corrosion, RIC
Canada	Copper	**Uniform corrosion**, localised corrosion, SCC, MIC, galvanic corrosion, RIC
China	Carbon steel	**Uniform corrosion**, localised corrosion, hydrogen embrittlement, RIC
Czechia	Carbon steel/stainless steel	**Uniform corrosion, localised corrosion (carbon steel only), MIC**, HIC, galvanic corrosion, RIC
Finland	Copper	**Uniform corrosion, localised corrosion, SCC, MIC**
France	Carbon steel	**Uniform corrosion, MIC**, SCC, HIC, RIC
Germany	TStE 355 C-steel	**Uniform corrosion, pitting**, SCC, IGA, RIC
Japan	Carbon steel	**Uniform corrosion, localised corrosion, SCC, HIC**, RIC
Spain	TStE 355 C-steel	**Uniform corrosion, localised corrosion**, SCC, IGA
Switzerland	Carbon steel	**Uniform corrosion, localised corrosion**, SCC, HIC
Sweden	Copper	**Uniform corrosion**, localised corrosion, SCC, MIC
Taiwan	Copper	**Uniform corrosion**, localised corrosion, SCC, MIC
USA	Alloy 22	**Uniform corrosion, crevice corrosion, SCC**, MIC
	Ti-7 drip shield	**Uniform corrosion, HIC, SCC**

[a] Corrosion processes considered to be most important highlighted in bold font. SCC stress-corrosion cracking, RIC radiation-induced corrosion, MIC microbiologically influenced corrosion, HIC hydrogen- or hydride-induced cracking, and IGA intergranular attack.

One of the most important characteristics of the near-field environment is that it evolves over time. This evolution of both the environmental conditions and the consequent corrosion behaviour has long been recognised and was described in the very first HLW/SF container corrosion assessment conducted in 1978 by the Swedish Corrosion Institute [3]. Understanding how the environmental conditions and the resulting container corrosion behaviour change over time is important for two reasons. First, it is useful for the justification of predictions over such long periods of time, since it demonstrates an understanding of the underlying corrosion mechanisms and their time dependence. Second, it indicates that a given corrosion process may only occur for certain periods of time during the lifetime of the container. For example, for many materials, pitting or crevice corrosion will be limited to the relatively short early warm, aerobic period which may only last for a few months or years. Thus, the difficult task of justifying long-term predictions of the corrosion behaviour over periods of thousands or tens of thousands of years is greatly simplified, since predictions for these localised forms of corrosion need only to be made over a period of a few years, a timescale which it is feasible to study experimentally.

The nature of the evolution of the near-field conditions depends on the repository design and its location with respect to the local water table. Common to all repository designs is the thermal transient caused by the radiogenic heating from the decay of the waste, which results in an initial increase in temperature over the first few decades postclosure, followed by a slower decrease in the ambient temperature of the host rock over a period of a few tens of thousands of years. For repositories below the water table, the early part of the thermal

transient corresponds to the period of oxic conditions, during which the O_2 trapped in the pores of the buffer and backfill materials at the time of closure is consumed by corrosion of the container, the oxidation of mineral phases in the sealing materials and host rock, and by aerobic microbial activity. Once the trapped O_2 has been consumed (and once the γ-radiation field has decreased to insignificant levels), the repository environment becomes anoxic and remains so indefinitely. The thermal and redox transients are accompanied by changes in the degree of saturation of the near field. Initially, the moisture in the buffer and backfill materials surrounding the container will be driven away from the surface under the influence of the thermal gradient. The near field will subsequently saturate as moisture and incoming groundwater move back towards the container at a rate dependent on the hydraulic conductivity of the host rock and the heat output from the container.

Figure 1 illustrates this evolution for a bentonite-backfilled repository design, along with indicative timescales. The overall evolution is divided into three phases:

- An initial aerobic, unsaturated phase;
- A subsequent anaerobic, unsaturated phase;
- A long-term anaerobic, saturated phase.

This classification is based on the current understanding that the redox transient will be complete prior to saturation of the near field. Indeed, the oxic period may only last for a period of months or a few years at most, meaning that a container with a design life of 10^5–10^6 yr will be exposed to anaerobic conditions for >99.99% of the target lifetime.

Figure 1 also illustrates the timescales for different forms of corrosion associated with the different environmental phases. All container materials will be susceptible to uniform corrosion at all stages of the evolution of the repository environment, initially supported by the cathodic reduction of the trapped O_2 (limited to the first few years) and oxidising radiolysis products and, subsequently, by the evolution of H_2 under anaerobic conditions (with the added presence of sulphide for copper containers). Localised corrosion, on the other hand, will be limited to the early oxic phase (perhaps extended to include the period when oxidised corrosion products, such as Fe(III) and Cu(II), persist). During the long-term anaerobic phase, H-related degradation mechanisms, such as the hydrogen-induced cracking of carbon steel and the hydride-induced cracking of Ti alloys, are possible, in addition to uniform corrosion.

Other repository designs will have different environmental evolution characteristics. For example, in the case of a cementitious backfill, the near-field chemistry is dominated by the highly alkaline pH of the cement pore water. The high pH will promote the passivation of carbon steel (as in the Belgian Supercontainer concept). It is, then, important to know how long such alkaline conditions will persist in the repository, as the cement backfill is slowly degraded by incoming groundwater. As another example, unlike the dominant redox transient characteristic of repositories located in the saturated zone, the unsaturated Yucca Mountain repository is expected to be oxic at all times [9]. There would still be a thermal transient, and an advantage is taken of the slow rate of saturation to ensure an extended period of dry conditions, during which the waste package is not initially expected to undergo corrosion.

This evolution in near-field environmental conditions and the associated corrosion processes has implications for modelling and lifetime prediction. One of the more important consequences is that localised corrosion processes, which historically have been considered to be difficult to predict, will only occur for a limited period of time. The pre-requisite conditions for localised corrosion are also known, either the non-uniform wetting of the surface or the presence of a passive film. In the former case, there is therefore a need for thermal hydraulic (TH) models to predict the time dependence of the temperature and relative humidity (RH) at the container surface. In the latter case, for alloys that are not inherently passive, such as copper and carbon steel, models are required to predict the conditions under which the container surface could passivate as well as the duration of that passivity. Furthermore, the period of localised corrosion will be limited to the early oxic phase for repositories located beneath the water table, since the presence of O_2 is

required to provide sufficient electrochemical driving force and the opportunity for the spatial separation of anodic and cathodic processes.

In contrast to the short-term nature of localised corrosion, some forms of corrosion continue indefinitely. For example, uniform corrosion will occur at all times, initially under oxic conditions and then during the long-term anaerobic phase (for saturated repositories). The microbial production of sulphide and the resulting container corrosion may also continue indefinitely. Lastly, hydrogen-related degradation mechanisms are most likely during the long-term anaerobic phase. Models for all of these processes must take into account the long-term evolution of the repository environment and the resulting evolving corrosion behaviour.
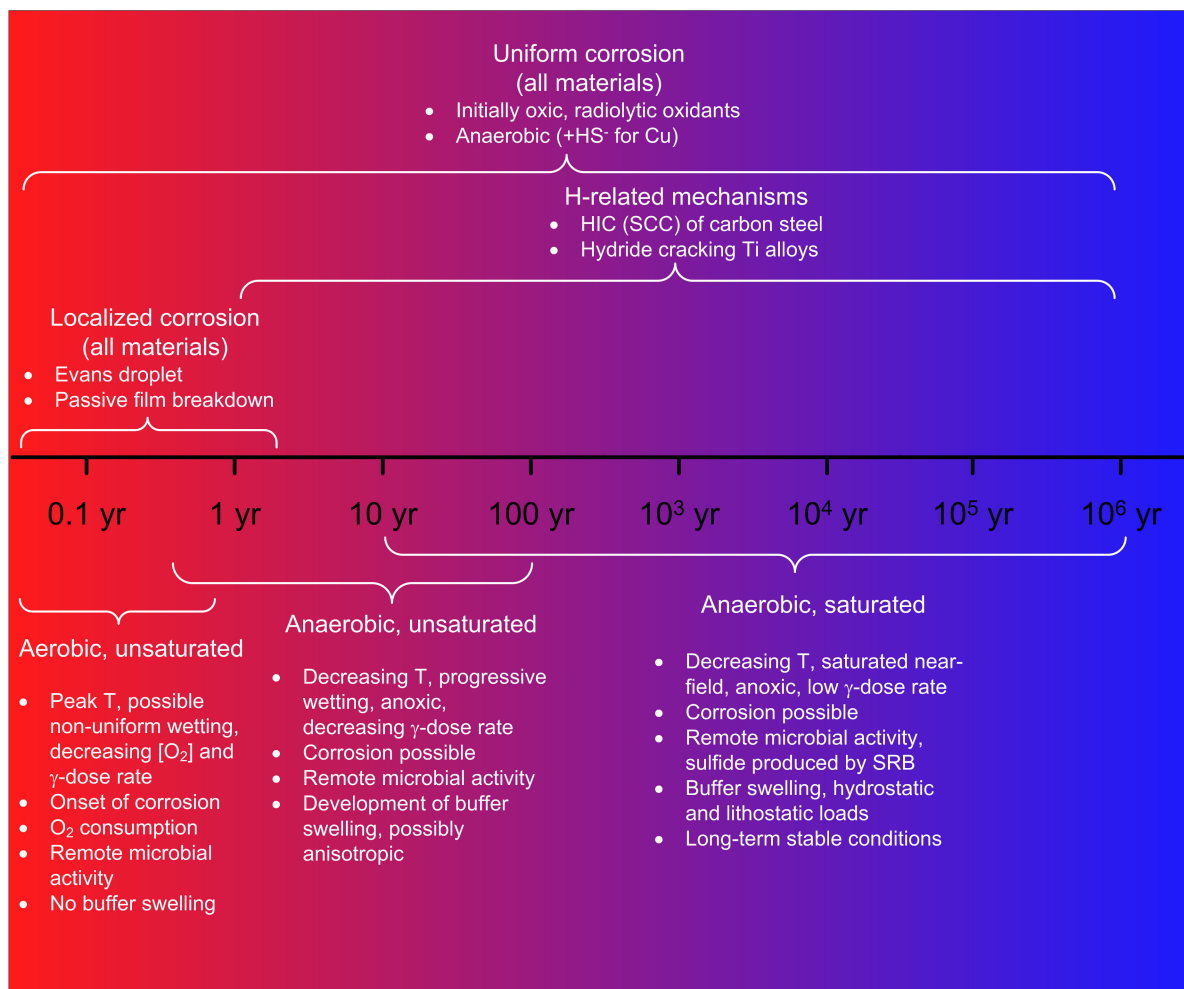

Figure 1. Schematic illustration of the evolution of the repository environment and the associated corrosion processes for a range of container materials. The evolution and the indicative timescales are for a bentonite-backfilled repository located in the saturated zone.

3. Process Models

Process models are defined here as models that can be used to interpret or predict the extent of a specific corrosion process (or, in a few cases, multiple processes). Process models are applied to laboratory-scale phenomena or on the scale of a single container, rather than on a repository scale. In general, process models can, and should be, validated against experimental data or empirical observations. Appendix A contains an extensive, but not exhaustive, list of process models that have been developed to account for the corrosion of HLW/SF containers and is divided into models for (i) uniform corrosion, (ii) localised corrosion (pitting or crevice corrosion), (iii) environmentally assisted cracking (EAC) (ei-

ther SCC or various forms of hydrogen-related degradation), (iv) MIC, (v) RIC, (vi) joint mechanical–corrosion processes, and (vii) miscellaneous corrosion-process models.

3.1. Uniform Corrosion

Models for the uniform corrosion of HLW/SF containers can be broadly classified into a number of different approaches, each with their own advantages and disadvantages (Table 5). Further examples for each of the different approaches listed in Table 5 can be found in Table A1.

Table 5. Approaches to the prediction of uniform corrosion processes for HLW/SF containers.

Approach	Examples	Advantages	Disadvantages
Empirical	Anaerobic corrosion of carbon steel [11,30,31]. Passive corrosion of Alloy 22 [9,32]	Conceptually simple. Conservative since the corrosion rate typically decreases with exposure time	Absence of any mechanistic basis.
Reactive transport	Point Defect Model [33–35] Steel–clay interaction model [36–38] Copper Corrosion Model (CCM) [39,40] Diffusion Poisson Coupled Model (DCPM) [41]	Mechanistically based. In some cases, provide additional information (e.g., E_{CORR} values) that is useful for predicting the long-term corrosion performance.	May require a lot of input data. Models tend to be mathematically complex, necessitating some skill in development and interpretation.
Mass transport	Corrosion of carbon steel under anoxic conditions in presence of corrosion-product film [42] Copper corrosion in O_2-free H_2O [43]	As for reactive transport models, couple the interfacial reaction to the (transport) properties of the near-field.	Non-conservative if a diffusing species reacts, resulting in a steeper concentration gradient but is not accounted for in the model.
Electrochemical	Mixed-potential model for copper in O_2-containing Cl^- environments [44,45] Corrosion of carbon steel in bentonite [46]	Typically involve prediction of the corrosion potential E_{CORR} which can provide additional insight. Inclusion of mass-transport effects provides link to near-field properties.	Can be overly conservative if protective properties of precipitated corrosion-product films are not taken into account.
Thermodynamic	Corrosion Domain and Volt Equivalent Diagrams [47,48] Corrosion of copper at high Cl^- concentration [49]	Sound physical basis and necessary data are widely available.	Unless coupled to a mass-transport expression, only provides information about what reactions are possible, not the reaction kinetics. Correction for activity coefficients at high concentrations somewhat uncertain.

3.1.1. Empirical

Empirical models for uniform corrosion are typically based on the extrapolation of experimental corrosion rates measured over periods of a few months to as long as 15–20 years [50]. Relatively short-term laboratory data may be supplemented by long-term data from large-scale in situ tests [51] and from archaeological analogue studies [52]. Empirical models have been used for both active and passive container materials. The corrosion rate generally decreases with exposure time due to the growth of the passive film on Ni or Ti alloys (or steel exposed to cementitious backfill) or the formation of a protective surface film on active materials such as Cu and carbon steel (Figure 2). Because of the decrease in corrosion rate with time, extrapolations of laboratory measurements to repository-relevant timescales are conservative, with predictions becoming increasingly reliable the longer the experimental exposure period. For saturated repositories, empirical extrapolation is generally used to predict the long-term rate of anaerobic corrosion, with mass-balance models based on the initial inventory of trapped O_2 used to predict the maximum extent of oxic corrosion.
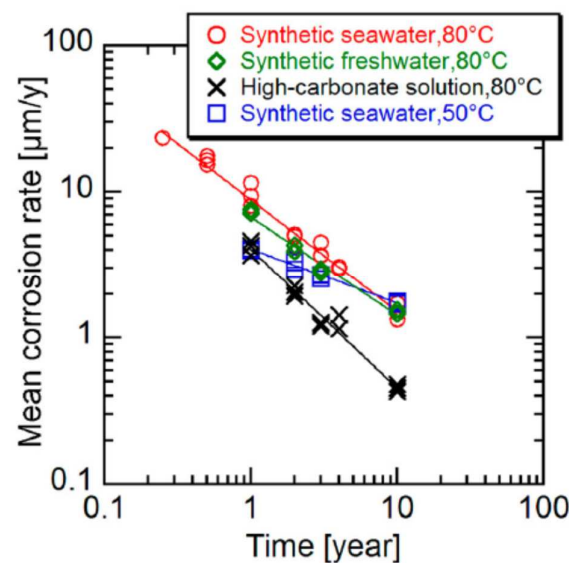
Figure 2. Decrease in the corrosion rate with increasing time for carbon steel embedded in compacted bentonite buffer saturated with various solutions during long-term exposure under anaerobic conditions [11]. Creative Commons attribution with a noncommercial, no derivative licence, reproduced with permission of the authors©.

In the simplest type of empirical model, a single value of the corrosion rate is selected, either from a statistical distribution or as a unique value (either a mean time-averaged rate or an "instantaneous" rate depending on the nature of the experimental data). For example, from the data shown in Figure 2, Ogawa et al. [11] selected a rate of 2 μm/yr to predict the long-term behaviour of the container, as it was the highest rate observed in the 10-y exposure tests. In other cases, the corrosion rate may be treated as temperature and/or time dependent, but it is not common for the corrosion rate to be dependent on the chemical environment. The absence of any chemical input in empirical models is partly because the corrosion rates are often found to be relatively insensitive to the nature of the environment (for example, Figure 2), and partly because, unlike the container temperature, it can be difficult to predict the time dependence of the near-field chemistry with certainty.

An Arrhenius-type expression was used to predict the temperature dependence of the rate of uniform corrosion of Alloy 22 in the Yucca Mountain Project (YMP) [9], with the form:

$$\frac{R_T}{R_{ref}} = \exp\left\{ -\frac{E_a}{R}\left(\frac{1}{T} - \frac{1}{T_{ref}} \right) \right\} \tag{1}$$

where R_T and R_{ref} are the corrosion rates at temperature T and reference temperature T_{ref}, R is the gas constant, and E_a is the activation energy for the corrosion reaction. The reference corrosion rate was determined from mass-loss measurements of creviced specimens exposed to three different simulated groundwaters and evaporated brines for a period of 5 yr at a temperature of 60 °C, fitted to a Weibull distribution (Figure 3). The activation energy was determined from experiments conducted at 60 °C and 90 °C (the upper end of the temperature range at which it was considered that an aqueous environment could exist on the waste-package surface at the elevation of the repository), with the E_a values fitted to a truncated normal distribution. Values for both the reference rate and E_a were sampled from the respective distributions for probabilistic performance-assessment modelling using the WAPDEG code [9]. Further details of the probabilistic waste-package degradation (WAPDEG) model are given in Part 2 of this review [25]. When applied to repository conditions, therefore, this modelling approach accounts for uncertainty in the measured values and the time-dependence of the container temperature, but not the decrease in rate due to the thickening of the passive film or any differences due to the nature of the chemical environment, although the experimental data indicated little effect of chemistry.
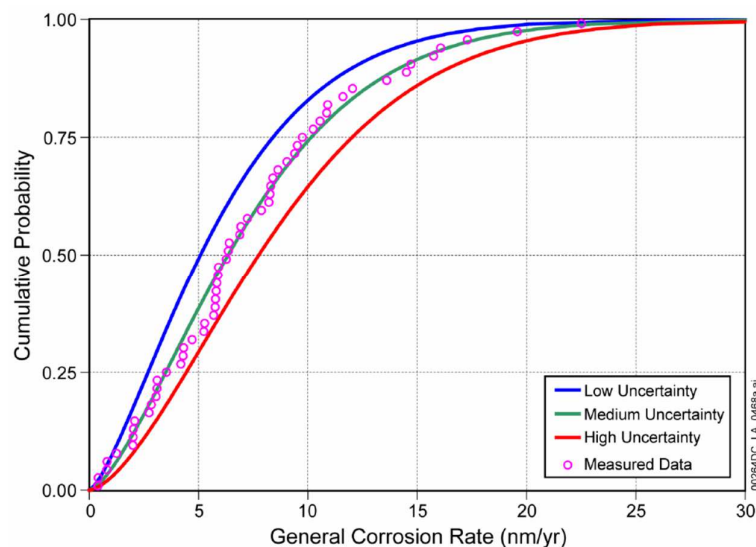
Figure 3. Cumulative distribution functions for the rate of uniform corrosion of Alloy 22 at 60 °C based on 5 yr mass-loss measurements fitted to a Weibull distribution [9].

An empirical model was also developed in the French program for the dry oxidation of carbon steel HLW containers during interim storage [53]. In this case, the time dependence of the corrosion rate was explicitly taken into account in the oxidation kinetics. Both logarithmic and parabolic kinetics were observed experimentally at different stages of film growth, but parabolic kinetics (for which the corrosion rate varies inversely with the square root of the exposure period) were selected as the most conservative of the two oxide growth laws. The rate of oxidation was found to be temperature-dependent (activation energy ~127 kJ/mol). So, when applied to the case of an HLW container in storage, the oxidation rate decreased with time both because of the thickening of the oxide and because of the decrease in temperature with time.

As described above, when extrapolating to times greater than the experimental exposure period, empirical models are inherently conservative, unless there is a loss of passivity or change in the environment or the mechanism. Hélie et al. [53] accounted for the effects of periodic spallation of the oxide film in their model. Ahn et al. [54] describe an approach for assessing the effect of the periodic depassivation of Alloy 22 due to the accumulation of S at the metal–film interface in an analogous mechanism to that observed under reactor operating conditions.

The inherent conservatism of empirical corrosion models is also based, of course, on the assumption that the corrosion rate does not increase with time. There was a suggestion in the Japanese program at one point that the accumulation of Fe_3O_4 corrosion product on carbon steel would lead to an increase in the corrosion rate [55]. The corrosion rate of carbon steel embedded in a Fe_3O_4 powder–bentonite mixture was found to increase with increasing magnetite content, possibly because the magnetite was acting as a cathode for the reduction of H_2O [56]. In the repository, this could lead to an acceleration of the corrosion rate, as the surface area of the cathode progressively increases as the corrosion product accumulates. However, Taniguchi [56] was able to demonstrate that the increase in corrosion rate was only transitory and was due to the reductive dissolution of the Fe_3O_4 involving the reduction of Fe(III) in the magnetite coupled to the dissolution of Fe to Fe(II). This is a good example of the need to support simple empirical models with a detailed mechanistic understanding of the underlying corrosion reactions.

Empirical models for uniform corrosion of HLW/SF containers are not limited to the prediction of the corrosion rate. An empirical expression was also developed in the YMP for the dependence of the corrosion potential E_{CORR} on the temperature and the solution composition [9]. The expression, derived from fitting experimental E_{CORR} values from 2 yr exposure tests in a range of simulated groundwater and brine solutions, is given by:

$$E_{CORR} = c_0 + c_1 T + c_2 pH + c_3 \frac{[NO_3^-]}{[Cl^-]} + c_4 T \frac{[NO_3^-]}{[Cl^-]} + c_5 pH \frac{[NO_3^-]}{[Cl^-]} + c_6 pHln[Cl^-] + \varepsilon_{CORR} \qquad (2)$$

where the different c terms were fitting coefficients, and ε_{CORR} was a residual not accounted for by the fitting procedure. Such an empirical fit is an alternative to the use of mixed-potential models for predicting E_{CORR}, as described below.

3.1.2. Reactive Transport

Reactive transport models are simply models in which the transport of reactants or products is coupled to one or more reactions in which they are produced or consumed. In the case of container corrosion, it is the transport of reactants towards, and of reactants away from, the container surface that is of most interest. Transport may occur by diffusion, advection, or electromigration (of charged species) and is described by a partial differential equation in space and time. Reactions are treated as either kinetic or equilibrium processes and are accounted for either as sources or sinks in the transport partial differential equation (PDE) or as a separate ordinary differential equation (in time only) for species that are not transported. Transport can be represented in 1, 2, or 3 dimensions. For example, the PDE for a species i that diffuses in 1D and participates in j reactions is given by

$$\frac{\partial c_i}{\partial t} = D_i \frac{\partial^2 c_i}{\partial x^2} + \sum_j R_j \qquad (3)$$

where c_i and D_i are the concentration and effective diffusivity of species i, R_j is the rate of the jth reaction, and x and t are the spatial and temporal variables.

The set of PDEs for the different species included in the model is mathematically solved subject to various initial and boundary conditions. The initial conditions are used to define the system, for example, whether it is initially aerated and the Cl^- concentration of the pore water. The boundary conditions are used to define the nature of the corrosion process at the boundary representing the corroding surface and of the other boundary (or boundaries) of the system being modelled, such as a location in the bulk solution of a laboratory experiment or at the buffer–host rock interface for a model of the container in the repository. Of interest here is how the corroding interface is treated mathematically, whether by coupled anodic and cathodic processes in a mixed-potential model (MPM) or by defining simpler non-electrochemical expressions for mobile reactants and products, such as finite-concentration or flux boundary conditions. As will be shown below, reactive transport models that use electrochemical boundary conditions for the corroding surface provide greater insight into the corrosion process than models based on non-electrochemical expressions.

The basic output of reactive transport models for the uniform corrosion of HLW/SF containers is similar regardless of the nature of the boundary conditions. The models predict the spatial and temporal variation of the concentrations of each of the species included in the model, as well as the rates of the various reactions. Spatial integration of the concentrations of various species can provide useful information about the evolution of the repository environment, such as the time dependence of the consumption of the initially trapped O_2. Integration of the rates of the various reactions can indicate which are the most important processes in the repository, for instance in the consumption of O_2, and where and when those reactions occur. In general, reactive transport models are useful for predicting the effects of the evolving environment on the corrosion behaviour of the container, and vice versa.

Of the large number of reactive transport models that have been developed (Table A1), the most suitable for the prediction of the corrosion behaviour of HLW/SF containers are those that explicitly treat the interfacial electrochemical processes. These models can be divided between those that treat the corroding surface as passive and those that assume active dissolution and the possibility of the formation of porous surface films. Of the former

type of model, the point defect model (PDM) is the best-known and most widely applied model [33–35,57]. The PDM predicts the growth (and breakdown, see Section 3.2) of the inner barrier layer responsible for the passivity of bilayer passive films comprising the inner barrier layer and an outer porous precipitated layer (Figure 4). Film growth and dissolution are determined by the generation, transport, and annihilation of different types of point defect, including cation (metal ion) vacancies (symbol $V_M^{\chi'}$), cation interstitials ($M_i^{\chi'}$), and oxygen (anion) vacancies ($V_{\ddot{O}}$). Cation vacancies are produced at the film–solution interface and consumed at the film–metal interface, resulting in recession of the metal surface. Anion vacancies are created and consumed at the opposite interfaces, resulting in a flux of cation vacancies inwards towards the metal and of anion vacancies in the opposite direction. The barrier-layer film also undergoes dissolution at the barrier layer–outer film layer interface. The (anodic) current is then expressed as a balance of these various transport and dissolution processes, and expressions can be derived for the steady-state current and passive film thickness.
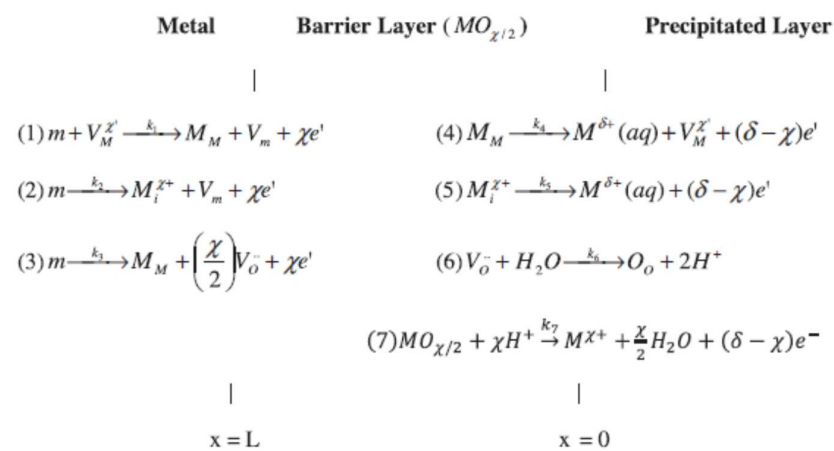
$$\text{Metal} \qquad \text{Barrier Layer } (MO_{\chi/2}) \qquad \text{Precipitated Layer}$$

$$(1)\, m + V_M^{\chi'} \xrightarrow{k_1} M_M + V_m + \chi e' \qquad (4)\, M_M \xrightarrow{k_4} M^{\delta+}(aq) + V_M^{\chi'} + (\delta - \chi)e'$$

$$(2)\, m \xrightarrow{k_2} M_i^{\chi+} + V_m + \chi e' \qquad (5)\, M_i^{\chi+} \xrightarrow{k_5} M^{\delta+}(aq) + (\delta - \chi)e'$$

$$(3)\, m \xrightarrow{k_3} M_M + \left(\frac{\chi}{2}\right)V_O^{\cdot\cdot} + \chi e' \qquad (6)\, V_O^{\cdot\cdot} + H_2O \xrightarrow{k_6} O_O + 2H^+$$

$$(7)\, MO_{\chi/2} + \chi H^+ \xrightarrow{k_7} M^{\chi+} + \frac{\chi}{2}H_2O + (\delta - \chi)e^-$$

$$x = L \qquad\qquad x = 0$$

Figure 4. Schematic of the seven reactions responsible for the growth and dissolution of the inner barrier layer of a bilayer passive film based on the PDM Generation II [35]. Reproduced with permission Elsevier©. The positions x = L and x = 0 represent the metal–film (barrier layer) and film–solution (outer precipitated layer) interfaces, respectively. The reactions and the notation for the various species involved are defined below.

Reaction (1): annihilation of a cation vacancy ($V_M^{\chi'}$) along with a metal atom (m) at the metal–film (barrier layer) interface resulting in the formation of a metal cation on the cation lattice (M_M) and a vacancy in the metal phase (V_m);

Reaction (2): generation of cation interstitials ($M_i^{\chi'}$) at the metal–film interface;

Reaction (3): generation of oxygen vacancies ($V_{\ddot{O}}$) at the metal–film interface;

Reaction (4): generation of cation vacancy and dissolved metal ion ($M^{\delta+}$(aq)) at the film–solution (precipitated outer layer) interface

Reaction (5): annihilation of metal interstitials at the film–solution (precipitated outer layer) interface

Reaction (6): annihilation of oxygen vacancies at the film–solution (precipitated outer layer) interface and the formation of oxygen ions in an anion site (O_O)

Reaction (7): dissolution of the barrier layer oxide ($MO_{\chi/2}$) at the film–solution (precipitated outer layer) interface

By coupling the expression for the anodic current to a Butler–Volmer expression for the cathodic reaction (generally the reduction of O_2 or H_2O), the PDM can be used to develop an MPM. This then allows the E_{CORR} of the passive system to be predicted [58–60], rather than relying on an empirical relationship such as that represented by Equation (2). Figure 5 shows an example of predictions from an MPM based on the PDM, in this case for Alloy 22 containers at the proposed Yucca Mountain repository. Predicted E_{CORR} values (as

well as the corresponding transpassive dissolution potentials) are shown for three different thermal loading scenarios for the entire evolution of the repository environment up to 1 million years.
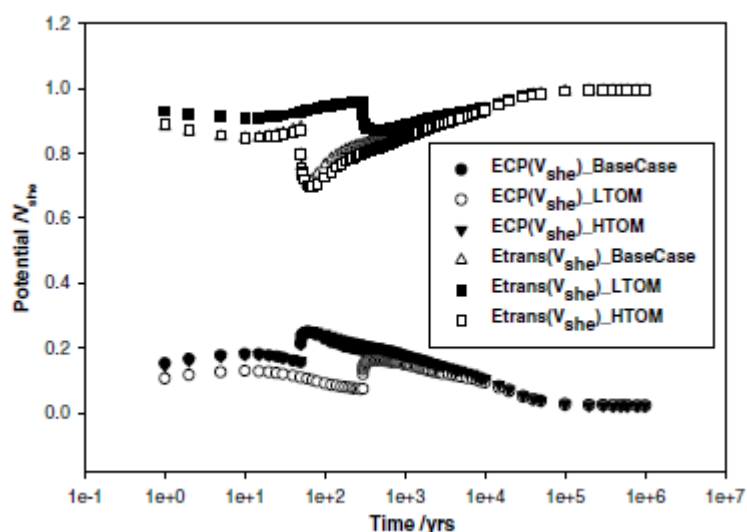

Figure 5. Predicted time dependence of the corrosion potential (ECP) of an Alloy 22 container in the Yucca Mountain repository for three different thermal-loading cases (a base case and for low (LTOM) and high (HTOM) temperature operating modes) [59]. Also shown are the corresponding transpassive dissolution potentials (Etrans). Reproduced with permission Elsevier©.

The PDM has been widely used to predict the growth and breakdown of passive films on metals in a wide range of industrial environments [34,35]. In terms of application to the prediction of the uniform corrosion behaviour of HLW/SF containers, the PDM has been used to predict the performance of Alloy 22 [58,59,61,62], carbon steel in a cementitious backfill [60,63], and copper in the presence of sulphide [64–66], although there has been some debate about whether the Cu_2S film in the latter system is truly passive or not [67,68].

As well as predicting E_{CORR} and the corrosion rate, the PDM has also been used to assess whether passive alloys could depassivate under repository conditions [63]. Depassivation is of concern because of the long-term deeply anaerobic conditions expected in saturated repositories. However, Lu et al. [63] were able to demonstrate using a combination of empirical evidence and analyses based on the PDM that depassivation of carbon steel in alkaline cementitious backfill is unlikely as the rates of film growth and dissolution decrease as the potential shifts to more negative values. This additional insight provided by such mechanistic models is a major advantage of the use of deterministic models for predicting the corrosion behaviour of HLW/SF containers.

The application of the PDM to the prediction of localised film breakdown will be discussed in Section 3.2.

The diffusion Poisson coupled model (DPCM) is based on a similar mechanism as the PDM for the growth of oxide films on passive surfaces [41,69]. Like the PDM, the DPCM is based on the movement of charge carriers in the barrier-layer oxide film and their generation and consumption at the metal–film and film–solutions interfaces. The major difference between the two models is that, whereas the electric field strength is treated as constant in the PDM, no such assumption is made for the DPCM, and the potential profile is calculated through a solution of the Poisson equation. The DPCM has been applied to the oxide formation on Fe in a neutral or slightly basic solution and predicts that the steady-state film thickness is a linear function of applied potential. Although the rest potential of a magnetite-covered surface in a mixed ferric and ferrous ion solution has been calculated, it does not appear that the model has been applied to a freely corroding system with either H_2O reduction or O_2 reduction as the cathodic reaction.

In contrast to the modelling of passivity using the PDM and DPCM, a number of reactive transport models have been developed on the basis of active dissolution of the container surface, along with the formation of porous non-passive surface films. Models have been developed for a range of corrosion systems, including copper in O_2-containing Cl^- environments [39,40], copper in the presence of sulphide [70–72], carbon steel in O_2-containing bentonite [5], carbon steel in bentonite under anaerobic conditions [73], and carbon steel in contact with bicarbonate-containing argillite clay [74,75].

In the models of King and co-workers, the interfacial electrochemical reactions representing the corrosion reaction are coupled to homogeneous reactions in the bulk medium representing a layer of compacted bentonite buffer in contact with the container. Various homogeneous processes are considered, such as redox reactions involving O_2 and dissolved Cu(I) and Cu(II) species; the precipitation and dissolution of solid phases; sorption of Cu^{2+} by the bentonite; and the diffusive mass transport of reactants towards, and of corrosion products away from, the corrosion surface. Figure 6 shows a typical reaction scheme (in this case for the copper sulphide Model (CSM)), illustrating the various homogeneous and interfacial reactions and diffusive mass-transport processes included in the models.
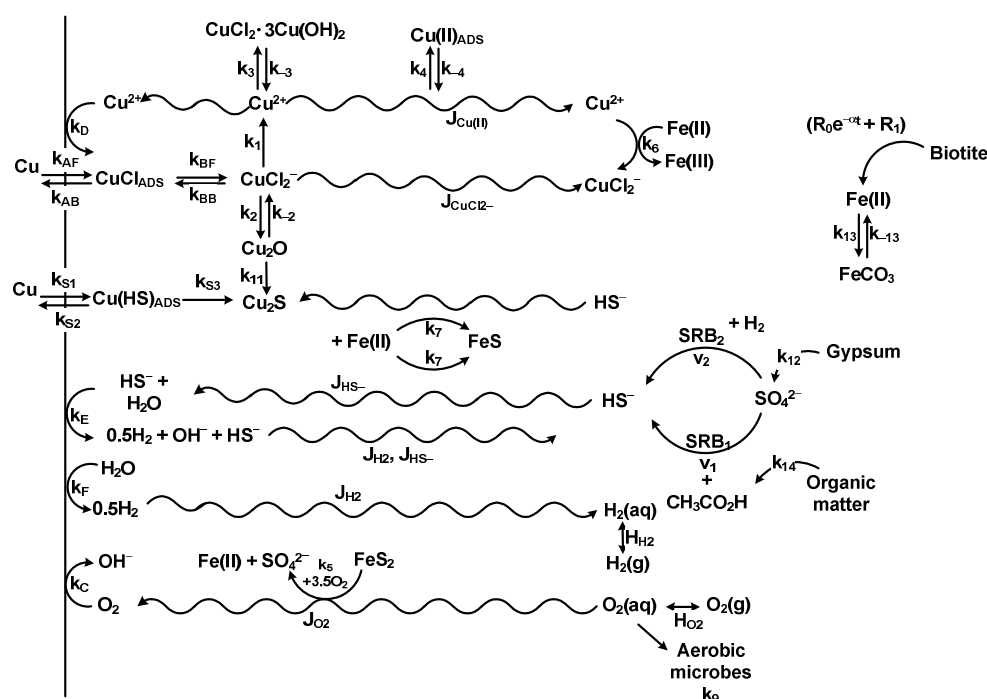

Figure 6. Reaction scheme for the version of the copper sulphide model (CSM) described by King et al. [72]. The ks represent rate constants for the various homogenous and interfacial reactions and the Js indicate diffusive fluxes represented by the wavy arrows. Creative Commons Attribution-NonCommercial-No Derivative Licence, reproduced with permission of the authors©.

The reaction mechanism shown in Figure 6, and other similar schemes for other models, is based on an extensive experimental program, the results from which not only provide the mechanistic basis for the model but also input data. Along with information and input-parameter values from the broader literature, this underlying mechanistic basis is the key feature of these deterministic approaches. The underlying mechanistic basis for the CSM and the earlier copper corrosion model (CCM) can be found elsewhere [39,76–80].

A basic component of the CSM and CCM is the inclusion of an MPM based on the interfacial electrochemical reactions representing the corrosion reaction. The reaction scheme in Figure 6 includes two anodic processes (the dissolution of copper as $CuCl_2^-$ species and the sulphidation of copper to form Cu_2S) coupled to four cathodic processes (the reduction of O_2 and Cu^{2+} and the evolution of H_2 from the reduction of either HS^- or

H$_2$O). Used as boundary conditions to solve the set of PDEs for the various species included in the model, these reactions define the MPM which is used to predict the time dependence of E$_{CORR}$ and the corrosion rate (as the corrosion current density i$_{CORR}$). Figure 7 shows an example of the prediction of the time dependence of E$_{CORR}$ for a copper container as the repository evolves from the initial aerobic phase (labelled "A" in the figure), through to the long-term anaerobic phase (labelled F). The evolution of E$_{CORR}$ also includes a period B where the surface of the container is too dry to support corrosion, as well as a precipitous drop in E$_{CORR}$ (at point E) when the dissolution of Cu as CuCl$_2$$^-$ in periods C and D switches to the sulphidation of copper to form Cu$_2$S. This further illustrates the mechanistic insight that can be obtained from deterministic models that are not available from simple empirical models.
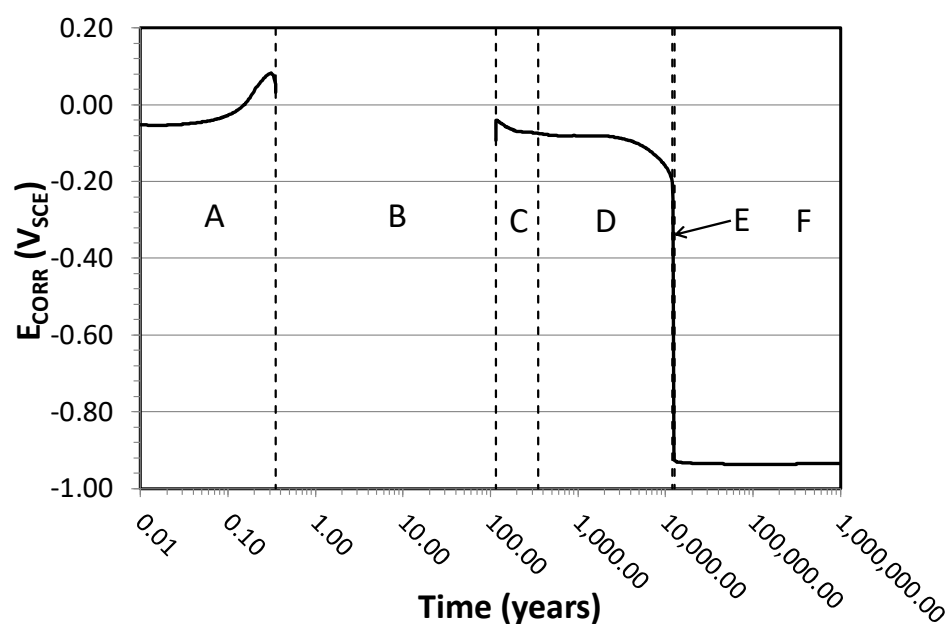

Figure 7. Predicted time dependence of the corrosion potential E$_{CORR}$ of a copper container in a deep geological repository under evolving redox conditions [72]. The near field is initially aerobic but becomes progressively anaerobic as sulphide reaches the container surface. The periods A–F represent different phases in the evolution of the near-field environment and container corrosion behaviour. Creative Commons Attribution-NonCommercial-No Derivative Licence, reproduced with permission of the authors©.

Two other variations of the CCM have been developed, the CCM-SCC to predict the initiation of aerobic forms of SCC of copper and the CCM-MIC to predict the effect of remote microbial activity. These models are described in Sections 3.3 and 3.4, respectively.

Reactive transport models have also been developed to predict the uniform corrosion behaviour of carbon steel containers. King et al. [73] applied the same modelling techniques described above for the CCM to the corrosion of carbon steel in contact with bentonite buffer under anaerobic conditions. The reactions considered in the model included the anodic dissolution of Fe supported by the cathodic reduction of H$_2$O; film formation involving the precipitation of a porous Fe$_3$O$_4$ layer; the generation, transport, and periodic release of H$_2$ gas; precipitation of Fe(OH)$_2$, Fe$_3$O$_4$, or FeCO$_3$ in the pores of the bentonite, thus reducing the buffer porosity; the sorption of Fe^{2+} on the clay; and the diffusive transport of dissolved and gaseous species.

The earliest reactive transport model for the corrosion of carbon steel containers was described by Marsh and Taylor [58]. In this model, the anodic dissolution of Fe^{2+} was coupled to the cathodic reduction of O$_2$, H$_2$O, or oxidising radiolysis products. Precipitation of Fe(OH)$_2$ or FeCO$_3$ was included in the model, but no other reactions other than the speciation of carbonate–bicarbonate. In this early model, the steel surface was assumed to

dissolve actively, and there was no effect of film formation on the rates of the interfacial processes. Mohamed-Said et al. [74,75] describe a model for the corrosion of carbon steel and the effects of $FeCO_3$ film formation on the corrosion behaviour. The various attempts at modelling the effect of porous film formation will be addressed in more detail below.

In addition to these electrochemistry-based reactive transport models for carbon steel, there is a large number of iron–bentonite interaction reactive transport models in the literature [see, for example, the models of Bildstein et al. [36], Samper et al. [37], and other models listed in Table A1]. These models tend to be developed by geochemists rather than electrochemists, and the focus is more on the reactions within the bentonite barrier than on the interfacial corrosion reactions. Indeed, in the majority of cases, the corrosion rate is a user-specified input rather than a parameter predicted by the model. Therefore, these models cannot be considered to be HLW/SF corrosion models, but rather geochemical models that predict the evolution of the near field as a consequence of container corrosion. Although these models do lack the mechanistic insight that can be obtained from electrochemical models that incorporate an MPM, they do tend to have a more robust treatment of homogeneous reactions in the buffer, typically based on the use of a geochemical thermodynamic speciation code to predict the equilibrium composition of the buffer porewater and the precipitation and dissolution of different solid phases.

Whereas the treatment of the properties of passive films has a sound basis in the science of point defects in solids [35], the most suitable manner for modelling the effects of a porous corrosion-product layer (CPL) is less clear. More specifically, the question is: how best to account for the spatial and temporal distribution of porosity as the film grows? The other question to address regarding porous surface films is what effect the film has on the interfacial dissolution processes. One effect of a porous film will be to block a fraction of the underlying surface from reacting, thus modifying the rates of the interfacial electrochemical reactions. In addition, the rates of transport of reactants to, and of dissolved corrosion products away from, the metal–film interface will be restricted by the pore structure. Lastly, if the film is electrically conducting, it could support electrochemical processes and could galvanically couple to the underlying metal surface [74].

The simplest approach is to assume that the porosity of the film is constant (in both space and time) with a value based either on experimental measurement or specified by the user [75,76]. The thickness of the CPL with time is then simply based on the rate of accumulation of precipitated corrosion product (either Cu_2S in the case of the CSM [76] or $FeCO_3$ in the case of carbon steel [75]). In the case of a Cu_2S film, this assumption of constant porosity was justified on the basis that experimental film growth rates were observed to be constant, which suggests that the film retains an open pore structure [76]. Because the porous film is typically assumed to block a fraction of the underlying metal surface (it can be shown that the fraction of the metal surface covered by a porous layer of randomly sised and randomly orientated pores that is exposed to the pore solution is equal to the bulk porosity), the value of the porosity becomes an important parameter in the model. For corrosion processes that are controlled by the rate of either the anodic or cathodic interfacial reaction, the predicted corrosion rate is proportional to the porosity (i.e., to the effective surface area exposed to the environment). On the other hand, if the corrosion rate is under mass-transport control (of either a reactant or product), the role of the film is simply to reduce the rate of transport across the CPL. If the container is in contact with compacted buffer material or cementitious backfill, the mass-transfer resistance of the buffer or backfill is generally higher than that of the thin CPL, and the corrosion film has little influence on the overall corrosion rate.

Another approach to modelling porous films is to calculate the spatial and temporal variation in porosity [75,81]. This is generally achieved by allowing the precipitate to form at the location at which saturation of the solution (or buffer porewater) with respect to a solid phase is achieved. Saturation will tend to occur close to the corroding interface, as this is the source of dissolved metal ions and is the location at which the highest concentration is achieved. However, very quickly, the interfacial porosity drops to zero and, if the

film is assumed to block the interfacial reaction, corrosion stops. That this is contrary to experimental observations of decreasing, but finite, corrosion rates over periods of up to 17 yr [50] suggests that either the precipitate does not block the surface or else some porosity is maintained in the film. King and Kolář [81] addressed this issue by defining a minimum interfacial porosity for the CPL but, because the rate of anaerobic corrosion of carbon steel in compacted buffer is kinetically controlled rather than transport limited, the predicted long-term corrosion rate is dependent on the assumed value of this minimum interfacial porosity. A more rigorous approach to this problem is to model the chemistry of the pore solution in the CPL since the continued corrosion suggests that open porosity is maintained by acidification of the pores due to the hydrolysis of dissolved metal ions. Mohamed-Said et al. [74,75] included the prediction of pore water pH, although the H^+ produced acted primarily as a cathodic reactant. In modelling the spatial distribution of the porosity of a $FeCO_3$ CPL, Mohamed-Said et al. [75] found that high rates of siderite precipitation resulted in denser and more protective CPL layers.

As well as potentially blocking the surface and restricting mass transport, porous CPL may also impact the distribution of electrochemical activity on the surface. If the CPL is electrically conducting and galvanically coupled to the underlying metal then catalysis of the cathodic reaction by the CPL could lead to an increase in corrosion rate, as was thought to be a possible explanation for the observation of Kojima et al. [55], described above. This was simulated by Mohamed-Said et al. [74] and, indeed, resulted in an increase in the corrosion rate. King and Kolář [79] also observed an increase in corrosion rate in the case of an electroactive Cu_2S layer, although King [76] argued that the experimental evidence argues against a conducting CPL in the case of copper in sulphide solutions. Furthermore, a conducting CPL will only lead to an increase in corrosion rate if the cathodic reaction is under kinetic or activation control. Thus, an increase in the effective size of the cathode due to the formation of a porous CPL would not lead to an increase in corrosion rate if the cathodic reaction were under transport control, as is the case for the corrosion of copper in sulphide environments [82] and the reduction of O_2 on steel in a compacted buffer [5].

One factor that is not generally considered in reactive transport models for HLW/SF containers is the extent to which rate constants and other input parameters determined in bulk solution can be used for the restrictive mass-transport conditions in highly compacted bentonite (HCB) or cementitious backfill [83]. Steric limitations in buffer and backfill materials would be expected to reduce the collision frequency of reacting species which, in turn, would be expected to slow the rate of reaction. On the other hand, long residence times due to slow rates of mass transport make it more likely that chemical reactions will be at equilibrium in porous systems. In fluid dynamics, the relative importance of reaction kinetics and mass transport can be expressed by the dimensionless Damköhler number Da, which is the ratio of the reaction rate to the mass-transport rate [84,85]. Extending this concept to reactive transport models in HCB, the slow rates of mass transport would tend to give Da > 1 [83]. Le Traon et al. [85] suggest that the effective reaction rate can be either enhanced or suppressed by local concentration gradients that can develop in porous media, with suppression of the reaction rate (compared with that measured in bulk solution) more likely for Da > 1 and for reaction orders of between 1 and 3 (requiring collisions between multiple species). This, then, implies that the rate constants in reactive transport modelling should be smaller than those measured in the bulk solutions that are typically used. However, Manaka [86] found that the rate constant for the oxidation of pyrite by O_2 was approximately 20 times higher in compacted bentonite than that measured in bulk solution. Thus, it seems that porous media will impact the reaction kinetics, but in ways that are not yet completely understood.

The various reactive transport models differ in the degree to which the corrosion reaction is coupled to the evolution of the near-field environment, specifically the thermal, saturation, and redox transients. The thermal transient will last for approximately 20,000 yr and will have a number of effects on processes relevant to the corrosion of HLW/SF containers. The rates of thermally activated electrochemical, chemical, microbiological, and

mass-transport processes will change over time, as will the solubilities of various solid phases, both corrosion products and other mineral phases in the near field. Although the effects of elevated temperature have been considered in various iron–bentonite interaction models, many of the models are isothermal (for example, [36,37,87,88]). Isothermal conditions were also assumed for the reactive transport models of Marsh and Taylor [5] and Mohamed-Said et al. [74,75]. On the other hand, Macdonald [59] explicitly investigated the effect of evolving temperature on the corrosion of Alloy 22 waste packages (see Figure 5), and the CCM and CSM models of King et al. [40,70–72] include a heat-conduction equation in addition to the PDEs for the various chemical species. The solution of the heat-conduction equation within the model allows the prediction of spatial and temporal variation in temperature, which is then used in conjunction with Arrhenius-type expressions for each of the temperature-dependent parameters to determine the effect of the thermal transient on the corrosion behaviour and near-field evolution.

The saturation transient will also have an effect on the corrosion behaviour of the container, impacting (i) partitioning of O_2 and H_2 (and possibly other species) between the gaseous and aqueous phases, (ii) the effective diffusivity of dissolved and gaseous species, (iii) the concentration and dilution of solutes as the relative volume of the aqueous phase changes, (iv) the activity of microbes through the effect on the water activity a_W, and (v) the rates of interfacial electrochemical processes in the event that the container surface dries out. The CCM and CSM suite of models account for all of these potential effects based on the spatial and temporal variation in the degree of saturation $S(x,t)$ of the compacted buffer material surrounding the container. While it would be feasible to predict $S(x,t)$ within the model through the solution of Richard's equation [89], the approach taken in the CCM and CSM is to define $S(x,t)$ as an input parameter based on the results of separate analyses. With this simplified approach, the CCM and CSM have been used to assess various effects of the saturation transient on the corrosion behaviour of the container, including (a) the evolution of the trapped O_2, the majority of which is initially present as gaseous O_2, but which reacts primarily as dissolved O_2; (ii) the possibility that the interfacial corrosion reaction ceases because the container surface dries out, corresponding to period "B" in Figure 7; and (c) the transport of gaseous H_2S and corrosion of the container at low degrees of saturation [79]. The coupled thermal–hydraulic–chemical (THC) sulphide transport model of Rashwan et al. [89] is discussed in more detail in Section 3.4.

A number of reactive transport models have addressed the early redox transient, since this period is particularly important for corrosion of the container. For their model of the corrosion of carbon steel containers in compacted buffer, Marsh and Taylor [5] assumed that the O_2 reduction reaction was transport limited and that the reduction of radiolytic oxidants was limited by their rate of production. As described in more detail in the discussion of localised corrosion in Section 3.2, these calculations were, in part, used to define the duration of the oxidising transient and, hence, the period for which localised corrosion was possible. There have been a number of attempts to predict the rate of O_2 consumption in the near field, mostly based on geochemical models that treated container corrosion in a peripheral manner, if at all (and which, therefore, are outside of the scope of this review). The CCM and CSM do account for the effect of container corrosion on the consumption of O_2, as well as the effects of aerobic respiration and pyrite oxidation [40,70–72]. In a recent CSM simulation in support of Posiva's operating-licence application [1], the initially trapped O_2 was predicted to be consumed within a period of 2–3 yr, although that is longer than the results of a full-scale in situ test suggest [90]. During this period, the canister surface was too dry to sustain aqueous corrosion processes, so the vast majority of the O_2 was predicted to be consumed by the oxidation of the pyrite present as an accessory mineral in the bentonite [1]. As well as the evolution in the O_2 content in the near field, the CSM also predicts the consequences of the formation and transport of sulphide to the container during the long-term anaerobic phase. Figure 7 is a representation of the entire redox evolution of the repository as indicated by the effect on the E_{CORR} of the container. From the relatively noble values of E_{CORR} during the initial O_2 transient,

the potential drops precipitously when sulphide reaches the container surface, and the potential-determining reactions shift from the dissolution as $CuCl_2^-$ to the formation of Cu_2S supported by the evolution of H_2.

In simulating the effects of repository conditions on the corrosion of the container material, the dimensionality of the models needs to be considered. All of the models discussed to this point have been 1D (either linear or radial geometry) in nature. However, the repository environment is clearly more complex, and 1D models may not properly account for the spatial arrangement of containers and potential oxidants, especially for in-floor disposal concepts such as the KBS-3 design. More complex 2D and 3D models are discussed in the context of sulphide transport simulations and the impact of remote microbial activity in Section 3.4.

3.1.3. Mass Transport

In addition to the reactive transport models described in the previous section, simpler transport-only models have also been used to predict the extent of HLW/SF container corrosion (Tables 5 and A1). Three such models are identified in Table A1, and in each case, the concentration of a corrosion product (either dissolved metal ions or H_2) at the container surface is calculated on the assumption of thermodynamic equilibrium. The corrosion rate is then determined by the rate of transport of the dissolved corrosion product away from the container surface. The three examples include:

- The corrosion of carbon steel under anaerobic conditions is determined by the rate of dissolution of a Fe_3O_4 film [42,91];
- Corrosion of copper in concentrated Cl^- solutions due to the anodic dissolution of cuprous–chloro complex ions supported by the cathodic reduction of H_2O [49,92];
- Corrosion of copper in O_2-free H_2O based on the assumption that the interfacial dissolved H_2 concentration is equivalent to that reported experimentally [43].

Models of this type are potentially non-conservative as they ignore reactions in the bulk environment that may potentially consume the transported species, such as the precipitation of Fe^{2+} or the microbial consumption of dissolved H_2. Consumption of the species undergoing transport will act as a sink and increase the concentration gradient at the corroding surface and, hence, the rate of corrosion. Vokál et al. [91] addressed this concern by including the sorption of Fe^{2+} by bentonite as a sink for the dissolved species produced by the dissolution of a Fe_3O_4-covered carbon steel container.

3.1.4. Electrochemical

The two electrochemical models identified in Table A1 are based on a simple mixed-potential model for copper in O_2-containing Cl^- environments. These models are based on the expressions developed by King et al. [44] for the steady-state E_{CORR} of copper as a function of dissolved O_2 concentration, Cl^- concentration, and the steady-state mass-transfer coefficient k_m, where $k_m = D_{eff}/\delta$ and D_{eff} is the effective diffusivity of the diffusing species (either $CuCl_2^-$ or O_2) and δ is the diffusion layer thickness. King et al. [44] validated the simple MPM against experimental data that covered three orders of magnitude variation in O_2, one order of magnitude variation in Cl^-, and five orders of magnitude variation in k_m. King and Briggs [45] subsequently developed a transient version of the same MPM and validated it against the time-dependent E_{CORR} values observed using a clay-covered copper electrode in O_2-containing 1 mol/L NaCl. This simple MPM forms the basis for the electrochemical interfacial reactions in the CCM reactive transport model described above [39,40,77,78] and was also used by Honda et al. [93].

3.1.5. Thermodynamic

Thermodynamic calculations are used in a number of modelling approaches, including the iron–bentonite interaction reactive transport models (Section 3.1.2) and for the calculation of the interfacial concentration of corrosion products in mass-transport models

(Section 3.1.3). Pourbaix diagrams are also extensively used in corrosion science and are classified here as an example of an "ancillary" model, as described in Section 3.8.

In addition to these uses of thermodynamics, there are two equilibrium-based approaches that have been directly used in the assessment of the corrosion behaviour of HLW/SF containers. Corrosion domain diagrams (CDD) were developed by Macdonald and Sharifi-Asl [47] to address the question of whether copper is immune to corrosion in O_2-free H_2O. A CDD is a pictorial representation of a given corrosion reaction of the conditions under which the metal is, and is not, thermodynamically stable (Figure 8). The parameter P is defined as the ratio of the activity a (or fugacity f for gaseous species) of the products of the corrosion reaction (raised to the power of the stoichiometric coefficients) divided by that of the reactants. For the corrosion of copper in pure water

$$Cu + H^+ = Cu^+ + \tfrac{1}{2} H_2 \tag{4}$$

the ratio P is given by

$$P = a_{Cu^+} f_{H_2}^{1/2} \tag{5}$$

Regions of stability and instability are separated by a line which represents the equilibrium conditions for the particular corrosion reaction as a function of pH (and temperature). If the ratio P for a given system is less than the value of P at equilibrium P^e, then corrosion is spontaneous. If $P > P^e$, then the system is thermodynamically stable and corrosion does not occur.
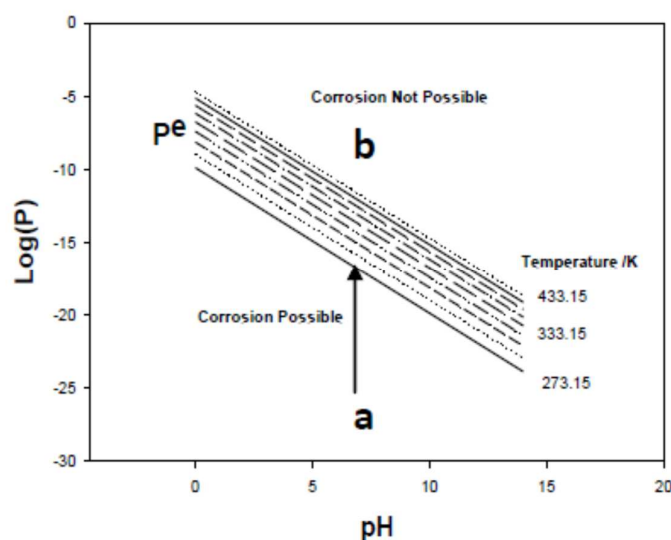

Figure 8. Corrosion domain diagram (CDD) for copper in pure H_2O as a function of temperature [47].

The CDD in Figure 8 shows that the equilibrium value for Reaction (4) is approximately 10^{-16} at 25 °C. Thus, metallic copper in an environment in which the value of $a_{Cu^+} f_{H_2}^{1/2}$ is greater than this value will not corrode. Clearly, although not "immune" to corrosion in pure H_2O, the extent of corrosion required to bring the system to equilibrium is infinitesimally small. Macdonald and Sharifi-Asl [47] calculated CDDs for a wide range of ligands, including a number of S-containing species, which enabled them to determine which species would "activate" copper, i.e., result in spontaneous corrosion.

A second thermodynamically based tool developed by Macdonald and Sharifi-Asl [47,48] is the volt equivalent diagram (VED). This approach is particularly useful for the S-H_2O system since there is a wide range of sulphur–oxy species with a wide range of S oxidation states. The "volt equivalent" for a species is the equilibrium potential for the reduction of the species to elemental sulphur multiplied by the average oxidation state of S in the species. The VED is then obtained by plotting the volt equivalents for the entire range of species against the respective average sulphur oxidation states. The resulting VED then allows the

products of the reactions between different species and the composition of the resulting solution to be predicted.

3.1.6. Current Status of the Process Modelling of Uniform Corrosion

The most common approaches to the prediction of the rate of uniform corrosion for HLW/SF containers are the use of empirical extrapolation and reactive transport modelling. The empirical approach is primarily used for predicting container lifetimes as part of the performance assessment (see Part 2 of this review) and is valuable for its transparency and ease of interpretation. However, empirical extrapolation should be supported by a demonstrated mechanistic understanding of the processes involved. Reactive transport modelling can provide that mechanistic insight, as well as be used to predict the corrosion rate instead of, or as well as, an empirical model. Of the various types of reactive transport models that have been developed, those that incorporate a mixed-potential model are particularly valuable in terms of the additional information and mechanistic understanding that they provide.

3.2. Localised Corrosion

Localised corrosion in the form of pitting or crevice corrosion is one of the more important processes to which HLW/SF containers may be susceptible in the repository, as evidenced by the large number of process models that have been developed (Table A2). Localised corrosion is important because, for saturated repositories, the amount of trapped O_2 is insufficient to lead to container failure by uniform corrosion and through-wall penetration is only possible if the attack is localised. For the proposed Yucca Mountain repository located in the unsaturated zone, the possibility of continuously aerobic conditions means that localised corrosion is a threat throughout the service life of the container.

Mechanistically, localised corrosion can be divided into initiation (birth), propagation (growth), and stifling (death) phases. Models have been developed for each phase and the following discussion will highlight which phase or phases are being simulated. Modelling the initiation process is useful if the aim of the simulation is to demonstrate that pitting or crevice corrosion will not occur under repository conditions, whereas modelling propagation (and stifling) is appropriate if the aim is to quantify the extent of damage.

Since most forms of localised corrosion are the result of the breakdown of a passive film, another important distinction is whether the container material is inherently passive (as in the case of Ti and Ni alloys) or whether the material is rendered passive because of the environmental conditions (as in the case of Fe and Cu). Inherently passive materials are potentially susceptible to localised film breakdown at any time, whereas active materials that become passive because of the nature of the environment will only remain susceptible while the conditions support passivation. Thus, conditions under which the corrosion-allowance materials Cu and Fe are susceptible to localised corrosion are also of interest. In this regard, it must be emphasised that, for saturated repositories, the period of susceptibility to localised corrosion will be limited to the initial aerobic phase (Figure 1), as the presence of O_2 is necessary to provide the electrochemical driving force to initiate and propagate a pit or crevice.

The various localised corrosion models in Table A2 are categorised in Table 6, along with the advantages and disadvantages of each approach.

3.2.1. Requirement for Passivation

For active materials, corrosion is expected to be uniform in nature unless the environment induces passivity that could increase the likelihood of the spatial separation of anodic and cathodic reactions. The two active HLW/SF container materials that may passivate due to environmental conditions are carbon steel and copper. In both cases, passivation becomes more likely with an increasing pH and HCO_3^-/CO_3^{2-} concentration, with the increasing temperature promoting the passivation of carbon steel but the active dissolution of copper [94,95]. The presence of compacted bentonite will tend to buffer the pH to a large

degree. Taniguchi et al. [96] observed the active dissolution of carbon steel in compacted bentonite saturated with a 0.1 mol/L HCO_3^-/CO_3^{2-} solution, with a pH ranging from 9 to 11, conditions under which the steel was passive in the absence of compacted bentonite. Thus, the presence of calcite and other minerals in the bentonite appears to buffer the pH at a value at which the carbon steel container would not passivate, and, hence, localised corrosion should not be of concern regardless of the redox potential.

Table 6. Approaches to the prediction of localised corrosion processes for HLW/SF containers.

Approach	Examples	Advantages	Disadvantages
Requirement for passivation	Period of susceptibility based on ability to sustain passive current density for carbon steel [97]. Suitable pH, $[Cl^-]$, $[SO_4^{2-}]$, $[HCO_3^-]$ and temperature for passivation of copper [98]	Establishes a period of time for which localised corrosion is of concern, which is typically a small fraction of the required service life.	-
Empirical	Pitting factor for copper [3] and carbon steel [10,99]. Extreme value analysis of maximum pit depth for copper [100] and carbon steel [101]). Time-dependent crevice propagation for Ti-Grade 2 [8]. Surface roughening factor of copper [16].	Conceptually simple. In the case of archaeological analogue samples and data from long-term in situ experiments, the exposure periods can exceed the duration of the oxic phase in the repository.	Limited mechanistic basis. Typically requires a large database. Environmental conditions for buried objects are different from those in the DGR. Material used in long-term exposure tests is often different from container alloy. Extrapolation beyond the length of the exposure periods and to containers with a larger surface area than the specimens that form the database can be challenging.
Reactive transport	Propagation of crevice corrosion for carbon steel [102]. Initiation of crevice corrosion for Ni and Ti alloys [103]. Pit propagation for copper [104,105]. Atmospheric corrosion stainless steel [106] Initiation, propagation, stifling of pitting on carbon steel in cementitious backfill [107].	Can provide additional mechanistic insight. Applicable to all phases of pit/crevice corrosion; initiation, propagation, stifling.	Difficult to define the cathode–anode surface area ratio. In some cases, no attempt to couple anode and cathode. Limited treatment of cathodic reduction of H^+ inside occluded region. Difficult to predict shape of corroded region inside a pit or crevice.
Electrochemical	Pit initiation and period of propagation based on comparison of E_{CORR} to film breakdown and repassivation potential for Alloy 22 [9,108] and copper [98].	Mechanistically based and, although most current modelling relies on empirical measurements of the critical potentials, these too can be predicted deterministically.	Critical potentials dependent on method of measurement and many experimental variables.
Stochastic	Pitting of passive alloys [109–111]	Addresses variability and uncertainty inherent to localised corrosion.	Lack of mechanistic basis.
Decision tree	Localised corrosion of Alloy 22 due to dust deliquescence [112].	Questions that form the decision tree are generally mechanistically based.	Less valuable if the answers to the question are qualitative.
Rules-based	Cellular automata model for carbon steel [113].	Rules can be mechanistically based.	Coupling of processes occurring on different spatial scales can be difficult, e.g., mass transport on the scale of metres and corrosion on the scale of μm.

In the case of copper, Briggs et al. [98,114] applied machine-learning techniques to the electrochemical data of Qin et al. [94] to predict the conditions of pH, $[Cl^-]$, $[HCO_3^-]$, $[SO_4^{2-}]$, and temperature at which passivation could occur. The experimental data were analyzed using a "bagged tree" algorithm to determine whether a given solution's composition and temperature would result in active (A) or passive (P) conditions. The bagged tree algorithm is a statistical classification and regression method designed to reduce variance and minimise overfitting to the data. As described in Section 3.2.4, the prediction of A or

P behaviour was then used to assess the likelihood of pit initiation and stifling based on electrochemical criteria.

The threshold pH criterion of Nakayama et al. [95] and the pore-water chemistry criterion of Briggs et al. [98,114] are useful for predicting the conditions under which passivation is possible. In contrast, Marsh et al. [97] proposed a redox-based criterion rather than a chemistry-based criterion for predicting the duration of passivity of carbon steel containers. These authors argued that even if the pore-water chemistry was suitable for passivation, passivity could only be sustained for the period that the flux of oxidants (either in the form of the initially trapped O_2 or as oxidising radiolysis products) could sustain the passive current density i_{pass}. Thus, the criterion for passivation can be expressed as (in terms of the initially trapped O_2):

$$D_{eff}\frac{\partial c(0,t)}{\partial x} \geq \frac{i_{pass}}{4F} \qquad (6)$$

where D_{eff} is the effective diffusion coefficient for dissolved O_2, $c(0,t)$ is the dissolved O_2 concentration at the container surface as a function of time, the factor 4 in the denominator on the right-hand side of the inequality represents the number of electrons transferred in the reduction of O_2, and F is the Faraday constant. Thus, as O_2 is consumed, the time at which the O_2 flux no longer satisfies this criterion represents the period of passivity. At this point, the surface would depassivate and localised corrosion would no longer be possible.

Whereas the discussion to this point has been focussed on determining the period during which passivation and, by inference, localised corrosion of copper or carbon steel is possible, the concept for the Belgian Supercontainer is to purposely passivate the carbon steel overpack in order to prevent localised corrosion and SCC [2]. This concept requires that the overpack is passivated so strongly that the $[Cl^-]$:$[OH^-]$ and $[S_2O_3{}^{2-}]$:$[OH^-]$ ratios are insufficient to initiate localised corrosion. Wang [115] has predicted the evolution of the near-field environment within the concrete buffer of the Supercontainer, including the time dependence of the pore-water pH and the concentrations of Cl^- and $S_2O_3{}^{2-}$ (both of which initiate localised corrosion and SCC) at the surface of the carbon steel overpack. The evolution of the pore-water pH follows the well-established mechanism for the leaching of concrete, with an initial period of 400–500 yr, during which the pH is controlled by the alkali metal hydroxides (~pH 13), followed by a subsequent period up to 80,000 yr postclosure when the pore-water pH is determined by the presence of $Ca(OH)_2$ at pH 12.5. This is, then, followed by a transition to C-S-H-dominated pore-water conditions (pH 11–11.5) beyond the simulation period of 10^5 yr. Thus, the passivation of carbon steel is expected throughout this time period. Furthermore, as Lu et al. [63] have demonstrated using the PDM, the passive state is predicted to be irreversible at these pH values, even when the overpack is exposed to deeply anoxic conditions.

In relation to the various stages of localised corrosion, the definition of a threshold pH [95] or of the necessary pore-water chemistry [98,114] for the passivation of carbon steel and copper, respectively, can be used to determine whether localised corrosion will initiate. The O_2 flux criterion for maintaining a passive film (Equation (6)) can also be used to determine whether localised corrosion will initiate but was primarily intended for predicting the duration of passivation and, in that sense, is more related to the propagation and stifling stages. For all of the approaches, however, if localised corrosion is possible, then a separate model is required to predict the extent of damage.

3.2.2. Empirical

As is the case for uniform corrosion, empirical models for localised corrosion of HLW/SF containers rely on an analysis of measured or observed localised damage from laboratory- of full-scale tests or from the study of archaeological analogues. As such, empirical models are focused on the propagation (and possibly stifling) stage, rather than on the initiation of pitting or crevice corrosion. Empirical models have been used to account

for the pitting of copper [3,100] and carbon steel [5,12,101,116], as well as the crevice corrosion of Ti [7,8] and Alloy 22 [9,117].

Pit propagation on copper has been predicted both on the basis of an empirical pitting factor [3] and a statistical analysis of pit depths [100]. The pitting factor (PF) is defined as the ratio of the maximum penetration depth (as measured from the original surface) to the average corrosion depth, with a pitting factor of one corresponding to uniform corrosion. The Swedish Corrosion Institute [3] was the first to propose this approach to account for the pitting of copper in their landmark assessment of copper SF canisters. The database used to estimate the value of the PF comprised measurements on copper objects that had been buried near the surface for various lengths of time and which could, therefore, be reasonably assumed to have been exposed to aerobic soil conditions [118,119]. As described in Part 2 of this review, the recommended value of the PF for performance-assessment purposes decreased over time as initial conservatism was relaxed. Despite the fact that the PF was based on objects exposed to aerobic conditions which only constitute a small fraction of the service life of the container in the DGR, the PF has tended to be used to predict the maximum depth of penetration for the entire assessment period of 10^6 yr [25].

The PF approach has also been used to predict the evolution of pitting for carbon steel [10,99,116]. Figure 9 shows the dependence of the PF on the average depth of corrosion based on data compiled for the Japanese program [10], which has been further supported by additional data from the French program [99]. There is strong evidence that the value of the PF decreases with an increasing depth of uniform corrosion so that, at a depth of 10 mm based on the data in Figure 6, the surface no longer exhibits localised corrosion. The data in Figure 9 can be fitted to a power-law expression for the purposes of container-lifetime prediction [99].

An alternative to the use of a PF is to extrapolate based on a statistical analysis of the time-dependent pit depth. Gumbel Type I generalised extreme value distributions have been commonly used to fit pit depths for both copper [100] and carbon steel [5,101,120]. The Gumbel distribution is used to represent the distribution of the "extreme values", i.e., either the maximum or minimum of the pit-depth distribution. Thus, extreme value analysis can be used to predict the maximum pit depth on a container, and therefore, the time to first penetration. But, it does not give any information about the distribution of pit depths.
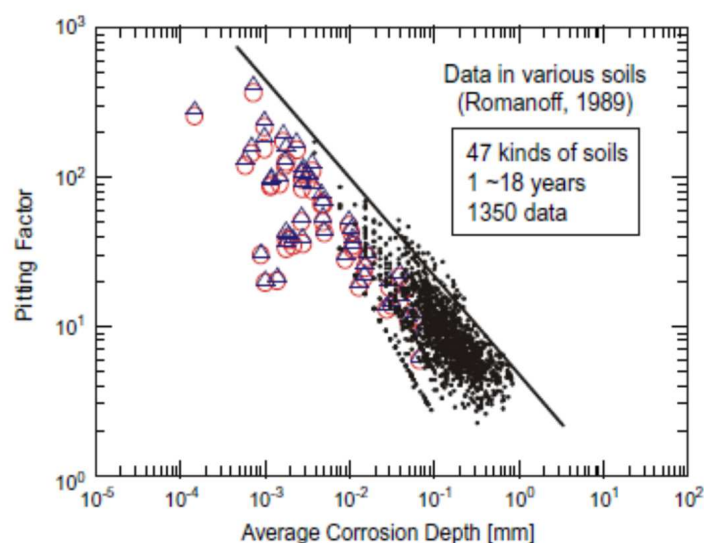

Figure 9. Variation of the pitting factor for steel and iron on the depth of uniform corrosion based on an analysis of data from long-term burial tests [121]. The soil data of Romanoff (shown as black dots) are supplemented by short-term experimental data from the Japanese program (blue triangles and red circles) [10]. Reproduced with permission Elsevier©.

A third empirical treatment used to represent localised corrosion of copper is the "surface roughness" allowance [16]. The concept of a surface-roughness allowance is based on the empirical observation that the surface of copper corroded in the presence of compacted bentonite does not exhibit discrete pitting but, instead, presents a roughened surface, where all regions have corroded but where the depth of penetration varies. Such a surface is consistent with a form of localised corrosion resulting from the non-permanent spatial separation of anodic and cathodic processes [16].

Having said the above that localised corrosion is only of concern in the presence of O_2, two cases of localised attack under anaerobic conditions have been considered in performance assessments for copper containers. These instances do not really represent process models and, therefore, are discussed in Part 2 on performance-assessment modelling [25]. However, briefly, the two cases relate to a proposed micro-galvanic process in sulphide environments (treated using a corrosion allowance [1,122]) and the possibility of localised corrosion under a biofilm on the surface of a canister where the surrounding bentonite has been chemically eroded and microbial activity becomes possible (treated using a localization factor [1]).

Empirical data have been used to assess the extent of localised corrosion of passive materials. Shoesmith et al. [7,8] fitted empirical crevice penetration rates for Ti Grade 2 (determined by mass loss of creviced samples exposed to a concentrated aerated NaCl solution at 100 °C) to a normal distribution (mean penetration rate of 10 μm/yr with a standard deviation of 5 μm/yr). A penetration rate was sampled from the distribution for each simulation of the Monte Carlo assessment of container lifetimes. This rate was adjusted for the time-dependent temperature of the container based on an Arrhenius expression with an empirically determined activation energy of 55 kJ/mol. Later, He et al. [123] presented a time-dependent power-law expression (also for Ti Grade 2) for the maximum penetration depth within the crevice (determined by successively polishing the creviced area until no further localised penetration was apparent), which could be used for predicting the stifling of the crevice corrosion. However, the fitted time exponent indicated that the penetration depth varied with $t^{0.87}$, so there was not a strong tendency for stifling under the particular experimental conditions (0.27 mol/L NaCl solution at 95 °C).

Empirical data have also been used to predict the crevice corrosion of Alloy 22. Initiation has been assessed based on a comparison of E_{CORR} to critical potentials for film breakdown and/or repassivation and is discussed in more detail in the section on electrochemical models below (Section 3.2.4). Dunn et al. [117] also measured the time dependence of the depth of crevice corrosion propagation and fitted the maximum depth to a power-law expression with a time exponent of 0.263, which is consistent with a strong tendency for stifling.

3.2.3. Reactive Transport

There is a surprisingly large number of reactive transport models that have been developed for pitting and crevice corrosion prediction (Table A2). We say "surprisingly" because, although it is entirely possible and informative to predict the chemistry and potential within the occluded region, the essential problem with simulating the initiation or propagation of localised corrosion is to predict the size and location of the anode and cathode. Although the location and size of the anode may be clear, especially in the case of crevice corrosion, the extent to which the anode can couple to the cathode is difficult to predict. The importance of this coupling lies in the fact that localised corrosion will likely be under cathodic control, i.e., the extent of dissolution will be limited by the capacity of the cathode to support the anodic reaction, especially in saturated repositories with a limited inventory of O_2, but also under aerobic atmospheric conditions [124]. While the factors that determine the extent of the anode–cathode coupling are understood, it is difficult to predict these with confidence. For example, the extent of coupling is dependent on the electrical conductivity of the environment and the resulting iR drop between the anode and the cathode. While the resistance of a bulk solution or a thin electrolyte layer can

be calculated [124], calculation of the resistivity of saturated bentonite is more difficult, especially since there is no consensus on the nature of the model that best describes the pore structure of compacted bentonite, let alone the resulting pore-water chemistry. When uncertainty in the number and distribution of anodic sites (especially sites for pit initiation) is added, it becomes very difficult to predict the relative cathode–anode surface area and the resulting extent of localised corrosion.

Nevertheless, reactive transport models have been developed to predict (Table A2) (i) the propagation of the crevice corrosion of carbon steel [102,125–129], (ii) initiation of crevice corrosion of Ni and Ti alloys [103,130,131] and of carbon steel [132], (iii) pit propagation for carbon steel [133], (iv) pit propagation of copper [104,105,134], (v) crevice corrosion under a porous dust deposit [135], (vi) atmospheric corrosion of stainless steel [106], (vii) passivity breakdown of Cu_2S films [64,65], (viii) dissolution of oxide particles in a friction stir weld [136], and (ix) initiation, propagation, and stifling of the pitting of carbon steel in a cementitious environment [107,137,138].

As a result of this difficulty in predicting the size and location of the cathode, a number of these reactive transport models focus only on the anodic reaction. For example, the early models of Sharland and co-workers [125–128] were used to predict the chemistry and potential within an occluded region as a function of crevice geometry and applied (external) potential, without any consideration of whether the cathode could establish or sustain that external potential. Alternatively, the rate of pit propagation could be predicted as a function of (assumed) cathode size [133]. In cases where the cathode is explicitly modelled, it is invariably assumed that the cathodic reaction (generally the reduction of O_2) occurs outside the occluded region, with the pit or crevice being the location of the anodic reaction. However, for the crevice corrosion of susceptible Ti alloys, it has been shown that the external O_2 reduction reaction only accounts for 20–30% of the total amount of corrosion [139], with the remainder supported by the cathodic reduction of H^+ inside the crevice, where the H^+ is formed by hydrolysis of dissolved Ti^{4+} ions within the occluded region.

Another difficulty in predicting the extent of propagation of localised corrosion is that the metal does not dissolve uniformly within the occluded region. Thus, the crevice corrosion of both Ti [123] and Alloy 22 [124] progresses at a number of sites within the crevice, resulting in localised penetrations ahead of a general corrosion front within the crevice. But, it is the depth of the deepest penetration that determines the time at which the container wall will be penetrated, and no mechanistically based model has yet been developed to predict these localised penetrations.

However, the atmospheric pitting model of Krouse et al. [106] does show promise in this regard. Although the model was developed for stainless-steel ILW containers, it is included here because it is potentially useful for predicting the development of pits for passive HLW/SF container materials. By predicting the distribution of the metal ion concentration within the pit during the propagation stage, Krouse et al. [106] were able to simulate the formation of the "lacy cover" that commonly forms over a growing pit, which is the result of the "undercutting" of the pit cross-section as dissolution spreads laterally at the same time that it proceeds in the depth-wise direction. The model can also account for the formation of different pit morphologies (hemispherical versus shallow, dish-shaped pits) observed at different combinations of RH and surface salt loadings.

By coupling an anodic dissolution model with a model for the cathode reaction, Krouse et al. [106] were also able to demonstrate the existence of a maximum pit depth for the atmospheric corrosion of stainless steel. Much work on this topic has been done by Kelly and co-workers in the area of the atmospheric corrosion of stainless steels (for example, [140,141]), and has also been applied to the crevice corrosion of Alloy 22 for the unsaturated Yucca Mountain repository [124]. Because of the iR drop between the anode and (external) cathode, there is a limit to the maximum current capacity that the cathode can deliver to the anode, which will then limit the extent of crevice propagation [142,143]. Furthermore, the iR drop within the crevice means that the rate of propagation varies

along the length of the crevice, thereby accounting for the localised penetrations commonly observed experimentally. Although these models have been developed for atmospheric corrosion conditions, they could also be applied to a saturated repository environment, provided that the electrical conductivity of the environment is known (or can be predicted).

Engelhardt and Macdonald [137] examined the conditions necessary for stable pit growth for carbon steel in cementitious environments. The presence of a low-conductivity, porous corrosion-product layer over the pit helps maintain differential aeration and prevents repassivation. However, if this cover over the pit is insufficiently conductive, then the resulting iR drop causes the pit to stifle. Taxén [104,105,134] also considered the effect of the precipitation of corrosion products within the pit-on-pit stability, in this case for copper. Based only on consideration of the anodic reaction, it was concluded that stable pit growth was only possible when a sufficient fraction of the dissolved Cu is transported out of the pit and does not precipitate and block the dissolving anode. The severity of pitting is, therefore, a function of the pore-water chemistry, since Cl^- and SO_4^{2-} promote dissolution, whereas high pH will tend to cause blocking of the pit by precipitation. The extent of pit growth, however, will depend also on the capability of the cathode to supply sufficient current to support the anodic dissolution reaction.

As well as the study of the propagation and stifling of localised corrosion, reactive transport models have also been used to predict the initiation of pitting or crevice corrosion. One common method for predicting the initiation of crevice corrosion is to determine the conditions under which a critical pH value is achieved within the occluded region [103,144,145] and, in some cases, a critical $[Cl^-]$ and potential [130–132]. Inevitably, however, the nature of the environment depends on the length and, especially, the width of the crevice, neither of which is easy to predict a priori. Therefore, such models are of more interest in terms of the mechanistic insight that they provide, rather than their truly predictive nature. Engelhardt et al. [135] investigated the properties of a porous layer on the container surface that would be necessary to act as a crevice former, which is of particular relevance for non-backfilled repository designs such as at Yucca Mountain.

The point defect model can also be used to predict pit initiation [33,34]. Pit initiation is postulated as occurring due to the condensation of cation vacancies at the metal–barrier layer interface at sites at which the flux of such vacancies is particularly high (Figure 10). Examples of such sites include the interfaces between the barrier-layer oxide and precipitates (such as MnS inclusions), grain boundaries, and emergent dislocations. Passivity breakdown is associated with the presence of aggressive anions, such as Cl^-, and two mechanisms have been proposed to account for the resulting enhanced flux of cation vacancies, namely Schottky pair generation and cation extraction. Expressions for the breakdown voltage and induction time can be developed on the basis of these mechanisms, which have been validated against experimental data for a wide range of systems [34]. Macdonald et al. [107] and Qiu et al. [138] have used the PDM to predict both the distribution of film breakdown potentials E_B and the induction time for carbon steel in cementitious environments for the Belgian Supercontainer concept. The effects of temperature, $[Cl^-]$, pH, and the presence of inhibiting oxyanions on E_B have been predicted and validated against experimental measurements. Macdonald et al. [107] applied these concepts to the "corrosion evolutionary path" (CEP) for the Belgian Supercontainer and concluded that, although pit initiation was possible during the early oxic phase, pits would stifle during the subsequent anoxic phase as the differential aeration cell necessary for pit growth could not be sustained. Therefore, it was concluded that the threat of pitting to the integrity of the container was negligible.

Mao et al. [65] have also applied the same principles to the possibility of film breakdown on copper in sulphide solutions. The effects of temperature and $[Cl^-]$ have been predicted and compared with experimental measurements, although, as noted above, there has been some debate about whether the Cu_2S films are passive or not [67,68].
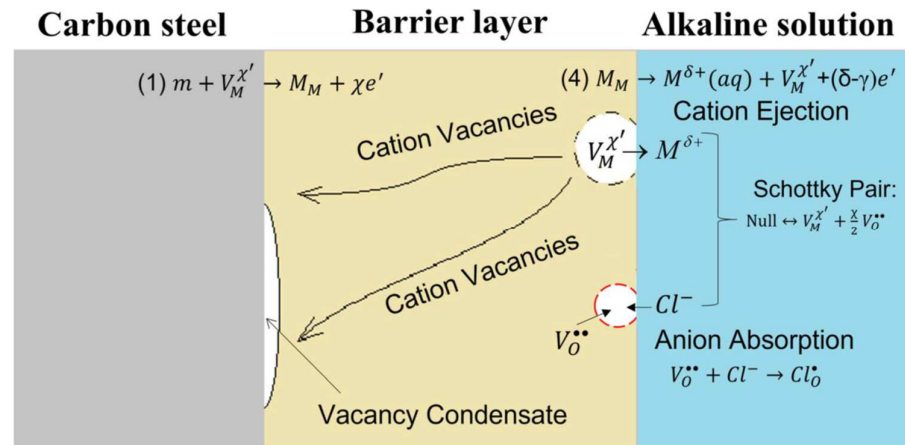
Figure 10. Schematic of the processes leading to film breakdown of carbon steel in alkaline environments according to the Point Defect Model [138]. Reproduced with permission The Electrochemical Society©.

3.2.4. Electrochemical

While electrochemistry plays an important role in various approaches to the modelling of localised corrosion, the focus of this section is on the use of critical potentials for predicting initiation and repassivation. The basic criterion for film breakdown and initiation of pitting or crevice corrosion is that the corrosion potential E_{CORR} must equal or exceed a critical potential E_{CRIT}, i.e.,

$$E_{CORR} \geq E_{CRIT} \tag{7}$$

The definition of critical potential is based on the typical current-potential behaviour of passive systems (Figure 11). Film breakdown occurs at a potential E_B, although pitting may not be sustained at that potential as it is preceded by metastable pitting events that exhibit a tendency to stifle without extensive dissolution. However, the increase in current at potentials more positive than E_B is an indication of pit propagation, as is the positive-current hysteresis observed, as the potential is scanned in the negative direction. The decrease in current as the potential is scanned in the negative direction indicates a slowing rate of propagation until such time that repassivation occurs at a potential (E_{RP}) defined here by the point of intersection of the forward and reverse potential scans. Although E_B defines the potential of film breakdown, it has been argued that a more reliable, and conservative, indication of pit or crevice initiation is to define the critical potential E_{CRIT} as the repassivation potential E_{RP} [108,146,147].

The use of E_{RP} as the indicator for crevice initiation has been broadly adopted in the Yucca Mountain Program [9,32]. The DOE developed an empirical expression for E_{RCREV} based on the results from a large number of current-potential scans for Alloy 22, similar to that shown in Figure 11. The fitted equation was given by

$$E_{RCREV} = a_0 + a_1 T + a_2 \ln\left[Cl^-\right] + a_3 \frac{\left[NO_3^-\right]}{\left[Cl^-\right]} + a_4 T\left[Cl^-\right] + \varepsilon_{RCREV} \tag{8}$$

where E_{RCREV} is the repassivation potential for crevice corrosion, and the coefficients a_0 to a_4 and the residual term ε_{RCREV} are derived from the fit. As can be seen from the fitted equation, increasing temperature T and $[Cl^-]$ promote film breakdown, whereas NO_3^- acts as an inhibitor. A similar fitted equation was developed by Dunn et al. [108,148], which also included the inhibitive effects of SO_4^{2-} and HCO_3^- on the initiation of crevice corrosion of Alloy 22.
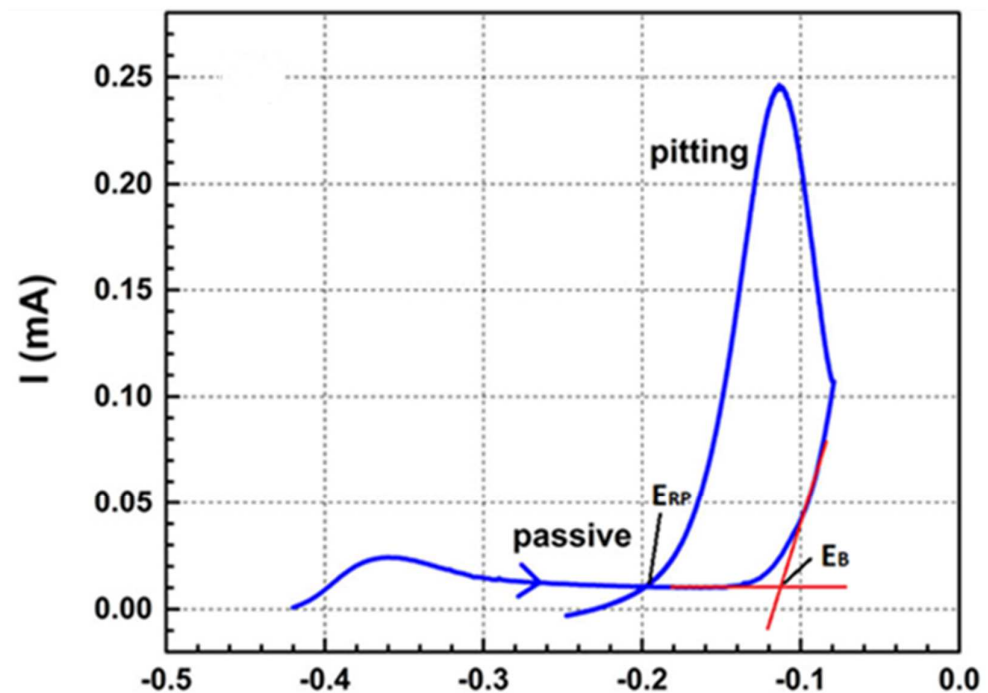
Figure 11. Illustrative current (I)-potential (E) scan for a system exhibiting passive behaviour. The film breakdown (E_B) and repassivation (E_{RP}) potentials are indicated. Figure modified from [94]. Creative Commons Attribution-NonCommercial-No Derivative Licence, reproduced with permission of the authors©.

To assess the likelihood of the initiation of crevice corrosion, the values of the critical potential from Equation (8) for various postulated environments that could be present in the YM repository were compared with corresponding E_{CORR} values from Equation (2). If the condition defined by Equation (7) was met, then localised corrosion initiation was assumed to occur. However, based on an analysis of many hundreds of possible aqueous solutions that could be present in the repository, the initiation criterion in Equation (7) was not met and localised corrosion was screened out as a possible waste-package failure mechanism.

For their probabilistic assessment of the pitting of copper canisters in aerobic saturated buffer material, Briggs et al. [98,114] based the criterion for pit initiation on the film breakdown potential rather than on the repassivation potential. Once initiated, pitting was assumed to propagate until such time that E_{CORR} fell below the repassivation potential. Thus, the criterion for stifling is

$$E_{CORR} \leq E_{RP} \tag{9}$$

The values of E_B and E_{RP} were taken from the parametric study of Qin et al. [94] and were fitted to a regression-tree algorithm with least squares gradient boosting using the built-in machine-learning capabilities of a commercial software package. In this way, values of E_B and E_{RP} could be estimated for any arbitrary combination of temperature, pH, [Cl$^-$], [SO$_4^{2-}$], and [HCO$_3^-$]. The value of E_{CORR} was a function of temperature, [Cl$^-$], and [O$_2$] and was predicted based on a mixed-potential model for copper under active conditions. If initiation was predicted to occur in any given run of the probabilistic Monte Carlo analysis, then the period of propagation was determined by the interval between initiation and repassivation. A separate empirical pit-growth law was then used to estimate the pit depth.

3.2.5. Stochastic

Localised corrosion, especially pitting, is often described as a stochastic process in the sense that various stages in the birth, growth, and death lifecycle appear to occur randomly in space or time. In reality, all of these processes, be it the initiation of a metastable pit or the stifling of that pit before it can become established, occur for specific mechanistically

based reasons. However, it may be that we lack the understanding to predict those events deterministically or that the variability in the system is too great to take into account; in which case, stochastic models of localised corrosion (generally pitting) may be useful.

Henshall [109–111] described a stochastic-based model for predicting the initiation and growth of pits for the YMP, but the approach is broadly applicable to any container material in any type of repository. The probability of pit initiation and stifling, of pit growth and the resulting distribution in pit depths can all be predicted based on this stochastic treatment, provided there is suitable empirical input data. Unlike the extreme value statistical analysis of pit depths described above, this stochastic treatment provides the time-dependent distribution of the depths of all of the pits on the container. Although a seemingly useful approach, it was not developed further in the YMP and has not been used to predict pit-depth distributions for a specific repository system.

3.2.6. Decision Tree

Decision trees are a type of model based on a series or hierarchy of events and their outcomes. Commonly used for decision making, the approach can also be used to support reasoned arguments for the exclusion of a given corrosion process from consideration. As such, the decision tree is usually structured as a series of prerequisite conditions that must be met so that the corrosion process is possible. If any one of the prerequisites is not fulfilled, then that process can be considered unlikely or impossible under repository conditions.

In the context of the localised corrosion of HLW/SF containers, the decision-tree approach has been used to support arguments that the localised corrosion of Alloy 22 due to either the deliquescence of dust deposits [112,149] or the evaporation of seepage drips [150] will not occur.

The use of decision trees will be discussed further in the context of the SCC of copper containers (Section 3.3.1).

3.2.7. Rule Based

Rule-based models are those in which the outcome is determined by a set of rules that govern, in the current case, interactions between various species and processes that describe the corrosion reaction. An example of a rule-based model that has been used to predict the corrosion behaviour of HLW/SF containers is the cellular automata (CA) model of di Caprio et al. [113]. An individual rule, for example, could be that a reactive state representing a metal atom converts to a passive state representing a metal oxide or hydroxide or that an electron-transfer step represents the reduction of H^+ to produce H_2. Pérez-Brokate et al. [151] used a set of seven such rules to represent the uniform corrosion of carbon steel. Probabilities were defined for each of the seven rules representing different reactions, which resulted in the roughening of the surface, as observed experimentally. The model also predicted the formation of isolated metal particles within a precipitated corrosion-product layer, which was also observed experimentally. Although the CA model can be used to predict the corrosion rate, the approach is more useful for providing insight into the corrosion mechanism.

3.2.8. Current Status of the Process Modelling of Localised Corrosion

A number of methods have been defined for determining when and if active materials may become passive and, hence, susceptible to localised film breakdown and pit or crevice initiation. The development and implementation of these models is a recognition that localised corrosion only occurs if certain prerequisite conditions are met and that the threat from pitting or crevice corrosion only needs to be assessed for a limited period of time. In addition to the breakdown of a passive film, localised corrosion may also initiate due to non-uniform wetting of the container surface and, while efforts in this area are underway, more work is needed to address the possibility of localised corrosion during the unsaturated phase of the repository evolution.

Mechanistically based models have been developed to predict the conditions under which pits or crevices may initiate, be it the electrochemical model based on a critical potential, reactive transport models to predict the time to develop critical crevice chemistry, or the PDM and the prediction of film breakdown based on the condensation of defects at the metal–film interface.

However, for pit and crevice propagation, empirical models still dominate. Empirical models are based on either laboratory measurements or data from long-term burial tests and large-scale in situ tests. This reliance on empirical data for predicting propagation is partly a reflection of the difficulty in deterministically modelling corrosion damage, although progress is also being made on this front.

3.3. Environmentally Assisted Cracking

Containers may be susceptible to two forms of environmental cracking (EAC); namely, stress-corrosion cracking and hydrogen-related degradation. The majority of the candidate container materials listed in Table 2 are susceptible to SCC to some degree, although not necessarily under repository conditions. A number of the materials may also be susceptible to hydrogen-related degradation, be it the hydrogen-induced cracking of carbon steel or the hydride-induced cracking of Ti alloys (both referred to here by the acronym HIC). Because the rate of crack propagation is fast compared with the timescales of interest, it is usual to make predictions on the basis of crack initiation. Either cracks will not initiate under repository conditions (the so-called "reasoned argument" or "exclusion principle" approach) or cracks will initiate, and the time to initiation represents the container lifetime. However, as described below, there have also been a couple of attempts at developing predictive models based on the concept of a limited propagation process.

The various process models developed for EAC are listed in Table A3 and are categorised in Table 7, along with the advantages and disadvantages of each approach.

3.3.1. Stress-Corrosion Cracking

Reasoned arguments against the possibility of SCC under repository conditions have been proposed for copper and carbon steel. Much of the evidence on which the arguments are made is empirical in nature, with relatively little deterministic underpinning. For example, Marsh and Taylor [5] argued that SCC of carbon steel containers could be prevented by stress relieving the fabrication residual stresses to less than 50% of the yield stress. Andra [152], on the other hand, argues that the use of a steel grade with low impurity and inclusion content, a fine-grained ferrite–pearlite (free from the susceptible banded microstructure), and good ductility will prevent SCC based on empirical evidence [153].

The reasoned argument against SCC for copper containers is based on a decision-tree approach [154,155]. Figure 12 shows the decision tree for the SCC of copper under aerobic conditions, with a corresponding one for anaerobic conditions also given by King [155]. In this approach, each of the prerequisite conditions for cracking is included in the decision tree in the form of a series of questions, all of which must be answered in the affirmative for SCC to be possible. Wherever possible, the question and the associated answer should be quantitative in nature, although it may be necessary to rely on qualitative responses where there is a lack of information or a high degree of variability and/or uncertainty.
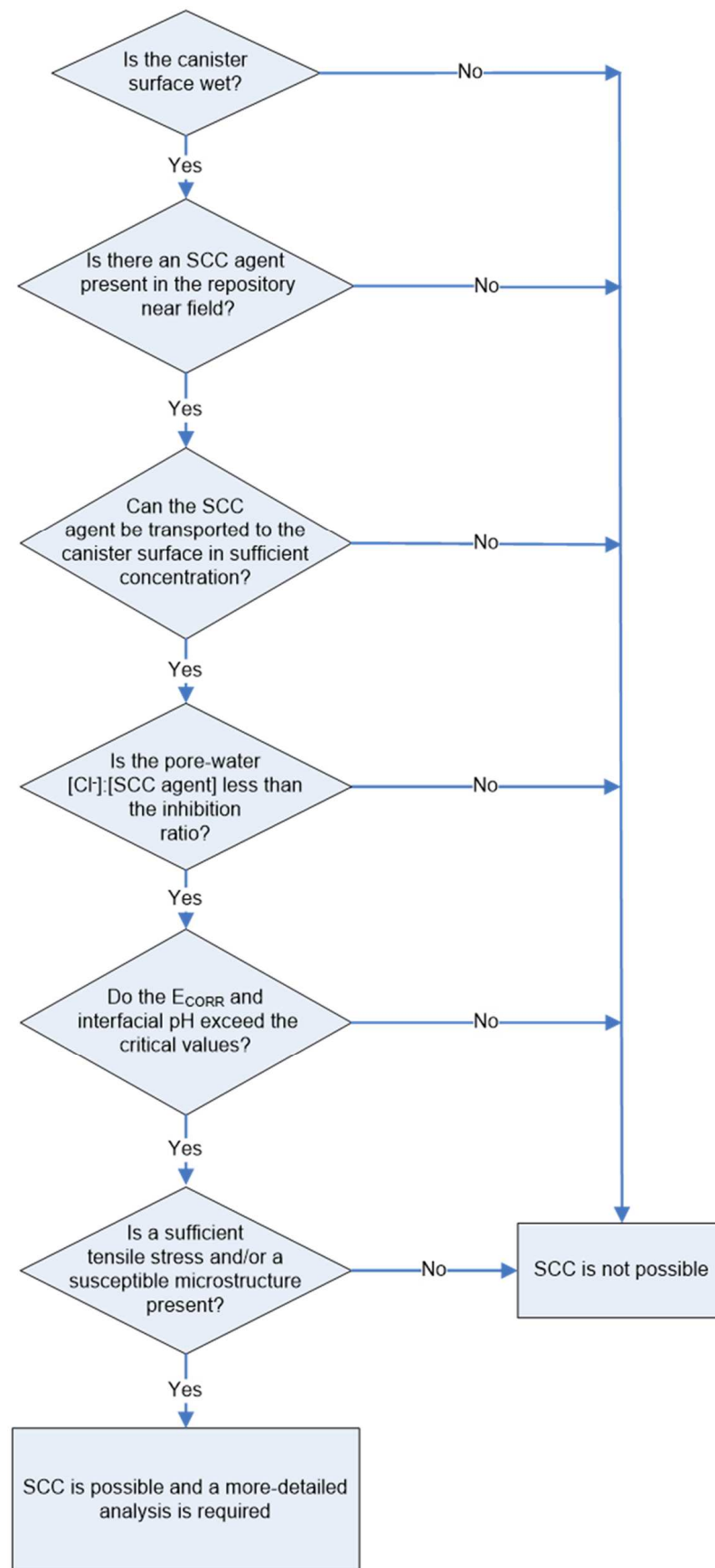
Figure 12. Decision tree for the stress-corrosion cracking (SCC) of copper containers under aerobic conditions [155]. Reproduced with permission Posiva Oy.

While most of the evidence underlying the decision tree is empirical, use is made of two modified versions of the copper corrosion model (CCM) to provide a mechanistic basis for the argument. The first modified version of the CCM that is used is for predicting the formation of microbial metabolic byproducts, specifically, ammonia and acetate, both of which are SCC agents. (The CCM-MIC is described in more detail in the next section). The second modified version of the CCM is the CCM-SCC [156,157], which includes the prediction of the pH at the container surface for comparison with empirical potential and pH boundaries for the SCC of copper in nitrite-, acetate-, and ammonia-containing environments.

Table 7. Approaches to the prediction of environmentally assisted cracking processes for HLW/SF containers.

Approach	Examples	Advantages	Disadvantages
Limited propagation (SCC)	Slip-dissolution model for Alloy 22 [158] Limited O_2 flux for aerobic SCC mechanisms for copper [159]	Mechanistically based. Avoids the need to demonstrate immunity over an extended period of time.	Large experimental database required.
Non-susceptibility (SCC)	Decision-tree analysis [154,155] Stress relief of fabrication stresses for carbon steel [5] Specification of steel grade with optimum chemical and microstructural properties [152,153]	Structure of decision tree is mechanistically based. Some evidence from pipeline operating experience to support benefits of stress reduction and improved material specification for steel	Relies heavily on empirical evidence
Threshold criterion (HIC)	Threshold [H_{ABS}] for onset of fast fracture for Ti alloys [160,161] Threshold hydride-layer thickness for crack initiation for Ti alloys [12,13,162] Threshold [H_{ABS}] for crack growth for carbon steel dependent on stress-intensity factor [20,26]	Conservative because of assumption of fast crack growth following initiation, except for hydride-layer thickness of Nakayama et al. [12,13,162].	Prediction of [H_{ABS}] for Ti alloys depends on hydrogen pick-up ratio which can be difficult to predict, especially in the event of crevice corrosion and/or for Pd-containing grades.
Non-susceptibility (HIC)	Low strength of selected grades of carbon steel are immune to HIC [5,10]	Extensive industrial experience from oil and gas industry.	No direct evidence for long-term exposure to repository environments.

Of the two models that have been proposed for the prediction of the crack growth rate, the most comprehensive is that of Andresen et al. [158] for the SCC of Alloy 22 for the proposed Yucca Mountain repository. While extremely corrosion resistant, the SCC of Alloy 22 has been observed during slow strain-rate testing in concentrated brine solutions at positive applied potentials, although no evidence for crack initiation was observed in U-bend tests [163]. Although the YM repository is continuously aerated, the absence of a backfill means that the only source of stress would be the residual stress from the final closure welds of the inner and outer lids, although the outer lid weld would be stress relieved by mechanical means so that the surface residual stress would be compressive. (The possibility of seismic activity leading to residual stresses from waste-package impacts has also been considered [163]). The SCC model was based on the slip dissolution–film rupture SCC mechanism and involved a threshold stress for crack initiation and a threshold stress-intensity factor K_{ISCC} for crack growth [158]. Crack growth was assumed to follow the commonly observed dependence on the stress-intensity factor K. The effect of pre-existing flaws and the stress-mitigated distribution of residual stress through the thickness of the closure weld were also accounted for in the model. The model was validated by comparing predicted crack growth rates with those observed experimentally, and, where there were discrepancies, the model was found to be conservative (i.e., it overestimated the observed rate).

The second attempt to predict the rate of crack propagation was the proposed correlation between the O_2 flux and the crack growth rate for aerobic forms of SCC of copper containers [159]. A relationship between the crack growth rate and the flux of O_2 to the container was developed based on the film rupture–anodic dissolution mechanism for the SCC of copper in nitrite solution, which involved a factor A_C–A_{CT} related to the ratio of the area of the cathode to that of the crack tip. Values for A_C–A_{CT} were derived by fitting the model to the literature's crack growth rate data, with A_C–A_{CT} found to be between 10 and 1000. The model was then coupled with calculations of the O_2 flux to the container and used to predict the maximum possible crack growth rate (assuming no periodic crack arrests due to film formation at the crack tip). Predicted crack depths ranged from 110 µm to 11 mm depending on the value of A_C–A_{CT}, but these were for a particularly slow rate of O_2 consumption over a period of 2400 yr. The much faster O_2 consumption now considered representative of the early redox transient (a matter of a few weeks [90]) would lead to a much shallower predicted crack depth.

3.3.2. Hydrogen- and Hydride-Induced Cracking

As for SCC, models have been developed for the HIC of carbon steel and Ti HLW/SF containers based on (i) non-initiation, i.e., that the selected grade of material will not be susceptible under repository conditions; (ii) initiation followed by fast fracture (i.e., fast crack propagation) once a threshold absorbed hydrogen concentration is reached; and (iii) initiation followed by predictable crack growth.

The non-susceptibility arguments are generally reserved for carbon steel (and copper) containers. Because of the importance of various forms of hydrogen-related degradation of carbon and low alloy steels in the oil and gas industry, there is an extensive industrial database relating susceptibility to hardness (which in turn is related to the yield strength), and, indeed, this relationship is the basis for the selection of steel for sour service. Both Marsh and Taylor [5] and JNC [10] claim immunity to HIC based on the relatively low strength of the grade of carbon steel to be used for HLW/SF containers. The immunity of copper alloys to hydrogen effects is generally attributed to the inherent lack of susceptibility of face-centred cubic (fcc) materials (due to the low solubility and diffusivity of hydrogen and because of the low strength of the proposed alloys) [1] and the fact that the effects observed in the laboratory involve absorbed hydrogen concentrations and/or charging rates many orders of magnitude greater than what is possible in the repository [164].

Crack initiation followed by fast propagation has been invoked as a model for both the hydrogen-induced cracking of carbon steel [20,26] and the hydride-induced cracking of Ti alloys [8,160,161,165,166]. The modelling of the HIC of carbon steel is an example of a joint mechanical–corrosion degradation mechanism and is discussed in detail in Section 3.6. Briefly, however, the model is based on a K-dependent (where K is the stress-intensity factor for a defect subject to a tensile stress) threshold absorbed hydrogen concentration at which an HIC crack initiates, with failure assumed to result immediately due to fast crack growth.

In the case of the hydride-induced cracking of Ti alloys, the threshold absorbed hydrogen concentration $[H]_C$ is defined by the intercept between the lines representing the onset of slow crack growth and the K-dependent fast fracture (Figure 13). The value of $[H]_C$ varies with the alloy type and increases with temperature because of the higher hydrogen solubility at elevated temperatures [165]. Fast fracture occurs at absorbed hydrogen concentrations greater than $[H]_C$ and failure is then assumed to be instantaneous. The prediction of the failure time, therefore, is based on the time-dependent increase in absorbed hydrogen concentration, which is a function of the rate of anaerobic uniform corrosion and the hydrogen pick-up fraction [161]. This approach has been used for the prediction of lifetimes of Ti Grade 2 containers in the Canadian program [160], replacing an earlier threshold-temperature criterion [8], and for Ti Grade 7 drip shields in the YMP [161].
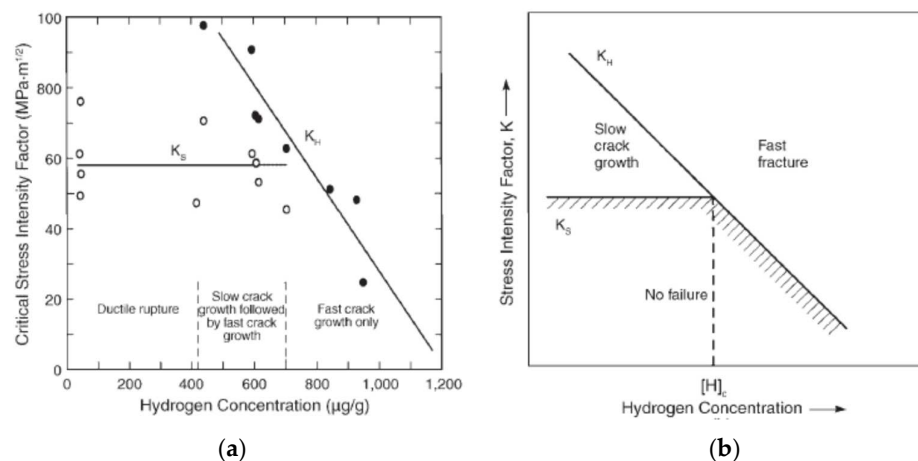
Figure 13. Basis for the definition of a threshold absorbed hydrogen concentration for the hydride-induced cracking of Ti alloys [165]. (**a**) Map of slow and fast crack growth as a function of stress-intensity factor and absorbed hydrogen concentration for Ti Grade 2. (**b**) Stylised basis for defining a critical or threshold absorbed hydrogen concentration for the onset of fast crack growth [H]$_C$. Reproduced with permission NACE International©.

An alternative approach to the prediction of failure due to HIC of Ti alloys has been proposed by Nakayama et al. [12,13,162]. This approach is based on the observation that crack formation occurs once the hydride-layer thickness reaches a critical thickness of approximately 10 μm. The hydride-layer thickness is a function of the cathodic current density and of the cathodic charge density, as well as temperature [162]. The charge density required to achieve the critical hydride-layer thickness of 10 μm can then be used as an initiation criterion, and the initiation time is predicted based on the anaerobic corrosion rate. However, unlike the model described above, fast fracture to failure is not assumed to occur once a crack has initiated. Instead, the rate of crack growth is predicted on the basis of the rate of thickening of the hydride layer (the length of the HIC crack is approximately 50% of the thickness of the hydride layer), which in turn is dependent on the anaerobic corrosion rate. Nakayama et al. [162] developed the Ti-H-iT model to predict the HIC behaviour of a Ti-0.01 wt% Pd transuranic waste container in cementitious backfill. After 60,000 yr (approximately 10 half-lives of C-14), the hydride-layer thickness was predicted to be only 1.3 μm, significantly less than the threshold of 10 μm for crack initiation. In an earlier analysis of a Ti Grade 17 (0.06 wt.% Pd) HLW overpack in compacted bentonite buffer, crack initiation (corresponding to a critical hydride-layer thickness of 20 μm) was predicted to occur after approximately 1000 yr, with a crack growth of <50 μm after 10,000 yr [12,13].

3.3.3. Current Status of the Process Modelling of the EAC of HLW/SF Containers

Process models for EAC have been developed on the basis of either non-initiation of cracking, initiation followed by rapid crack growth, or a limited propagation rate. Although there is widespread experience in the nuclear and other industries with the use of limited propagation models to manage SCC, such models are always coupled with periodic inspection. For the case of HLW/SF containers, it is difficult to believe that a limited crack-propagation argument would be acceptable given the inability to periodically inspect and, if necessary, repair the container.

A more suitable approach, therefore, may be to argue on the basis of either non-initiation or initiation followed by rapid crack growth. Models have been developed for both approaches, although it is always more difficult to guarantee immunity from EAC, especially for H-related processes that are feasible over the extended anaerobic phase of the repository evolution.

3.4. Microbiologically Influenced Corrosion

When assessing the impact of microbial activity on HLW/SF container corrosion, the overriding question is where will that activity occur [167]? For repository designs with either compacted bentonite or cementitious buffer, it is plausible to argue that microbial activity will not occur in the buffer and, most importantly, at the container surface. In these cases, MIC is only possible if aggressive metabolic byproducts, produced by microbial activity in regions of the repository where such activity is possible, reach the container surface. In contrast, for unbackfilled repository designs, or in backfilled repositories with buffer or backfill that does not suppress microbial activity, the possibility of microbial activity and biofilm formation on the container surface must be considered. The significance of biofilm formation is that, while we may have robust models for predicting the impact of remote microbial activity (see below), there are no such models for predicting the consequences of the spatial distribution of microbial and electrochemical activity within the biofilm [168].

Microbes may have detrimental or beneficial effects on container corrosion. Perhaps the detrimental effect that has received the most attention is the formation of sulphide by sulphate-reducing bacteria (SRB). Microbes may also produce other aggressive species, such as ammonia and acetate that are known to induce the SCC of copper [155]. On the other hand, the consumption of the initially trapped O_2 in many repository designs will result, in part, from the beneficial activity of aerobic microbes.

The various process models developed for MIC are listed in Table A4 and are categorised in Table 8, along with the advantages and disadvantages of each approach.

Table 8. Approaches to the prediction of microbiologically influenced corrosion of HLW/SF containers.

Approach	Examples	Advantages	Disadvantages
Empirical	Suppression of microbial activity in highly compacted buffer material [169,170] Empirical corrosion rate for carbon steel that includes microbial effects [152] or enhancement factor for uniform corrosion of Alloy 22 [9]	Absence of microbial activity in buffer material obviates the need to predict corrosion under a biofilm.	Mechanistic basis required to support argument of suppression of microbial activity. Difficult to justify specific corrosion rates or enhancement factors. Empirical corrosion rates often measured in presence of added nutrients and/or under non-repository conditions, so relevance is questionable.
Mass balance	Mass-balance calculations for nutrients, electron acceptors, and energy [5,171].	Establishes an upper limit to the extent of corrosion, assuming a closed system in which no additional electron acceptors or donors enter the system.	Prediction of maximum microbial population is not informative. No account taken for possible recycling of organic material.
Reactive transport	Copper Corrosion Model for MIC (CCM-MIC) [172–174]. Sulphide production, transport, and consumption models [175–178]	Mechanistically based and supported by analogues in nature. Allows optimization of repository design (for example, buffer density and mineralogical composition). Models available in 2D and 3D to assess multidimensional aspects.	Treatment of all possible microbial processes requires a large database of input values.
Transport	Sulphide transport model [89,179]	Extended to include effect of near-field re-saturation. Multidimensional models available to explore complex geometrical effects.	Based on an assumed source term (sulphide concentration). Absence of reactions in models, especially sinks for sulphide (Fe(II)/Fe(III)).

3.4.1. Empirical

Much of the evidence used to predict the absence of microbial activity is based on empirical evidence. For example, the evidence that microbial activity is suppressed by highly compacted bentonite or cementitious backfill is largely empirical ([169,170,180,181] for compacted bentonite and [182] cementitious backfill). While research in this area still continues [183,184], it would seem that the most important factors limiting microbial

activity in highly compacted bentonite are the high swelling pressure, low water activity, and the lack of physical space or a combination of all three.

Empirical evidence is also used to predict the effects of microbes for non-backfilled repository designs. For example, a microbial enhancement factor (sampled from a uniform distribution of between one and two) was used to account for the effect of microbes on the rate of uniform corrosion of Alloy 22 waste packages in the YMP [9,32]. The value of two was based on the doubling of the corrosion rate in short-term electrochemical tests in the presence of microbes and added nutrients compared with that measured in control experiments. Similarly, Andra [152] uses a conservative corrosion rate of 10 μm/yr for carbon steel to account for both abiotic and biotic corrosion processes, justified largely by the results from laboratory and full-scale in situ experiments.

Of the various candidate container materials in Table 2, the only one that may be immune to MIC is Ti. This immunity, which is based on empirical evidence, may result from the absence of multiple oxidation states in the stable TiO_2 passive film, which will tend to inhibit the redox processes associated with microbial activity [167].

Another example of the use of empirical evidence to support the prediction of the consequences of biofilm formation is the use of a "localization factor" to account for possible surface roughening [1]. The loss of buffer density due to chemical erosion of the bentonite could result in microbial activity in the deposition hole of a KBS-3 style repository at Olkiluoto. Under these circumstances, the possibility of biofilm formation on the copper canister cannot be excluded, and an empirically determined pitting or localization factor is used to account for the resulting MIC.

3.4.2. Mass-Balance Approaches

Mass- and energy-balance equations have been used to predict the maximum microbial population [171] and the maximum amount of sulphate reduction by SRB [5]. While knowledge of the maximum microbial population is interesting, we are really concerned about microbial activity. Larger microbial populations do not necessarily correlate with higher microbial activity [167]. Prediction of the maximum amount of sulphide produced by SRB based on the stoichiometry of the sulphate reduction reactions and the mass balance of electron donors and acceptors is more useful [5], although it does not account for the long-term supply of reactants from the far field. In fact, detailed reactive transport modelling of sulphide production, transport, and consumption (see below) reveals that the near field of a KBS-3 repository can be considered a relatively closed system for a period of the order of 10^5 yr [1,72]. Thus, mass-balance calculations of the relative amounts of electron acceptor (sulphate) and electron donors (organic matter) initially present in the repository are useful for identifying the limiting reactant and, hence, the maximum amount of sulphide that can be produced within the closed system.

Mass- and energy-balance calculations do not take into account the effects of mass transport of reactants and products, nor do they discriminate based on the location of the microbial activity.

3.4.3. Reactive Transport Models

These shortcomings of the mass-balance approach were overcome by developing reactive transport models for the effect of remote microbial activity, i.e., microbial activity that occurs away from the container surface. These models generally treat microbial reactions in an analogous fashion to that of chemical reactions in the reactive transport models for uniform corrosion discussed in Section 3.1.2 but use Monod kinetics to describe the rate of microbial reactions. The first such model developed for HLW/SF containers was the microbial activity model (MAM) of King et al. [174]. In terms of microbiology, the model was limited to the remote microbial reduction of sulphate by SRB but included the following features:

- 1D representation of the buffer, backfill, and host rock, with all materials treated as equivalent porous media;

- diffusive mass transport of reactants and products but not of microbes, which were deemed to be immobile in the compacted bentonite buffer;
- organotrophic and lithotrophic reduction of sulphate using organic carbon (represented by acetate) and H_2, respectively, as electron donors;
- Monod kinetics to describe the rate of microbial reactions;
- death, or alternatively the dormancy, of microbes due to desiccation (low water activity) or irradiation, with recycling of a fraction of the dead cell material;
- corrosion of the copper container based on the assumption of a sulphide-transport limited corrosion process;
- precipitation of mackinawite FeS as a sink for sulphide;
- spatial and temporal variation of temperature.

At the time of this model, it was considered that γ-irradiation of the near field would deplete the microbial population and, along with desiccation of the buffer due to the heat output of the container, limit microbial activity to locations remote from the container surface. The vast majority (>99%) of the sulphide produced by the SRB was predicted to precipitate as mackinawite, with only 1.4 μm of corrosion after 10^6 yr [174].

The use of Monod kinetics to represent microbial activity in the repository was extended to include a number of other microbial processes, including [172,173,185]:

- aerobic respiration;
- organotrophic and lithotrophic denitrification;
- nitrogen fixation;
- nitrosofication;
- nitrification;
- ammonia oxidation;
- fermentation;
- organotrophic and lithotrophic Fe(III) reduction;
- organotrophic and lithotrophic sulphate reduction.

Monod kinetic expressions for the 15 different microbial processes were incorporated into the reaction scheme for the CCM, with the resulting model being denoted the CCM-MIC. The microbial reactions were selected for their relevance to the corrosion of copper containers, including (i) the consumption of initially trapped O_2 by aerobic respiration, (ii) the denitrification of nitrate produced by γ-irradiation to form N_2 and the subsequent fixation of that nitrogen to form ammonia, (iii) the nitrosofication of ammonia to form nitrite and the oxidation (nitrification) of nitrite back to nitrate, (iv) the oxidation of ammonia, (v) fermentation of complex organic matter to produce acetate suitable for SRB, (vi) the reduction of Fe(III) to Fe(II) to act as a possible sink for sulphide via mackinawite precipitation, and (vi) the reduction of sulphate to sulphide via organotrophic and lithotrophic routes. The N-cycle was included in the reaction scheme as nitrite and ammonia are SCC agents for copper. The reaction sequence listed above is arranged in order of redox potential, and, in addition to the other limiting factors, each of the 15 microbial reactions only occurred over a range of redox potentials. Other factors, such as the necessary energy balance and biomass production associated with microbial activity, were also simulated in the model. The end result was a very comprehensive model, but it had the disadvantage that it required a large amount of input data, much of which was not available. Therefore, only a limited number of sensitivity analyses were ever performed with the model [172,173,185].

More recently, there have been a number of sulphide production, transport, and consumption reactive transport models developed and used to predict the extent of corrosion of copper due to remote SRB activity [79,80,175–178,186–191]. All of these models share the same Monod kinetic treatment of organotrophic and lithotrophic sulphate reduction, with the dissolution of gypsum and the groundwater acting as sources of sulphate, and with reactions with Fe(II) and/or Fe(III) species acting as potential sinks for the sulphide (Figure 14). Microbial activity is generally assumed to be suppressed in the compacted buffer material surrounding the container, with sulphate reduction occurring instead in the EDZ surrounding the tunnel and/or deposition hole, as well as in the backfill and host

rock. Since the buffer material is a major source of sulphate (from gypsum dissolution) and organic matter, these species must first diffuse away from the container to the EDZ (and backfill and host rock) where they react, with the resulting sulphide then diffusing back to the container surface, where it is consumed either by reaction with Fe(III) and/or precipitation as mackinawite or in the corrosion reaction itself.
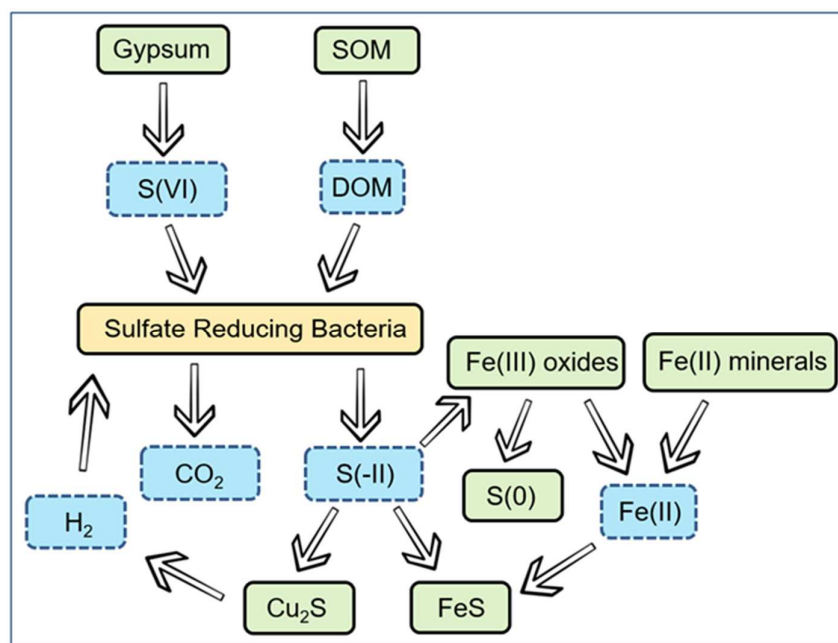

Figure 14. Illustration of the basic microbial reaction scheme for the University of Bern sulphide model (UBSM) used in Posiva's safety case for the construction licence application [192]. SOM and DOM refer to solid and dissolved organic matter, respectively. Reprinted with permission of Posiva Oy.

Although the models listed above share a common reaction scheme, there are distinct differences between the different codes. For example, the model of Idiart et al. [175], the CSM [79,80,190,191], and the INER sulphide model (ISM) [178] are all limited to 1D, whereas the model developed at the University of Bern [176,177,186–189] has been implemented in 1-, 2-, and 3D, with the 2D and 3D models useful for highlighting the effects of the spatial relationship between the location at which microbial activity occurs and the container and buffer material where the resulting sulphide is consumed. Another major difference is the treatment of the interfacial boundary condition for sulphide on the container surface. For all models except the CSM, the rate of consumption of sulphide at the container surface is assumed to be under transport control, simulated either by using a high value for the rate constant or by assigning a zero-concentration boundary condition for sulphide. The CSM, on the other hand, uses electrochemical expressions for the interfacial boundary conditions in the form of a mixed-potential model (Figure 6). In this regard, only the CSM and ISM treat the reactions at the container surface as truly interfacial processes, while the other models simulate the interface as an element or volume with the heterogeneous process simulated using a homogenous rate constant. This "homogenization" of the interface is common with the use of geochemical codes that are not capable of handling true interfacial processes. One advantage of these geochemical codes, however, is that they incorporate thermodynamic speciation models so that the treatment of the homogeneous processes in the University of Bern and Idiart et al. [175] models is more rigorous than that in the CSM and ISM, which are both based on a simplified treatment of the pore-water chemistry.

Despite all of these differences, the various models produce similar results, as revealed by the extensive inter-model comparisons that have been performed [21,178,192]. In all cases, the models predict that the most important source of sulphate initially (for the first

10^5 yr or so) is the gypsum impurity in the bentonite clay, with the sulphate supplied by the ground only becoming significant at longer times. Whether the availability of electron acceptor (sulphate) or donor (organic matter, hydrogen) is limiting depends on the amounts of these species in the buffer material and on the assumption made about the fraction of the organic matter that is bioavailable. However, of the sulphide produced, all models predict that the vast majority (90–99%) is sequestered by reaction with Fe(III) minerals and/or by precipitation as mackinawite. As a result, the extent of corrosion is limited and is predicted to be in the range of 0.1–0.3 mm after 10^6 yr [178], with maximum corrosion rates of the order of 1–10 nm/yr. Equally as importantly, the maximum flux of sulphide to the container surface is less than the threshold fluxes for transport control of the rate of uniform corrosion [82] and of the empirically observed threshold for the formation of crack-like defects on copper in sulphide environments [1,164].

Although the modelling of the production, transport, and consumption of sulphide from remote SRB activity is well developed, some uncertainties still remain. For example, attempts have been made to simulate the formation, transport, and consumption of gaseous H_2S during the early unsaturated period [79,193]. Gaseous H_2S reacts rapidly on copper surfaces, even at RH values below that at which a continuous adsorbed H_2O layer would be expected to exist on the surface. However, there is uncertainty about the location of the source of $H_2S(g)$, since the extent of microbial activity will be limited in an unsaturated system, but vapour-filled pores are necessary for the partitioning and transport of $H_2S(g)$. There is also uncertainty about the treatment of iron sulphide precipitation and whether the resulting solid (generally assumed to be mackinawite) serves as a permanent sink for a fraction of the total sulphide produced [178]. Mackinawite has a lower solubility product than Cu_2S. So, in a sulphide-limited system, any FeS that precipitates in the buffer would be predicted to redissolve and diffuse to the container, where it would then produce Cu_2S. The CSM and ISM treat mackinawite precipitation as irreversible, but some redissolution of the FeS is predicted in some cases using the geochemical models of Idiart et al. [175] and the University of Bern. Another possibility is that the initially precipitated FeS will transform to the more stable and less soluble iron sulphide phases greigite (Fe_3S_4) and/or pyrite (FeS_2), for which there is some evidence from archaeological analogues [52,178].

Notwithstanding these uncertainties, the reactive transport modelling of the remote production of sulphide by SRB, and the consequences for container corrosion, has developed into a mature subject over the past 5 years. The robustness of the model's predictions is demonstrated by the agreement between different models from the different benchmarking exercises. Because of their deterministic basis, these models provide additional insight into not only MIC but also the uniform corrosion and SCC behaviour of the container that is not provided by the other microbial models described here.

3.4.4. Mass Transport

In addition to the reactive transport models for microbially produced sulphide described above, there is a series of models that can best be described as mass-transport models for sulphide-induced corrosion [89,179,194–196]. Unlike the reactive transport models, these transport models do not take into account the kinetics of the microbial reduction of sulphate or any reaction involving the resulting sulphide other than corrosion of the container; the latter is calculated from the rate of supply of sulphide to the surface.

These models have been developed in the Canadian program in which the reference repository design is based on the in-room emplacement of an upper and lower row of containers with associated compacted bentonite. Given the additional feature of a container with a hemispherical head, this repository design represents a complex geometrical arrangement of the sources (the EDZ and host rock surrounding the disposal room) and sinks (the two rows of containers) of sulphide. For this reason, 1-, 2-, and 3D transport models have been developed to determine the resulting distribution of corrosion over the surfaces of the containers. In addition, the effects of spatial and temporal variation in temperature [89,179,196] and of the degree of saturation [89] have been considered,

although, in the latter case, not the effect of gaseous H_2S. In place of kinetic expressions to calculate the rate of sulphide production, a constant sulphide concentration boundary condition is used, with a concentration typical of that observed in deep ground waters. Since there are no reactions considered, the sulphide flux at the container surface scales with the source concentration so that the predicted corrosion rate can be normalised with respect to the source concentration.

Figure 15 shows the variation of the steady-state corrosion rate over the surfaces of an array of thirteen containers, highlighting the importance of geometrical considerations. The constant sulphide concentration boundary condition was applied on all faces of a box around the array of containers representing the walls, ceiling, and floor of the disposal room (not shown). The steady-state corrosion rate varies by a factor of 7–8 over the surface of the containers, with the highest rates at the end of the hemispherical head and the lowest rate on the "inner" surfaces of the containers that are shielded from the sulphide source by the rest of the container. The addition of reactions to these models, particularly the sequestration of sulphide by reaction with Fe(II) and Fe(III) in the bentonite, may exacerbate these spatial variations, as the already shielded inner surfaces may be further protected by the precipitation of iron sulphide.
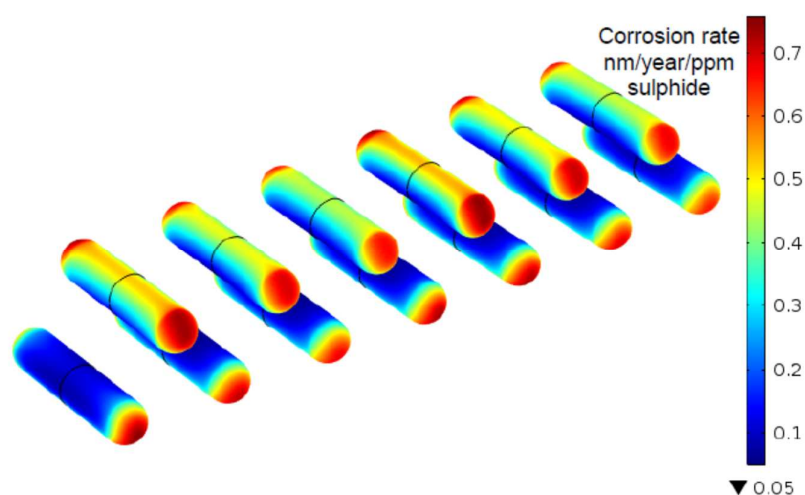

Figure 15. Distribution of predicted steady-state corrosion rates over the surfaces of an array of thirteen containers for the reference Canadian DGR design [179]. The corrosion rate is normalised with respect to the constant sulphide concentration used as the source term. Reproduced with permission of the Nuclear Waste Management Organization©.

3.4.5. Current Status of the Process Modelling of the MIC of HLW/SF Containers

The current state of the art for modelling MIC depends on whether we are considering biofilm formation or only microbial activity remote from the container. For un-backfilled repository designs or for other circumstances where a biofilm could be present on the container surface, there is still a reliance on empirical corrosion rates. While biofilm corrosion models do exist, they do not appear to be sufficiently reliable to be used for the prediction of the long-term MIC of HLW/SF containers.

In contrast, there are robust reactive transport models for predicting the effects of remote microbial activity. These models are quite mature for the prediction of the effects of SRB, and the framework is in place to extend these models to other microbial species. Only the input data are lacking.

3.5. Radiation-Induced Corrosion

Even though the absorbed dose rates at the surface of HLW/SF containers are modest by the standards of in-reactor exposures, there have been a number of models developed to predict the effect of long-term γ-irradiation (Table A5). This interest stems in part from

uncertainty over the effects of long-term exposure to low levels of radiation and whether such effects should be predicted based on the dose rate or the total absorbed dose. While maximum dose rates are on the order of a few Gy/h or less, absorbed doses can exceed a few hundred kGy after 1000 yr and, because of the in-growth of γ-emitters due to the decay of spent fuel, a few MGy after 10^6 yr [197].

Irradiation could have a number of effects on the corrosion behaviour of HLW/SF container materials [198]:

- neutron- and/or γ-irradiation could embrittle the material, rendering the container more susceptible to fracture, especially cast iron and carbon steel;
- the production of radiolytic oxidants could increase the rate of uniform corrosion;
- ennoblement of E_{CORR} by radiolytic oxidants could increase the probability of the initiation of localised corrosion of passive materials;
- radiolysis could produce species that induce localised corrosion or EAC, such as ammonia or nitrite which are SCC agents for copper;
- the absorption of hydrogen could lead to embrittlement of various container materials.

The neutron- and γ-dose rates are too low to induce embrittlement or other forms of radiation damage to the container material [164]. All of the other effects are caused by the radiolysis of the external environment (either buffer pore water or humid gas phase), and this is where the modelling activities have been focussed. The different approaches to the prediction of the radiation-induced corrosion (RIC) of HLW/SF containers are summarised in Table 9, along with their advantages and disadvantages.

3.5.1. Empirical

Although one might think that it would be possible to make long-term predictions based on an empirical relationship between the corrosion rate and dose rate, there have been few such models published. Westerman et al. [199] developed a semi-empirical model based on fitting experimental corrosion rates to a conceptual model for the competing production and consumption reactions for radiolytic species. In addition, Marsh and Taylor [5] describe the estimation of an effective G-value for the yield of radiolytic oxidants based on the degree of enhancement of the rate of uniform corrosion of carbon steel (By convention, the notation g-value is used here to refer to the yield of primary radiolysis products and the term G-value is used to refer to the net yield of a species based on both primary interactions and secondary reactions.).

However, the major use of empirical data has been in the development of reasoned arguments for the exclusion of γ-radiation effects. These arguments tend to be based on an early review of the effects of irradiation on container materials [200], in which it was suggested that the effects of radiation for various materials were insignificant for dose rates in the range of 1–10 Gy/h and, for some materials in some environments, up to 100 Gy/h. Based on this review, a number of waste-management organizations (WMO) have argued that, since their maximum dose rate is below these levels, the effects of γ-radiation do not need to be considered [11,30,31,201]. The danger of this approach, of course, is that what might be considered to be an insignificant effect over laboratory timescales could be significant over the long timescales of interest in the postclosure period, especially if the total dose is important in determining the extent of corrosion.

3.5.2. Uncoupled Radiolysis Models

The deterministic approaches to the prediction of RIC are based on some form of radiolysis modelling to predict the yield of oxidising (and reducing) radiolysis products. Here we distinguish two types of radiolysis-based models, namely uncoupled models in which the rate of consumption of the radiolysis species due to the corrosion reaction does not affect the radiolytic yields and coupled models in which the interfacial processes are incorporated into the bulk radiolysis reaction scheme.

Uncoupled models involve a two-step process. First, the yield of radiolysis products is predicted using a bulk radiolysis model, with a focus usually on the production of oxidising

species, such as H_2O_2, O_2, and $OH^\bullet$ radicals. Second, the steady-state concentration of one or more oxidising species is used to calculate the resulting corrosion rate. The justification for this approach is generally that the kinetics of the homogeneous radiolysis reactions are so much faster than those of the interfacial corrosion reactions that the two processes can be de-coupled.

Table 9. Approaches to the prediction of the radiation-induced corrosion of HLW/SF containers.

Approach	Examples	Advantages	Disadvantages
Empirical	Effective G-value for radiolytic oxidants for carbon steel [5]. Dose rate limit for significant effect of irradiation [11,30,31,201]	Concept of a "threshold" dose rate is useful for engineering purposes	The definition of "significant" depends on the container material, as well as on the experimental methodology and duration.
Bulk radiolysis (uncoupled)	Humid air radiolysis model (HARM) for copper [197]. RIC mixed-potential model for copper [202]	Mechanistically based. Computationally simpler to uncouple radiolysis reactions from interfacial processes.	Assumes steady-state concentrations of radiolysis products are not affected by interfacial reactions.
Bulk radiolysis (coupled)	Thin-layer mixed-potential model (TLMPM) [203] Coupled corrosion-bulk radiolysis model for copper [204,205] Copper corrosion model for radiation-induced corrosion (CCM-RIC) [206]	Yield of radiolysis products takes into account their interfacial consumption. Mechanistically rigorous approach.	Some software requires that the interfacial reaction be "homogenized", i.e., that the heterogenous process be converted to a homogeneous reaction. Interfacial rate constants may be difficult to obtain, especially for radical species.

Uncoupled radiolysis-based corrosion models were first developed by the Swedish Corrosion Institute [4]. Instead of directly calculating the concentration of oxidants, it was argued that, because the radiolytic decomposition of H_2O quickly establishes a steady state, the net rate of production of oxidants would be equal to the rate of loss of reductants from the system. The latter was estimated based on the diffusive flux of radiolytic H_2 away from the canister surface.

The uncoupled model of Marsh et al. [97] was based on the empirically determined effective G-value for radiolytic oxidants described above. This effective G-value of 2.13 molecules/100 eV (based on the assumption of a two-electron reduction process) was used to account for the yield of both primary radiolytic oxidants H_2O_2 and $OH^\bullet$ and secondary species O_2, O_2^-, and $HO_2^\bullet$. This effective G-value compares with typical g-values for primary radiolytic oxidants of 0.7 molecules/100 eV for H_2O_2 and 2.7 molecules/100 eV for $OH^\bullet$ [207]. Assuming a one-electron reduction process for $OH^\bullet$ ($OH^\bullet + e^- \rightarrow OH^-$), the sum of the g-values corrected for a two-electron reduction reaction would be 2.05 molecules/100 eV (i.e., $0.7 + \frac{1}{2} \times 2.7$). If 100% of the primary species cause corrosion, then the difference between this weighted g-value and the empirical effective G-value of 2.13 molecules/100 eV suggests that the secondary oxidants do not contribute very much to the overall extent of corrosion.

Other uncoupled RIC models have been developed by Morco et al. [197], Henshaw and Spahiu [208], and King and Behazin [202]. Morco et al. [197] used a simplified version of the 730-reaction set for the humid air radiolysis model (HARM) [209] to arrive at a bounding estimate of the yield of HNO_3 produced by the radiolysis of humid air representative of the unsaturated repository environment during the initial saturation transient. The amount of HNO_3 produced in a given volume of vapour was then presumed to dissolve in a surface water droplet of assumed volume, from which the depth of corrosion could be estimated based on a mass-balance calculation. King and Behazin [202] also used a simplified radiolysis model to predict the time-dependent concentration of H_2O_2 at the

container surface as the dose rate decreased with time. This steady state [H_2O_2] was then coupled to a simple mixed-potential model to predict the time-dependent value of E_{CORR} and the corrosion rate. Wu et al. [210] also used the HARM to predict the amount of HNO_3 that could be produced inside a sealed container due to the radiolytic decomposition of air and moisture that remained following incomplete drying and evacuation of the internal atmosphere prior to sealing. The case of internal residual H_2O was also considered by Henshaw and Spahiu [208], in this case with a 266-reaction humid air radiolysis model.

3.5.3. Coupled Radiolysis Models

The problem with uncoupled radiolysis models is that it is not apparent that interfacial processes are slow in comparison to the bulk homogeneous reactions. In some cases, it takes several hours for the concentration of different radiolytic species to reach a steady state [207], a timeframe that is certainly not fast in comparison to the kinetics of interfacial electron transfer processes. For this reason, it is important to take into account the effect of the interfacial processes on the yield of radiolytic species. We refer to such models as coupled radiolysis models and they can be distinguished based on the treatment of the interfacial processes.

Soroka et al. [204] and Jonsson [205] have developed a coupled radiolysis model using the MAKSIMA-CHEMIST software package extensively used for bulk radiolysis modelling [211]. One limitation of this software is that all reactions must be treated as homogeneous reactions. As a consequence, the interfacial reaction(s) must be "homogenized" by multiplying the interfacial rate constant (in units of, say, mol/($m^2 \cdot$s)) by a suitable surface area–volume ratio (in units of m^{-1}) to derive a corresponding homogeneous rate constant (in units of mol/($m^3 \cdot$s)).

Jonsson and co-workers considered two interfacial processes, namely the decomposition of H_2O_2 to produce O_2 and the corrosion of copper by O_2. Originally, H_2O_2 had been considered to be the species leading to corrosion, but Soroka et al. [204] were unable to account for the experimentally observed corrosion on the basis of radiolysis modelling with H_2O_2 as the oxidant. Better agreement between the experiment and model was obtained if the interfacial decomposition reaction was included and O_2 was assumed to be the oxidant. However, from a purely mass-balance point of view, the two H_2O_2 molecules that decompose into H_2O and O_2 will corrode the same amount of copper as the one molecule of O_2 that they produce.

$$2H_2O_2 \rightarrow H_2O + O_2 \tag{10}$$

Therefore, the better agreement is not just a result of the difference in the oxidising species but must also be because of an increased radiolytic yield of H_2O_2, possibly because of the inclusion of the interfacial H_2O_2 decomposition in the reaction scheme. If so, this would confirm the hypothesis that the interfacial reactions can impact the radiolytic yield.

Further evidence for the effect of the interfacial reactions on the bulk homogenous processes comes from the early modelling work of Macdonald and Urquidi-Macdonald [203]. The problem of having to "homogenize" the interfacial process is solved by treating the interfacial reaction(s) explicitly, as done for many of the electrochemically based reactive transport models for uniform and localised corrosion described in earlier sections. Macdonald and Urquidi-Macdonald [203] coupled the interfacial reduction and oxidation of nine molecular and radical radiolysis products to the radiolytic production and transport of these species in a thin water film assumed to be present on the container surface. One downside of this approach is that it requires the interfacial rate constants (or exchange-current densities) and Tafel slopes for each of the electrochemical reactions, many of which are unknown, especially for the radical species. Therefore, sensitivity analyses were performed using different assumed values for the Tafel slopes, with the result that the predicted concentrations of radiolysis products (averaged over the H_2O film thickness) varied by orders of magnitude for a reasonable variation of the values of the transfer coefficients defining the Tafel slopes. These results confirm that the interfacial processes do impact the

bulk radiolytic yields, but also highlight the importance of understanding the kinetics of the oxidation and reduction of molecular and radical species on the surface.

The use of electrochemical interfacial expressions to couple the corrosion and bulk radiolysis processes is also the basis of a conceptual RIC model described by Behazin et al. [206]. This model is an extension of the CCM suite of reactive transport models for uniform corrosion, MIC, and SCC, with this particular variant referred to as the CCM-RIC. Figure 16 shows the reaction scheme for the conceptual model, with the interfacial oxidation and reduction of various radiolytic species combined with the anodic dissolution of copper and the reduction of Cu^{2+} to form a mixed-potential model. These interfacial reactions are used as mathematical boundary conditions to solve the set of PDEs (Equation (3)) that describe the radiolysis reactions occurring in the bulk and interlayer water of the compacted buffer material in contact with the container. In doing so, it is recognised that the system being modelled is characterised by a high surface area–volume ratio of solids to H_2O and is quite unlike the bulk solution systems for which the radiolysis models were developed. Many of these solids are oxides, either metal (copper) oxide on the container surface or aluminosilicate clay particles, the presence of which can alter the radiolytic yield of various species [206]. Fe(II) and Fe(III) species in octahedral sites in the clay lattice may also undergo redox processes with radiolytic species, as can pyrite present as an impurity in many commercial bentonites. The model is still under development and care is being taken to validate the model at every stage, particularly because it is being implemented using a general finite-element software package instead of the traditional custom-designed software generally thought necessary for handling the stiff computational aspects of radiolysis models.
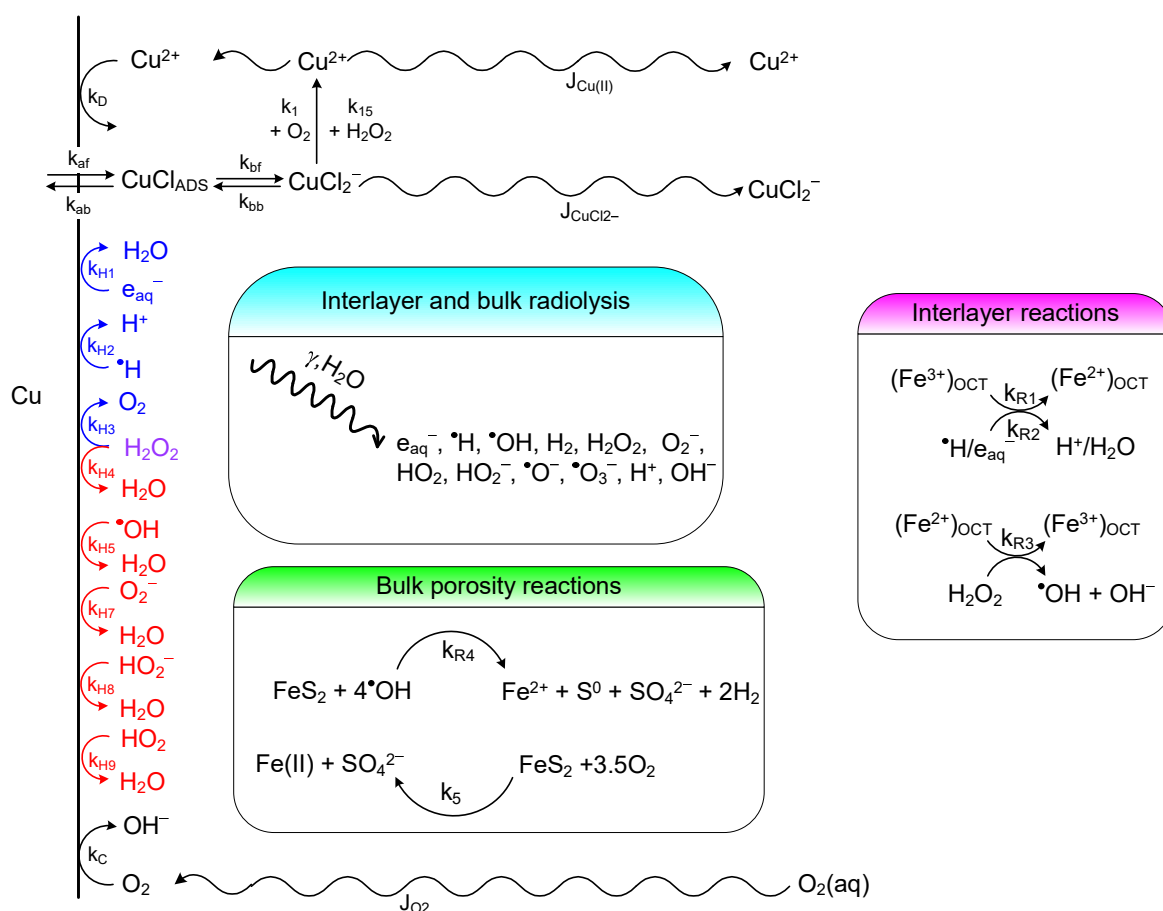

Figure 16. Conceptual model for the copper corrosion model for radiation-induced corrosion (CCM-RIC) [206]. Reproduced with permission Wiley©.

3.5.4. Current Status of the Process Modelling of the RIC of HLW/SF Containers

The importance of coupling interfacial processes to the bulk homogenous reactions is now recognised and some of the models include this coupling, either through the use of electrochemical boundary conditions or by "homogenizing" the interfacial reaction into a corresponding homogeneous process. Where validation has been done, this approach appears to predict corrosion rates consistent with experimental observations.

However, no model yet accounts for the lower corrosion rates of copper and ferrous alloys often observed in the presence of radiation at low dose rates [198]. Although the mechanism for this apparently beneficial effect of radiation is still unknown, visual evidence suggests that it is associated with the properties of corrosion-product films. As noted in the discussion of reactive transport models for uniform corrosion, it is difficult to predict the properties of such films a priori, so the prospects for improved RIC models to account for this phenomenon are not good.

3.6. Joint Mechanical–Corrosion Degradation Models

Historically, container lifetimes have been predicted based on time-dependent corrosion behaviour only. In many waste-management programs, the tendency was for designers to design the container to withstand the expected (and, in some cases, extreme) external loads and to determine the minimum wall thickness required to provide structural stability, with the remainder of the wall thickness available as a corrosion allowance. This approach, based on separate "mechanical" and "corrosion" allowances, is reasonable if there is no significant interaction between the mechanical and chemical (corrosion) loads and if there is no time-dependent degradation of the material properties. Another consequence of this historical separation of corrosion scientists and structural engineers was that lifetime predictions were based on the assumption of a pristine container, with little analysis in the early waste-management programs of the possible effects of defects.

More generally, however, we are interested in predicting the container failure time regardless of whether that failure results from purely mechanical, purely corrosion, or from some combination of mechanical and corrosion factors. It is most likely that the container will fail due to structural instability following a period of material degradation and/or the loss of the load-bearing wall thickness as a result of corrosion. For a robust container lifetime prediction, therefore, it is important that we consider the possibility of joint mechanical–corrosion degradation modes.

The probability of significant joint mechanical–corrosion interactions depends on the container design and materials of construction. Dual-wall container designs in which an outer corrosion barrier is supported by an inner structural component tend to be less prone to such interactions than single-wall designs in which the single shell provides both the corrosion-resistance and load-bearing functions. This is especially the case if that single shell is fabricated from a material that is prone to time-dependent degradation due to exposure to the corrosive environment or γ- and neutron-radiation fields.

Table A6 summarises a number of models that have been developed to investigate joint mechanical–corrosion interactions for HLW/SF containers.

3.6.1. Environmentally Assisted Cracking

Environmentally assisted cracking is generally the result of the conjoint action of both an applied (or residual) stress and a corrosive environment, although some forms of hydrogen-related degradation can create their own stress. In this sense, the EAC models described in Section 3.3 are examples of joint mechanical–corrosion models, although some were based only on environmental arguments. The models which do have a specific mechanical component include the slip dissolution SCC model for Alloy 22, where both crack initiation and crack growth are dependent on the level of tensile stress [158], and the decision-tree analysis for the SCC of copper, where the requirement for a sufficient tensile stress is one of the prerequisite conditions in the decision tree [1].

3.6.2. Effect of the Formation of Expansive Corrosion Products

The consequences of the volume change that accompanies corrosion in constrained systems have been of concern in a number of waste-management programs. Unlike the case of EAC where the presence of the mechanical load induces an effect on the corrosion behaviour, in this case, the formation of corrosion products can lead to the development of stresses in the system.

An issue that was investigated experimentally and with the use of analytical models during the development of the copper–cast iron KBS-3 canister was whether expansive corrosion products could "unzip" the copper shell [212,213]. It was suggested that a small through-wall penetration of the copper shell could be transformed into a more extensive opening with resulting consequences for the ingress of groundwater and the release of radionuclides. Although it was concluded from the modelling work that the stresses resulting from the formation of magnetite (Pilling-Bedworth ratio 2.1) could cause plastic deformation of the copper shell, no such deformation was observed experimentally [214]. This discrepancy between experiment and model highlights the importance of developing conceptual and mathematical models on the basis of a sound mechanistic understanding of the processes involved.

An assessment was carried out in the Japanese program of whether the formation of expansive carbon steel corrosion products would exert an additional stress on the container [10]. The volume expansion due to the formation of magnetite by corrosion of the steel container was offset to some degree by the consolidation of the surrounding buffer and the creep of the host rock. An additional stress on the container of up to 1.9 MPa was predicted.

The effect of expansive corrosion products is also of concern for the Belgian Super-container concept since the carbon steel overpack and concrete buffer are encased in an outer stainless-steel envelope. Engelhardt et al. [215] considered the changes in porosity of the corrosion-product layer and concrete buffer in response to the strain produced by the change in volume associated with the conversion of Fe to Fe_3O_4. It was predicted that the porosity change in the corrosion-product layer was larger than that in the concrete because of the respective mechanical properties and because the thickness of the concrete layer was greater. The reduction in the porosity of the corrosion-product layer is sufficient in that corrosion is predicted to eventually cease as the porosity of the outer portion of the bilayer oxide film drops to zero.

3.6.3. Fracture Mechanics

The development of joint mechanical–corrosion models for HLW/SF containers also introduced the concept of fracture mechanics to lifetime prediction and a consideration of the effect of flaws and defects. All fabricated components contain flaws; the important question is whether those flaws are serious enough to be considered defects that might impact the integrity of the container.

Asano and co-workers developed a procedure for assessing the integrity of the closure weld in a carbon steel container based on fitness-for-service principles for nuclear power plants [19]. Figure 17 illustrates the underlying conceptual model. Failure is assumed to occur when a flaw grows to a critical length or at such a time that the wall thickness has been reduced sufficiently by uniform corrosion to lead to plastic collapse. The critical crack length is defined by an engineering critical assessment and may involve detailed finite-element structural analysis or simpler fracture-mechanics calculations. The maximum tolerable flaw size is the critical flaw size divided by a suitable safety factor. Asano et al. [19] used a safety factor of 10 based on general practice in the Japanese nuclear industry. Smaller safety factors might be appropriate [216], although it can be argued that a value of 10 is appropriate since the HLW/SF container cannot be inspected after disposal. In the illustration in Figure 17, the flaw is assumed to grow to the critical size before the wall thickness has been reduced sufficiently by uniform corrosion to lead to plastic collapse.

Growth of the flaw could be the result of SCC (if the flaw is surface-breaking) or by HIC (for surface-breaking, embedded, or internal flaws).
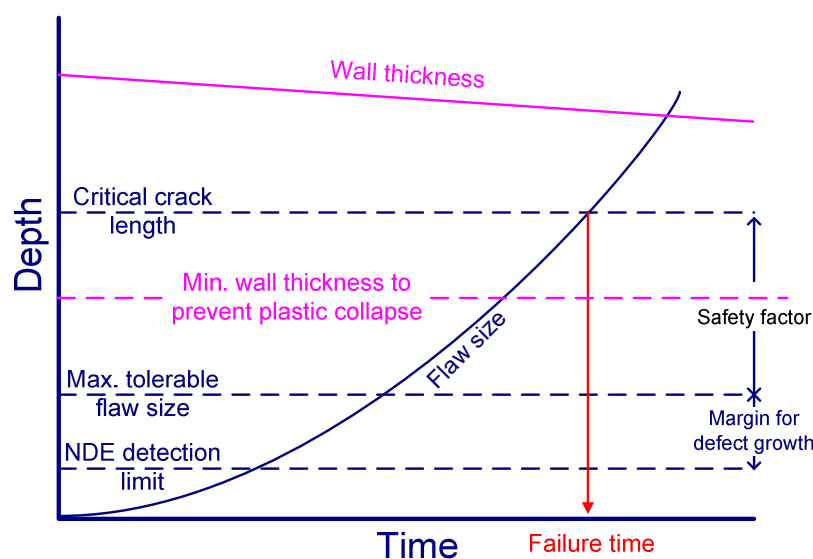

Figure 17. Conceptual model for the joint mechanical–corrosion assessment of defects in the closure weld of a carbon steel HLW container (modified based on [19]). In this example, the flaw grows to the critical size, leading to container failure (indicated by the red arrow) before the wall thickness has been reduced sufficiently to lead to plastic collapse.

Patel et al. [216] proposed the use of failure-assessment diagrams (FADs) to assess the time-dependent integrity of HLW/SF containers. Originally developed as part of the R6 assessment of the integrity of structures containing defects for nuclear power plants in the UK and subsequently incorporated in standards such as BS7910 [217], FADs provide a visual representation of the proximity of the structure to failure by either fracture or plastic collapse. Figure 18 shows a representative FAD for a carbon steel SF container with a 30 mm surface-breaking flaw in the closure weld. The horizontal axis L_r is the ratio of the applied load divided by the limit load and represents the proximity to plastic collapse. The vertical axis K_r is the ratio of the stress-intensity factor divided by the fracture toughness and represents the proximity to fracture. The "envelope" represents the boundary between "safe" and "unsafe" conditions, with the structure considered to be stable if the assessment point for the flaw falls below the curve, and failure is possible if the assessment point lies above the curve. Methods for locating the safety envelope are defined in the various standards and depend on the fracture toughness and the proof stress (the average of the yield and ultimate tensile strengths) of the container material. The figure also shows the location of the assessment point for the surface-breaking defect subject to a residual stress equivalent to the yield strength of 220 MPa. The assessment point is well within the safe region of the FAD for the assumed fracture toughness of the as-received material of 220 MPa$\sqrt{m}$ but moves closer to the safety envelope as the fracture toughness decreases, for instance, due to the absorption of hydrogen.

King et al. [20] developed this approach further and determined the evolution of the structural integrity of a carbon steel container with defects when subjected to a hypothetical evolution of external loading conditions. For each defect considered, a "trajectory" of assessment points was established in response to the time-dependent changes in container-wall thickness (due to external corrosion), the loss of fracture toughness of the container material (due to the absorption of hydrogen), and changes to the size and location of the flaw (again due to external corrosion). Figure 19 shows the trajectories for three assumed weld flaws, namely a surface-breaking external flaw, an embedded flaw located three-fourths through the wall thickness, and an internal flaw. Assessments were done for each defect for various intervals along the evolutionary path representing loading events at specific

junctures, including asymmetric buffer swelling and the development of the hydrostatic pressure, and culminating with an elevated hydrostatic load due to the formation of an ice sheet at an assumed time of 55,000 yr postclosure.
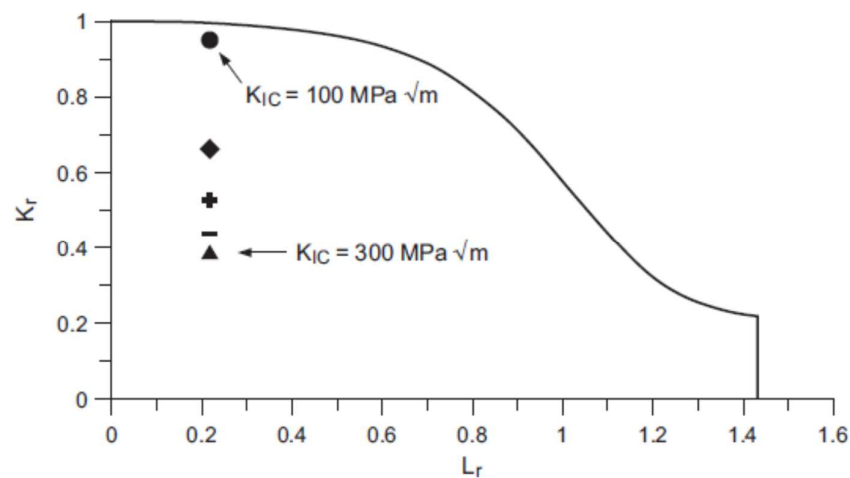

Figure 18. Failure-assessment diagram (FAD) for a carbon steel SF container subjected to asymmetric in situ stresses of 29 and 22 MPa, a membrane axial stress of 46 MPa, a residual stress of 220 MPa, a flaw size of 30 mm, and various fracture toughness values between 100 and 300 MPa$\sqrt{}$m [216]. Reproduced with permission of Nagra ©.
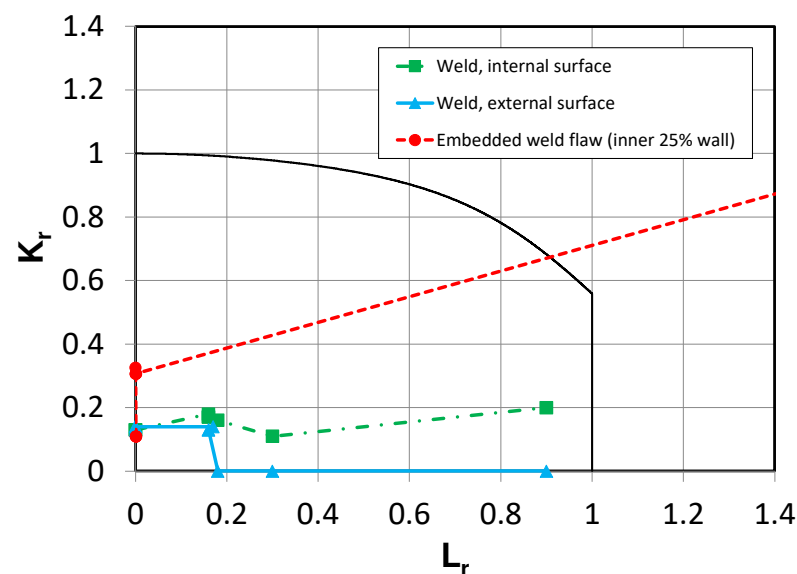

Figure 19. Examples of the assessment-point trajectories for three different assumed defects in a carbon steel container subject to a hypothetical series of external loads (modified based on [20]). Starting from the origin, the trajectories of assessment points (identified by the symbols) have been determined at various time intervals up to a maximum of 55,000 yr corresponding to the assumed time of the next ice sheet.

As can be seen from the figure, the trajectories for the different flaws depend on their location. The initial conditions for all three flaws are benign with the assessment points lying close to the origin and well within the safety envelope. Although still relatively benign, the external flaw is the most deleterious initially, with the assessment point (shown by the solid blue triangles) lying on the vertical K_r axis, indicating that fracture would be the most likely failure mode. As the container-wall thickness is reduced by external corrosion, the possibility of plastic collapse increases (although still unlikely), as indicated by the horizontal trajectory of the assessment point. However, at some point, the external

flaw is removed by corrosion and the assessment point moves to the horizontal L_r axis and remains there until such time (beyond 55,000 yr) that the wall thickness has been reduced sufficiently that plastic collapse occurs. The size of the internal weld flaw (indicated by the green square assessment points) does not change with time, and the assessment point moves vertically (due to increased possibility of fracture due to hydrogen absorption) as well as horizontally (due to decreased load-bearing capacity as the wall thickness is reduced by external corrosion). After 55,000 yr, the assessment point indicates that plastic collapse is the most likely cause of container failure. Interestingly, it is the initially embedded defect that leads to failure because, after a period of external corrosion, the original buried flaw becomes surface breaking at the same time that the load-bearing capacity has been reduced due to external corrosion. Failure is predicted to occur at some time prior to 55,000 yr due to a combination of plastic collapse and fracture, based on the point at which the trajectory crosses the safety envelope.

Nagra [26] has further extended this approach in the probabilistic canister breaching model (PCBM). The PCBM is a performance-assessment model rather than a process model and is described further in Part 2 of this review [25]. However, the PCBM is based on the application of the FAD approach to the assessment of canister breaching due to fracture or plastic collapse associated with flaws or global plastic collapse due to wall thinning. The model accounts for both external anaerobic corrosion of the carbon steel canister and HIC due to the absorption of hydrogen. Variability and uncertainty in various input parameters are taken into account using Monte Carlo simulations of the evolution of the structural integrity of the canister, with the main output of the model being the distribution of canister breaching times.

3.6.4. Current Status of the Process Modelling of Joint Mechanical–Corrosion Effects

After many years of separate assessments of the structural stability and long-term corrosion performance of HLW/SF containers, attention is now being paid to the importance of considering joint mechanical–corrosion degradation modes. Such considerations are not necessarily important because these interactions will lead to container failure, but by carefully considering the possibility of such interactions, it demonstrates a degree of robustness in the container-lifetime prediction.

It is probably unnecessary to develop joint mechanical–corrosion models for container materials and designs that exhibit a low probability of such interactions, for example, dual-wall container designs where the two components serve separate functions. However, joint mechanical–corrosion models are necessary for some container materials and designs, particularly carbon steel containers that can undergo a time-dependent change in material properties due to the effects of anaerobic corrosion. This need has been recognised and suitable approaches have been developed.

3.7. Miscellaneous Corrosion Models

Table A7 in Appendix A lists a number of process models that do not fall into any of the categories described above. Many of these models are based on first principles or atomistic approaches and include:

- thermodynamic analysis of the effects of phosphorus and sulphur on the properties and structure of pure copper and the implications for the creep behaviour [218];
- calculation of bulk and surface properties of Cu(I) sulphides using the interface Green's function method [219];
- density functional theory (DFT) and linear response theory calculations of the stability of various Cu-H-O species that have been proposed to be formed during the corrosion of copper in O_2-free H_2O [220];
- DFT model of the conversion of Cu_2O to Cu_2S by sulphide, including an assessment of the relative reactivities of different crystal planes and different sulphide species [221–223];
- DFT calculations of copper vacancy diffusivity in a Cu_2S film in support of PDM characterization of the film [224].

Other miscellaneous models of interest include:

- CALPHAD (calculation of phase diagrams) calculations of the temperature-time-transformation (TTT) and the possible thermal ageing of various Ni-Cr-Mo alloys for the Yucca Mountain program. Phase transformation could impact the localised corrosion behaviour of the alloy [225];
- Model for predicting the possibility of the separation of solutes due to the flow of electrolytes over the surface of a waste package in an unsaturated environment. The model addresses the question of whether the composition of the surface electrolyte in an evaporating droplet (and, crucially, the ratio of the concentration of aggressive ions such as Cl^- to that of inhibitive ions such as NO_3^-) will vary circumferentially around the waste-package surface due to solute solubility differences as the drip moves over the surface under the effects of gravity [226];
- Calculation of the time-dependent internal pressure due to hydrogen diffusion through the wall of a carbon steel container during the long-term anaerobic phase. Internal pressurisation offsets the compressive load from the buffer swelling and hydrostatic pressures, but will also lead to an increased risk of hydrogen-induced cracking due to internal or embedded flaws [227];
- The use of multiple models to determine the number and timing of canister failures due to earthquakes and shear across deposition holes in a KBS-3-type repository in crystalline rock [228].

3.8. Ancillary Models

In addition to the models used directly to describe or predict various corrosion processes, use is also made of other models in the assessment of the long-term performance of HLW/SF containers. As noted in Section 2, it is essential to understand the nature and evolution of the near-field environment, and many such models have been developed, including:

- Models for the nature of the pore structure and pore-water chemistry of compacted bentonite [229–232];
- Evolution of the pore-water pH of cement [115,233];
- Evaporation of seepage drips and the deliquescence of surface deposits in the YM repository [234–236];
- Thermal-hydraulic-mechanical-chemical (THMC) models of the time-dependent temperature, saturation, bentonite swelling pressure, and pore-water chemistry [237–241];
- Predictions of the γ- and neutron-dose rates at the surface of the container [242,243];
- Models for the evolution of the near-field redox conditions [90,244,245];
- Prediction of the response to mechanical loads on the container [216,246].

The use of Pourbaix diagrams is fundamental to the analysis of corrosion mechanisms, including not only the conventional diagrams based on bulk thermodynamic properties [247,248] but also those that consider adsorbed surface phases [249,250].

4. Conclusions and Outlook

As highlighted by some of the examples presented in this review, a wide range of models have been developed to predict and interpret the corrosion behaviour of HLW/SF containers over the past 45 years. These models range from the simple (e.g., an empirical corrosion rate) to the complex (e.g., reactive transport models such as the CCM and PDM). Although there has been a general progression in the level of complexity and the depth of the mechanistic basis of these models over the decades, it is interesting to note that we are still relying on some of the same approaches that were first proposed by the Swedish Corrosion Institute in 1978.

Some of the progress that has been made is in the development of more mechanistically based models and a (partial) move away from empiricism to determinism. Determinism is the focus of this Special Issue, and it is appropriate that we should present our position on the question of determinism versus empiricism. While deterministic models provide additional insight that is not available from purely empirical models, we are less focused

on the type of model and more on how reliable the prediction is. Empirical extrapolations are acceptable, provided they are supported by a sound mechanistic understanding of the underlying processes involved in the corrosion reaction. Thus, a sound mechanistic understanding is vitally important, either to provide the basis for a deterministic model or to support the prediction of an empirical model.

Having reviewed the historical development of corrosion models for HLW/SF containers, it is of interest to look forward into the future. There has been a tendency among international WMOs to move away from the selection of passive materials for HLW/SF containers in favour of the two active materials, namely copper and carbon steel. This shift has, in part, been the result of the perceived difficulty in making long-term predictions for passive materials that are potentially susceptible to localised corrosion, such as Ti [22] and Ni alloys [23]. As described here and elsewhere [29,251–253], there have been considerable advances in the mechanistic understanding and modelling of localised corrosion over the past few decades. It is to be hoped that such progress will persuade those responsible for reviewing future licence applications for regulatory and government organizations that it is indeed possible to make reliable long-term predictions of the localised corrosion behaviour of passive materials. We may then see a shift back towards the consideration of passive materials for HLW/SF containers, as in the Czech program [254].

Along with greater confidence in our understanding of the mechanisms of various corrosion processes and in our ability to model them comes an opportunity for optimization of the container designs. Thus, some of the conservatisms characteristic of earlier models may be relaxed. We are already seeing evidence of this in the NWMO-designed copper-coated container with a corrosion allowance of just 3 mm for a predicted lifetime of more than 1 million years [17].

We would also like to see a greater emphasis on the validation of process models against either laboratory-scale experiments or the results of full-scale in situ tests. There should also be more discussion about the limitations of such models. Perhaps a good starting point would be a description of the assumptions inherent to the model and a discussion of the consequences of these assumptions on the reliability of the predictions.

Notwithstanding the progress in HLW/SF container corrosion modelling that has been made, there are still opportunities for future progress. For example, many of the models described here treat the container surface as being pristine. In reality, the surface will have a certain degree of surface roughness, with asperities and other surface features and contaminants. At a minimum, the surface will be oxide-covered but may also feature organic residues, deposited salts, and other potentially detrimental species. There will also be a range of flaws, both on the surface and embedded within the container wall, especially associated with the final closure weld. Although some effort is being made to include the effects of these "real-life" container features in the corrosion models, more could be done.

There also seems to be continuing uncertainty about the duration of the oxic transient in repositories located in the saturated zone. There is full-scale experimental evidence that the transient may only last for a few weeks [90], but predictive models still indicate an oxic period of several years or longer. Having greater confidence in the length of the oxic phase is of great importance for container corrosion modelling, especially for the possible use of passive materials. If the oxic period is indeed only a few weeks or months in duration, possibly at a time that the container surface is too dry to support aqueous corrosion processes, then there is no reason why a range of passive materials (including austenitic stainless steels) cannot provide long-term containment.

Appendix A

Table A1. Summary of process models developed for the prediction of the uniform corrosion of HLW/SF containers *.

Model Name or Brief Description	Model Type	Description	Reference(s)
Generic reactive transport model for copper or steel containers in a saturated repository	Reactive transport	2D cartesian or axisymmetric cylindrical reactive transport model with electrochemical boundary conditions. Assumes film-free container surface. Includes effects of sulphate reduction to sulphide and radiolytic oxidants. Not applied to a specific repository system due to cancellation of basalt project in the U.S.	[255]
Mixed-potential model for carbon steel in bentonite buffer	Reactive transport	Mixed-potential model for the uniform corrosion of carbon steel in compacted bentonite buffer in a DGR in granitic host rock. The anodic dissolution of Fe as Fe^{2+} was coupled to the cathodic reduction of O_2 (assumed to be under transport control) and of H_2O (assumed to be kinetically controlled). The production and consumption of radiolytic oxidants were also considered. Model used to predict a steady-state E_{CORR} value and a conservative corrosion rate at an assumed constant temperature of 90 °C. The reduction in corrosion rate due to precipitated corrosion products was not taken into account. Also used for assessment of corrosion of carbon steel for disposal in marine sediment.	[5,6]
Point defect model (PDM)	Reactive transport	General framework for the prediction of the growth and breakdown of passive films. Applied to a number of HLW/SF container corrosion issues (see below).	[33–35]
Mixed-potential model for copper in O_2-containing Cl^- environments	Electrochemical	Analytical mixed-potential model for copper validated against experimental data covering five orders of magnitude variation in mass-transfer coefficient, three orders of magnitude in $[O_2]$, and one order of magnitude in $[Cl^-]$. Subsequently implemented using COMSOL.	[44,45]
Copper corrosion model (CCM)	Reactive transport	Mixed-potential model based on coupling of interfacial electrochemical reactions to mass-transport, redox, adsorption/desorption, and precipitation/dissolution reactions occurring in highly compacted bentonite buffer. Model assumes initially aerated, Cl^- dominated conditions. Effects of thermal and saturation transients included.	[39,40,77,78,83]
CAMEO	Reactive transport	3D cylindrical geometry of copper canister in deposition hole with assumption that corrosion rate is determined by either the rate of transport of oxidants (O_2 or HS^-) towards or of corrosion products ($CuCl_2^-$) away from the container.	[256]
Threshold corrosion product spalling thickness	Analytical	Time-dependent decrease in corrosion rate due to build up of protective corrosion product affected by assumed spalling of corrosion products on carbon steel container in an un-backfilled disposal tunnel.	[257]
Uniform corrosion of carbon steel in bentonite	Mixed-potential model	Coupled interfacial electrochemical kinetics for Fe dissolution and O_2 and H_2O reduction with O_2 transport in bentonite	[46]
CUPRS	Electrochemical	Mixed-potential model for copper in O_2-containing Cl^- environments. Based on model of [44]	[93]
Steel–clay interaction models	Reactive transport	Geochemical models focussed on the prediction of alteration of the clay barrier due to reactions with dissolved Fe. Generally based on a thermodynamic speciation code coupled to a transport model. However, with the exception of the study of Marty et al. [38], the corrosion rate is an input parameter and is not predicted by the codes.	[36–38,87,88,258,259]

<div align="center">**Table A1.** *Cont.*</div>

Model Name or Brief Description	Model Type	Description	Reference(s)
General corrosion model (GCM) and accumulated damage model (ADM) for Alloy 22	Reactive transport	Based on the PDM for prediction of barrier layer thickness and Butler–Volmer expressions for the cathodic reactions (reduction of O_2 and/or H_2O). Model predicts E_{CORR}, corrosion rate, and transpassive dissolution potential. Application of model to predict transients in passive film growth on Alloy 22	[28,58,61,62]
Long-term passivity of Alloy 22	Reactive transport	Mechanistic model for the long-term passive dissolution of Alloy 22 based on an extension of the PDM. Conclude that dissolution of alloy is congruent provided diffusivities for the alloying elements are similar. Periodic film spalling should not drastically increase the corrosion rate. Therefore, long-term prediction based on the extrapolation of empirical corrosion rates is justified.	[260]
Uniform corrosion of carbon steel	Empirical	Arrhenius temperature-dependent fit to empirical data for oxic and anaerobic conditions in compacted clay or clay–water systems	[116]
Wet–dry cycle atmospheric corrosion	Reactive transport	Atmospheric corrosion of iron during a wet–dry cycle.	[261]
Diffusion Poisson coupled model (DPCM)	Reactive transport	Based on the point defect model but with the potential profile within the barrier oxide layer explicitly calculated based on the Poisson equation	[41,69,262–264]
Low-temperature oxidation model	Empirical and reactive transport	Simple empirical and advanced reactive transport models for predicting the extent of dry oxidation of carbon steel containers at repository-relevant temperatures	[265,266]
Transport model for the uniform corrosion of carbon steel	Reactive transport	1D cylindrical reactive transport model for the corrosion of carbon steel in bentonite buffer. Corrosion rate assumed to be determined by the rate of transport of dissolved Fe^{2+} away from the container surface. Sorption of Fe^{2+} by bentonite was the only reaction considered. Corrosion rate depends on solubility of assumed corrosion product.	[91]
Uniform corrosion rate of copper and carbon steel	Empirical	Power-law time-dependent corrosion rates for Cu and carbon steel derived from experiments in bentonite slurry	[267]
Uniform corrosion Alloy 22	Empirical	Uniform corrosion rate derived from mass-loss results from 5-year exposure tests and assumed to be temperature dependent but constant over time. Rates independent of solution chemistry.	[9,32]
Corrosion potential model for Alloy 22	Empirical	Empirical fit to long-term E_{CORR} measurements expressed as a function of T, pH, [Cl^-] and [NO_3^-]. For use with E_{RCREV} relationship to determine if crevice corrosion initiates.	[9,32]
Uniform corrosion Ti Grade 7	Empirical	Uniform corrosion rate derived from mass-loss results from 2.5- and 5-year exposure tests and assumed to be independent of temperature and constant over time. Rates independent of solution chemistry.	[9]
Diffusion-limited corrosion model for carbon steel	Reactive transport	Interfacial dissolution of Fe under anaerobic conditions described by an equilibrium expression with Fe^{2+} and H_2 as corrosion products. Corrosion rate is then determined by the flux of Fe^{2+} and/or H_2 away from the container surface, with equilibrium corrosion product concentrations calculated using PHREEQC. Corrosion rate decreases with decreasing effective diffusivity.	[268]
Copper sulphide model (CSM)	Reactive transport	Extension of the copper corrosion model (CCM) to include the effects of sulphide present either in the groundwater or generated by sulphate-reducing bacteria (SRB) activity. Based on the assumption of the formation of a porous Cu_2S corrosion-product film.	[70–72,76,79,80,190–192]
Mixed-potential model for predicting H_2 generation in ONDRAF/NIRAS supercontainer	Reactive transport	Mixed-potential model to predict the evolution of the consumption of initial O_2 and the subsequent generation of H_2 within the cementitious backfill due to corrosion of the carbon steel container and stainless steel envelope	[269]

Table A1. *Cont.*

Model Name or Brief Description	Model Type	Description	Reference(s)
Corrosion domain and volt-equivalent diagrams	Thermodynamic	Assessment of the thermodynamic driving force for corrosion of copper in pure water and in the presence of sulphur species and other ligands.	[47,48,270]
Uniform corrosion of carbon steel	Empirical	Assumption of a constant corrosion rate based on empirical data.	[11,30,31,254]
Point defect model for copper in presence of sulphide	Reactive transport	Application of PDM to passivation of copper by sulphide and development of a mixed-potential model for the prediction of E_{CORR}	[65,271]
Uniform corrosion of carbon steel in anoxic environments in presence of corrosion-product film	Coupled chemical equilibrium and mass-transport model	Effect of bilayer oxide film on corrosion rate of carbon steel in anoxic environments. Model accounts for H_2O diffusion through film and film dissolution at the film–solution interface.	[42]
Steel corrosion model (SCM)	Reactive transport	1D reactive transport model for carbon steel corrosion under anoxic conditions, solved using a mixed-potential model for the boundary conditions on the container surface. Model accounts for the development of a mixed bentonite–corrosion-product layer, as well as the production and periodic release of H_2.	[73,81,272,273]
Oxide growth on copper during friction stir welding (FSW)	Empirical	Estimation of amount of oxygen incorporated into an FSW during welding based on expected thermal profile and empirical copper oxidation data.	[274]
Effect of precipitated porous corrosion products on carbon steel	Reactive transport	1D finite element model to predict the effect of precipitated $FeCO_3$ on the time-dependent corrosion rate of carbon steel. Considered both a constant porosity and variable porosity corrosion-product layer, with the latter in better agreement with experimental data. Effect of conductive corrosion-product layer also considered.	[74,75]
PDM for steel in cementitious environments	Reactive transport	Coupling PDM with Butler–Volmer expressions for the cathodic reaction (H_2 evolution) constitutes a mixed-potential model from which the corrosion rate and E_{CORR} can be determined. Model also used to demonstrate the irreversibility of the passive state for carbon steel in the cementitious environment,	[60,63]
Copper corrosion in pure O_2-free H_2O	Mass transport, empirical	What-if calculations for the corrosion of copper in pure H_2O based on (a) temperature-dependent corrosion rate derived from the proposed literature rates or (b) mass transport of H_2 away from canister surface.	[43]
Extent of copper corrosion based on results from large-scale in situ tests	Empirical	Regression analysis of extent of copper corrosion as a function of temperature and buffer thickness from large-scale in situ tests.	[275]
Corrosion of copper at high Cl^- concentration	Coupled thermodynamic speciation–mass transport	PHREEQC thermodynamic speciation code used to predict equilibrium-dissolved Cu concentration, which was then used as a source concentration in simplified mass-transport expressions to predict the corrosion rate as a function of pH, [Cl^-], T, and mass-transfer coefficient	[49,92]
Anaerobic corrosion of carbon steel in bentonite	Reactive transport	Model based on observations from various bench-scale and in situ experiments. Fractures in bentonite can occur as a result of desiccation due to H_2O consumption in the corrosion reaction. Oxygen is assumed to be immobile but reacts with Fe^{2+} diffusing away from the corroding interface. Precipitation of corrosion products results in decoration of fractures in bentonite with Fe(II)/Fe(III) and, ultimately, clogging of the pore structure.	[276]

* Arranged in chronological order of publication.

Table A2. Summary of process models developed for the prediction of the localised corrosion of HLW/SF containers *.

Model Name or Brief Description	Model Type	Description	Reference(s)
Pitting factor for copper	Empirical	Ratio of the deepest penetration (measured from the original surface) to the mean depth of penetration. Thus, a pitting factor of 1 represents uniform corrosion. Pitting factors typically determined from long-term exposure of archaeological or anthropogenic objects to near-surface burial conditions.	[3]
Pit propagation rate for carbon steel	Empirical	Time-dependent pit depth expression based on electrochemically grown pits in Cl^-/HCO_3^- environments.	[277]
Period of passivation of carbon steel	Electrochemical	Maximum duration for which carbon steel is deemed to be passive and, therefore, susceptible to localised corrosion is defined as the period that the flux of oxidants (initially trapped O_2 and/or oxidising radiolysis products) is sufficient to sustain the passive current density.	[97,278,279]
Extreme value analysis (EVA) of pit depths for carbon steel	Statistical analysis of empirical data	EVA of laboratory pit depths fitted to limited and unlimited distribution functions to predict time dependence of maximum probable pit depth on container.	[5,128]
Propagation of pitting or crevice corrosion of carbon steel	Reactive transport	1D or 2D finite-element model of chemistry inside and dissolution rate within an occluded pit or crevice as a function of external electrode potential and crevice dimensions. Propagation assumed not to be limited by external cathode.	[102,125–127]
Model for large-scale corrosion cells	Reactive transport	Reactive transport model for predicting localised corrosion due to long-range electrochemical cells, as might develop due to differential aeration or spatial variations in current/potential behaviour of the (steel) substrate. Such long-range cells tend to result in surface roughening rather than discrete pits.	[280]
Pit or crevice chemistry and electrochemical potential model	Reactive transport	Coupled speciation, transport, and electrochemical model for the prediction of the evolution of the chemistry and potential distribution within the occluded region.	[281]
Crevice corrosion initiation time	Reactive transport	Prediction of initiation for crevice corrosion of titanium and stainless steels based on time to establish a critical pH within the crevice. Effect of crevice length and gap found to be important.	[103,144,145]
Damage function analysis (DFA)	Deterministic	General deterministic approach to predicting corrosion damage. Applied to the pitting of Alloy 22 using the point defect model for determining passivity breakdown, deterministic models for cavity growth, and the assumption of delayed repassivation.	[59,282,283]
Model for the initiation of crevice corrosion	Reactive transport	Development of the earlier model for crevice propagation, with initiation determined by the time to establish critical pH, $[Cl^-]$, and potential within the crevice.	[132]
Stochastic pitting models	Stochastic, Monte Carlo	Stochastic models for predicting the initiation time, survival probability, and pit-depth distribution. Time to container failure and the time dependence of the number of through-wall pits can also be predicted.	[109–111]
Extreme value analysis (EVA) of pit depths on copper	Statistical analysis of empirical data	EVA of empirical pit depth data from long-term buried corrosion study and Bronze Age archaeological artefacts. Time dependence of location parameter permitted extrapolation in time for prediction of probability of maximum pit depth as a function of time.	[100]
Extreme value analysis (EVA) of pit depths for carbon steel	Statistical analysis of empirical data	EVA of maximum and average corrosion depths on galvanostatically polarised specimens. Derived a maximum pit depth–average corrosion depth ratio for any one of 20,000 containers.	[101,120]
Crevice corrosion initiation model for Fe-Ni-Cr-Mo alloys	Reactive transport	Prediction of chemistry and distribution of potential within crevice for Type 316L stainless steel and Alloy 825. Initiation based on time for pH, $[Cl^-]$, and potential to result in depassivation of surface inside crevice.	[130]
Crevice corrosion propagation model for Ti Grade 2	Probabilistic, empirical	Rate of crevice corrosion based on empirical measurements and treated as temperature dependent.	[7,8,123]
Use of repassivation potential as a criterion for the initiation of localised corrosion	Electrochemical	Definition of the electrochemical criterion for the initiation of localised corrosion (in the form of either pitting or crevice corrosion); $E_{CORR} \geq E_{RP}/E_{RCREV}$. Repassivation potential is argued to be a more conservative criterion for initiation than the film breakdown potential.	[108,146,147]

Table A2. *Cont.*

Model Name or brief Description	Model Type	Description	Reference(s)
Pitting of carbon steel in compacted bentonite	Electrochemical	Maximum pit depth predicted based on duration of pitting and maximum pit growth rate. Duration of pitting equated to length of time that the O_2 flux can sustain the passive current density. Pit growth rate based on Sharland localised corrosion model and empirical pit growth expression	[46]
Pitting of carbon steel	Reactive transport	Reactive transport model of pit propagation in carbon steel. Pit kinetics dependent on assumed cathode size.	[133]
Crevice chemistry model for Alloy 22	Reactive transport	Prediction of the evolution of the chemistry inside a crevice on Alloy 22 as a function of crevice geometry. Predicted decrease of pH in crevice insufficient to lead to crevice initiation, especially in combination with the decrease in potential within the crevice.	[131]
Environmental conditions for passivation of carbon steel	Empirical	Based on active or passive characteristics of voltammograms measured in compacted bentonite	[10]
Equilibrium-mass transport model for pitting of copper	Reactive transport	Pit propagation model based on the need to prevent pit stifling by precipitation of corrosion products within the pit. Equilibrium calculations of dissolved species coupled with transport expressions determine the rate of removal of oxidised copper from pit. Assumes pit propagation is anodically limited.	[104,105,134]
Stochastic localised corrosion model	Rule based	Generic rule-based model for predicting passivation and evolution from uniform to localised corrosion.	[284]
Depth-dependent pitting factor for carbon steel	Empirical	Pitting factor decreases with increasing depth of uniform corrosion	[116]
Critical potential for initiation and repassivation of passive alloys	Based on the concept of a critical electrochemical potential that must be exceeded for the initiation of pitting or crevice corrosion. Pit or crevice stifling occurs below the repassivation potential	Crevice corrosion of Ti alloys Crevice corrosion Alloy 22	[9,12,148,285]
Extreme value analysis (EVA) of pit depths	Statistical analysis of empirical data	Carbon steel	[12,286]
Propagation of crevice corrosion of iron	Electrochemical-based reactive transport	Prediction of chemical conditions and potential distribution within an occluded region and the conditions under which precipitation and, hence, crevice stifling might occur.	[129]
Cathodic limitation of crevice corrosion under atmospheric conditions	Electrochemical	Analytical expressions for the extent of coupling between an external cathode and an occluded pit or crevice under atmospheric conditions. Initially developed for stainless steel, subsequently applied by Payer and Kelly to the case of the crevice corrosion of Alloy 22 under dust deposits. Model provides conditions of crevice dimensions and electrolyte conductivity (related to salt loading and RH) under which pits will either propagate or stifle.	[124,142,143]
Localised corrosion of Alloy 22 under dust deposit	Decision tree	Analysis of the possibility of crevice corrosion of Alloy 22 due to deliquescence of soluble minerals in a dust layer deposited on a waste package	[112,149]
Localised corrosion of Alloy 22 due to seepage drips	Decision tree	Crevice corrosion requires that (i) seepage drips contact waste-package surface (no thermal or capillary barrier, drip shield failed), (ii) the composition of seepage water leads to development of aggressive aqueous phase after evaporation, (iii) a crevice exists, and (iv) conditions are sufficiently oxidising.	[150]
Crevice corrosion of Alloy 22	Empirical	Model accounts for initiation, propagation, and stifling of crevice corrosion of Alloy 22. Initiation based on the $E_{CORR} \geq E_{RCREV}$ criterion, with the value of E_{RCREV} dependent on temperature and $[Cl^-]$ and the inhibitive effects of NO_3^-, CO_3^{2-}, and SO_4^{2-}. Propagation based on empirical time-dependent penetration depth. Empirical expression for E_{CORR}. Monte Carlo simulations run to account for variability and uncertainty.	[117]
Crevice corrosion under porous deposit	Reactive transport	General model for prediction of crevice initiation and propagation for a metal covered by a permeable layer, such as a dust layer on a HLW/SF container in an open disposal tunnel	[135]
Crevice corrosion initiation for Alloy 22	Empirical	Empirical expression for the crevice repassivation potential E_{RCREV} as a function of T, $[Cl^-]$, and $[NO_3^-]$. E_{RCREV} used as a conservative indicator of crevice initiation.	[9,32]

Table A2. *Cont.*

Model Name or brief Description	Model Type	Description	Reference(s)
Surface roughening factor for copper	Empirical	Localised corrosion of copper under repository conditions takes the form of surface roughening rather than discrete pits, and is consistent with the non-permanent spatial separation of anodic and cathodic processes. Treated in lifetime predictions as an allowance of 50–100 µm.	[15,16]
Crevice chemistry model for Alloy 22	Reactive transport	Model for predicting the development of the chemistry inside and outside an occluded region, but link to either the initiation or propagation of crevice corrosion not stated.	[287]
Cellular automata (CA) model for surface roughening of carbon steel	Rule based	CA approach for pitting and surface roughening of carbon steel. Extended to include a probabilistic treatment of the probability of the transitions between different states.	[113,151]
Critical potential for initiation and repassivation of passive alloys	Based on the concept of a critical electrochemical potential that must be exceeded for the initiation of pitting or crevice corrosion. Pit or crevice stifling occurs below the repassivation potential	Attempt to apply literature expressions for pitting and repassivation potentials to bentonite pore-water solutions. Correlation fails because copper not passive in bentonite pore water	[288,289]
Atmospheric pitting corrosion of stainless steel	Reactive transport	Reactive transport model for the pitting of stainless steel in contact with a thin electrolyte layer representative of atmospheric conditions. The extent to which the external cathode can couple to the anodically dissolving pit due to the limited conductivity of the thin electrolyte layer is taken into account in the model.	[106]
Passivity breakdown of Cu_2S films	Reactive transport	Determination of the effect of chloride ions and elevated temperatures on the breakdown of passive Cu_2S films and interpretation using the point defect model	[64,65]
Dissolution of oxide particles in copper friction stir welds	Reactive transport	Finite-element model for the dissolution of Cu_2O particles embedded in the surface of FSW based on the assumption of chemical equilibrium between the oxide and dissolved Cu(I) species	[136]
Pit repassivation model	Reactive transport	Deterministic model for predicting pit repassivation based on the concept that there exists a critical pit propagation rate (and, hence, a critical coupling current between internal anode and external cathode) necessary to maintain aggressive conditions within the pit. Applied to the case of the pitting of the carbon steel overpack for the Belgian Supercontainer concept.	[137]
Pitting of carbon steel in alkaline cementitious porewater	Reactive transport	Application of the PDM and DFA to predict the initiation (incubation time and critical potential), propagation, and stifling of pits on Belgian Supercontainer.	[107]
Effect of chloride ions on passivity breakdown of carbon steel in alkaline solutions	Reactive transport	Use of PDM to predict the effect of $[Cl^-]$ on the breakdown potential of passive films on carbon steel in simulated cementitious pore water solutions. No passivity breakdown for $[NaCl] \leq 1$ mol/L.	[138]
Environmental conditions for passivation of copper	Machine learning	Machine-learning algorithms applied to empirical electrochemical database to predict conditions of T, pH, $[Cl^-]$, $[SO_4^{2-}]$, $[HCO_3^-]$ for passivation of Cu as a prerequisite condition for pitting	[98,114]
Probabilistic pitting model for copper under aerobic, saturated conditions	Electrochemical/Machine Learning	Pit initiation based on requirement for a passive surface and exceeding a critical potential, with propagation based on empirical growth law. Probabilistic model accounts for variability and uncertainty in repository environmental conditions	[98,114]

* Arranged in chronological order of publication.

Table A3. Summary of process models developed for the prediction of the environmentally assisted cracking of HLW/SF containers *.

Model Name or Brief Description	Model type	Description	Reference(s)
Hydrogen degradation (embrittlement and/or hydrogen-induced cracking) of carbon steel	Empirical	Excluded based on the use of a relatively low-strength grade of carbon steel with limited empirical susceptibility to effects of absorbed H.	[5,10]
Stress-corrosion cracking (SCC) of carbon steel	Empirical	Excluded based on the proposed use of stress relief to reduce the residual stress to less than 50% of the yield strength.	[5]
Limited propagation model for SCC of copper	Empirical	For aerobic forms of SCC of Cu (e.g., in NO_2^- solutions), rate of crack propagation determined as a function of applied anodic current density. Under repository conditions, corresponding current density is due to flux of oxidant (O_2) to the container surface, from which the rate of crack growth as a function of time can be estimated.	[159]
Critical absorbed hydrogen concentration for HIC of Ti alloys	Empirical	Based on empirical threshold of absorbed H concentration for the loss of fracture toughness of Ti alloys and the assumption that a defect of appropriate size, location, and orientation will be subject to a sufficient tensile load that the fracture toughness will exceed.	[160]
Critical hydride-layer thickness HIC of Ti alloys (Ti-H-iT model)	Empirical	Cracks propagate due to the repeated fracturing of Ti hydrides when the hydride layer reaches a critical thickness of approximately 10 μm. Hydride-layer thickness is proportional to the square root of time and the corrosion current density. Threshold charge density below which no cracks are observed experimentally. Crack depth approximately 50% of thickness of hydride based on empirical data.	[13,162]
Copper corrosion model for stress-corrosion cracking (CCM-SCC)	Reactive transport	Modified version of the CCM to include the prediction of the interfacial pH. Used in conjunction with the CCM-MIC to predict the time dependence of the interfacial concentration of SCC agents (nitrite, ammonia, acetate), of E_{CORR} and the interfacial pH, the latter two parameters then compared with potential and pH at which SCC of copper has been observed empirically. CCM suite of models based on active dissolution of surface instead of passive, as required for SCC.	[156,157]
Slip dissolution model for SCC of Alloy 22	Empirical	Crack initiation and propagation model based on the requirements of a threshold stress for crack initiation and a threshold stress-intensity factor K_{ISCC} for crack growth. Crack growth rate a function of K_I.	[158]
SCC of copper	Decision-tree analysis	Logical basis for reasoned argument to exclude possibility of SCC of copper. Each prerequisite environmental, material, and stress-related condition must be met for SCC to be possible. Applied to SCC under aerobic and anaerobic, saturated and unsaturated near-field conditions.	[154,155]
Stress-corrosion cracking (SCC) of carbon steel	Empirical	Excluded based on the absence of suitable environmental conditions and/or of cyclic loading found necessary to support crack growth in anaerobic near-neutral pH environments.	[290]
HIC Ti Grade 7	Probabilistic	Based on concept of a threshold absorbed H concentration above at which fast fracture occurs and the time-dependent absorption of H due to uniform corrosion. Under oxic conditions, only a fraction of the total cathodic current is supplied by H_2 reduction and only a fraction of the resulting H is absorbed.	[161,165,166]
Hydrogen degradation of copper	Transport	Model developed to predict H_2 bubble formation during electrochemical charging of OFP copper. For H charging rates typical of anaerobic corrosion in the repository (1 nm/yr), effects of absorbed H would be minimal.	[291,292]

* Arranged in chronological order of publication.

Table A4. Summary of process models developed for the prediction of the microbiologically influenced corrosion of HLW/SF containers *.

Model Name or Brief Description	Model Type	Description	Reference(s)
Maximum extent of sulphidation by SRB	Mass balance	Mass-balance calculation of the maximum amount of FeS that could be produced based on the stoichiometry of organotrophic sulphate reduction and the assumption that organic carbon is the limiting factor, and on the assumption of 100% bioavailable organic matter in the bentonite buffer.	[5]
Nutrient and energy balance analysis	Mass and energy balance	Analysis of the inventory of nutrients and potential energy sources in the repository, leading to a calculation of the maximum microbial population	[171]
Radiation-induced microbial-depleted zone	Empirical	Creation of "sterilized" zone around container due to reduction in microbial population due to γ-irradiation of buffer material and empirical radiation-sensitivity of indigenous microbes.	[293]
Microbial activity model (MAM)	Reactive transport	Monod kinetics used to describe rates of organotrophic and lithotrophic sulphate reduction by SRB under repository conditions, and the reaction of the sulphide with Fe(II) and the copper container.	[174]
Copper corrosion model for microbiologically influenced corrosion (CCM-MIC)	Reactive transport	Extended version of the CCM to include various forms of microbial activity, including aerobic respiration, denitrification, nitrogen fixation, nitrosofication, ammonia oxidation, fermentation, iron reduction, and sulphate reduction. Microbial activity described using Monod kinetics. Limitations on the rate of microbial activity based on (i) the availability of electron donors and acceptors, (ii) water activity, (iii) temperature, (iv) redox potential	[172,173,185,294]
MIC of copper	Reactive transport	2D model of fracture intersecting deposition hole for the KBS-3 system, with assumed first-order reduction of sulphate to sulphide. Fraction of sulphide swept away in flowing groundwater, with remainder causing corrosion of the canister. No other sink for sulphide considered.	[295]
MIC of Alloy 22	Empirical	Multiplication factor for MIC based on electrochemical corrosion rates measured with and without microbes indigenous to Yucca Mountain (determined at ambient temperature with added organic nutrient). The MIC enhancement factor f_{MIC} is a uniform distribution between values of 1 and 2.	[9,32]
Suppression of microbial activity by cementitious backfill	Empirical	Evidence that while SRB may remain viable after prolonged exposure to alkaline conditions similar to those in a cementitious backfill, the microbes are not active.	[182]
Suppression of microbial activity by highly compacted bentonite	Empirical	Based on empirical observations that the ability to cultivate microbes from highly compacted bentonite (HCB) diminishes with increasing buffer density, with indications of a threshold HCB dry density of approximately 1600 kg/m^3 for complete suppression of microbial activity. The physiological cause of this apparent threshold is not known but is likely to be due to one or more of the following factors: (i) low water activity a_W, (ii) high swelling pressure, and/or (iii) lack of physical space.	[169,170,180,181]
Sulphide transport model	Mass transport	1D, 2D, and 3D sulphide transport models based on assumed constant sulphide source and zero-concentration boundary condition at copper surface to simulate a transport-limited corrosion reaction. Extended to consider the temporal and spatial variation of the near-field saturation and temperature.	[89,179,194–196]
Sulphide transport and reactive transport models for copper containers in a Nagra repository	Reactive transport	Two sulphide transport models were used to estimate the extent of corrosion of a copper-coated container for the Nagra repository design and for various backfill properties. In the simpler model, the sulphide flux was estimated based on the flux of sulphate subject to solubility control by an iron sulphide phase; equivalent to assuming fast sulphate reduction kinetics dependent only on the availability of the electron acceptor. For the second, more complex, model, the rate of sulphide production was explicitly calculated based on Monod kinetics (as in the UBSM, see below).	[176,177,186,187]
Assessment of damage under biofilm for copper and carbon steel	Empirical	Empirical determination of localised damage under a biofilm in the presence of sulphate-reducing bacteria. Carbon steel exhibits pitting and little uniform corrosion, whereas copper exhibits both forms of corrosion. Damage can be expressed in terms of a pitting factor.	[296]

Table A4. *Cont.*

Model Name or Brief Description	Model Type	Description	Reference(s)
Amphos21 sulphide model	Reactive transport	Reactive transport model for the production, transport, and consumption of microbially produced sulphide and the consequences for container corrosion. Transport based on interlayer bentonite pore-water model.	[175]
University of Bern Sulphide Model (UBSM)	Reactive transport	1D, 2D, and 3D reactive transport models for the production, transport, and consumption of sulphide due to remote microbial activity by SRB. Corrosion rate determined based on the assumption of sulphide transport control. 2D and 3D models permit the effect of the spatial relationship between the sulphide source (typically the excavation damaged zone around the rock openings) and the sulphide sink (i.e., the canister) to be determined.	[176,177,188,189]
Effect of SRB on corrosion of copper containers	Reactive transport	Reactive transport model for the effect of sulphate reduction by SRB based on assumed first-order kinetics for the sulphate reduction reaction. Sulphate reduction rate assumed to be a function of bentonite density. No limitation due to the availability of electron donors. No attenuation of sulphide flux by reaction with ferrous or ferric species.	[297]
INER Sulphide Model (ISM)	Reactive transport	COMSOL-based 1D, linear reactive transport model for the production, transport, and consumption of sulphide due to organotrophic and lithotrophic SRB. Microbial activity described by Monod kinetics.	[178]

* Arranged in chronological order of publication.

Table A5. Summary of process models developed for the prediction of the radiation-induced corrosion of HLW/SF containers *.

Model Name or Brief Description	Model Type	Description	Reference(s)
Extent of radiation-induced corrosion (RIC) of copper canisters	Uncoupled bulk radiolysis model	Net production of oxidants equated to the rate of diffusive loss of reductants (H_2) away from canister surface. Concentration of H_2 calculated based on bulk radiolysis model for H_2O containing 5 mg/L Fe^{2+}. Corrosion rate assumed to be controlled by rate of production of oxidants.	[4]
Radiolysis effect on iron-base materials	Empirical	Semi-empirical model based on fitting experimental corrosion rates to conceptual model for competing production and consumption reactions for radiolytic species.	[199]
Effective G-value	Empirical	The overall yield of radiolytic oxidants (the effective G-value) was calculated from empirical data based on the enhancement of the rate of corrosion in the presence of radiation. The effective radiolytic yield was then used as an input to a reactive transport, mixed-potential model.	[5]
Effective G-value	Uncoupled bulk radiolysis model	An effective G-value of 2.13 molecules/100 eV was defined assuming an average valence of 2 for the radiolytic oxidants. This effective G-value appears to include contributions from both the primary species ($OH^\bullet$, H_2O_2) and secondary species (O_2, O_2^-, HO_2).	[97]
Thin-layer mixed-potential model (TLMPM)	Reactive transport, coupled bulk radiolysis model	Fully-coupled radiolysis–interfacial electrochemical reactive transport model for radiation-induced uniform corrosion in thin adsorbed H_2O layer. Coupled with passive current-potential expressions for Types 304L and 316L stainless steel and oxygen-free copper, aluminium bronze, and 70:30 Cu:Ni.	[203]
Dose rate limit	Empirical	Argument that effects of γ-radiolysis are insignificant below a given dose rate. Based on the review of Shoesmith and King [200] who reported no observable effect for dose rates of the order of 1–10 Gy/h. Subsequently adopted by others with varying dose rate limits between 1 Gy/h and 25 Gy/h.	[11,30,31,200,201]
Humid air radiolysis model (HARM)	Uncoupled bulk radiolysis model-corrosion damage	HARM bulk radiolysis model used to predict yield of HNO_3 due to radiolysis of humid air, which was then assumed to dissolve into a droplet of arbitrary diameter from a volume of air of arbitrary size leading to corrosion of the copper substrate	[197,209]
Uncoupled mixed-potential model for copper	Uncoupled bulk radiolysis–mixed-potential model	Anodic dissolution of copper coupled to cathodic reduction of H_2O_2. Yield of H_2O_2 calculated from simplified bulk radiolysis model.	[202]

Table A5. *Cont.*

Model Name or Brief Description	Model Type	Description	Reference(s)
Coupled corrosion–bulk radiolysis model for copper	Coupled corrosion–bulk radiolysis model	RIC model based on a bulk radiolysis model for H_2O with O_2 as the species supporting oxidation of the Cu. Interfacial reaction incorporated as a homogeneous reaction between Cu and O_2. Model subsequently extended by Jonsson [205] to examine the effect of groundwater species, such as chloride, sulphide, dissolved Fe, bicarbonate, dissolved O_2, and dissolved organic matter.	[204,205]
Radiolysis of moist air inside canister	Uncoupled bulk radiolysis model	Radiolysis model for humid air/Ar gas phase inside canister due to entrainment of liquid H_2O in defected spent fuel assemblies. While not a corrosion model as such, predictions do highlight the possibility of the formation of NH_3, a potential SCC agent for copper. Ammonia only produced once O_2 has been consumed.	[208]
Copper corrosion model for radiation-induced corrosion (CCM-RIC)	Reactive transport, coupled bulk radiolysis model	Fully-coupled radiolysis/interfacial electrochemical reactive transport model for radiation-induced uniform corrosion of copper. The effects of oxide interfaces (clay particles and on container surface) on the effective radiolytic yield taken into account. Reactions between oxidising and reducing radiolysis products and structural Fe(II)/Fe(III) in octahedral lattice sites, as well as reactions between radiolysis products and accessory minerals in the bentonite clay also considered.	[206]

* Arranged in chronological order of publication.

Table A6. Summary of process models developed for the prediction of the joint mechanical–corrosion effects for HLW/SF containers *.

Model Name or Brief Description	Model Type	Description	Reference(s)
Development of stress due to corrosion of inner vessel of advanced cold process canister (ACPC)	Analytical	Calculation of the hoop stress in the copper outer barrier due to the formation of expansive corrosion products from the corrosion of the inner carbon or cast steel vessel.	[212,213]
Consolidation stress due to formation of expansive corrosion products	Analytical	The formation of carbon steel corrosion products with a volume greater than that of the corroded Fe is assumed to lead to a load on the container, after accounting for the effects of consolidation of the buffer and creep of the host rock (if any). Resulting stress depends on buffer thickness, but is predicted to be of the order of 1 MPa to >20 MPa.	[10]
Assessment of effect of surface-breaking flaws	Fracture mechanics	Effect of surface-breaking flaws on the possibility of SCC of copper containers due to stress concentration or intensification by notch-like and crack-like flaws, respectively.	[298]
Consequences of seismic activity and/or rockfall on waste-package integrity	Finite element model	Impact damage of waste packages by falling rocks or by collisions due to seismically induced ground motion could induce plastic deformation and residual stresses, which would then render the waste packages susceptible to SCC.	[9]
Structural integrity of closure weld of carbon steel HLW container	Fracture mechanics	Fracture mechanics assessment of the critical flaw size for an assumed defect in weld material susceptible to uniform corrosion but not SCC or HIC	[19]
Structural integrity of carbon steel container containing defects	Fracture mechanics	Application of the failure-assessment diagram (FAD) approach to a defected carbon steel container subjected to internal and external mechanical loads and time-dependent reduction in wall thickness due to corrosion and degradation of fracture toughness due to hydrogen absorption.	[20]
Modelling of physically constrained systems	Mechanical	Prediction of time-dependent porosity of carbon steel corrosion-product layer in cementitious backfill constrained at the inner and outer boundaries, as in the Belgian Supercontainer concept. Model predicts that corrosion ceases as porosity of outer corrosion-product layer is reduced to zero.	[215]
Probabilistic canister breaching model (PCBM)	Fracture mechanics	Based on the same general principles as the model of King et al. [20], but run probabilistically to account for variability and uncertainty in the values of the different input parameters. Model used to predict the distribution of breaching times for a carbon steel canister in a DGR in Opalinus Clay.	[26]

* Arranged in chronological order of publication.

Table A7. Summary of models developed for the prediction of miscellaneous processes related to the corrosion of HLW/SF containers *.

Model Name or Brief Description	Model Type	Description	Reference(s)
Assessment of effect of environmental uncertainties on predicted container lifetime	stochastic	Study addresses the question of how well the evolution of environmental conditions needs to be known in order to predict container lifetimes with a given scatter.	[299]
Hydrogen production from advanced cold process canister (ACPC)	Analytical	Assessment of the rate and extent of H_2 generation from the corrosion of carbon steel inner vessel of ACPC in the event of a through-wall defect in the outer copper corrosion barrier.	[300]
Effect of defect interactions in copper	Atomistic	Effect of P and S (and Ag) impurities on properties and structure of pure copper studied using first principles thermodynamic calculations. Results are useful for understanding the effects of P and S on creep properties.	[218]
Surface properties of digenite	Atomistic	Calculation of bulk and surface properties of copper(I) sulphides using the interface Green's function method. Digneite $Cu_{2-\delta}S$ found to contain stable cation vacancies and high cation mobility, consistent with the ionic nature of digenite	[219]
Phase stability of Ni alloys	CALPHAD (calculation of phase diagrams)	Temperature–time–transformation (TTT) assessment of the thermal ageing of various Ni-Cr-Mo alloys for the Yucca Mountain program. Phase transformation could impact the localised corrosion behaviour of the alloy.	[225]
Flow separation processes on waste-package surface	Reactive transport	Model for predicting the possibility of the separation of solutes due to the flow of electrolyte over the surface of a waste package in an unsaturated environment. The model addresses the question of whether the composition of the surface electrolyte in an evaporating droplet (and, crucially, the ratio of the concentration of aggressive ions such as Cl^- to that of inhibitive ions such as NO_3^-) will vary circumferentially around the waste-package surface due to solute solubility differences as the drip moves over the surface under the effects of gravity.	[226]
Hydrogen accumulation inside steel canister	Mass transport	Calculation of the time-dependent internal pressure due to H diffusion through the wall of a carbon steel canister due to the generation of hydrogen on the external surface of the canister during the long-term anaerobic phase. Internal pressurisation will offset the compressive load from the buffer swelling and hydrostatic pressures, but will also lead to an increased risk of hydrogen-induced cracking due to internal or embedded flaws.	[227]
Quantum-mechanical calculations of stability of Cu-H-O species	Atomistic	Density functional theory and linear response theory calculations of the stability of various Cu-H-O species have been proposed to be formed during the corrosion of copper in O_2-free H_2O.	[220]
Density functional theory (DFT) model of the sulphidation of Cu_2O	Atomistic	DFT model of the conversion of Cu_2O to Cu_2S by sulphide, including an assessment of the relative reactivities of different crystal planes and different sulphide species	[221–223]
Diffusivity of copper vacancies in copper sulphide film	Atomistic	DFT calculations of copper vacancy diffusivity in Cu_2S film in support of PDM characterization of film.	[224]
Consequences of canister failure due to seismic activity	Multiple	Use of multiple models to determine the number and timing of canister failures due to earthquakes and shear across deposition holes in a KBS-3 type repository in crystalline rock in Taiwan. A total of five canisters are predicted to fail, with the first failure after 230,000 yr.	[228]

* Arranged in chronological order of publication.

References

1. Posiva. *Canister Evolution*; Working Report WR-2021-06; Posiva Oy: Eurajoki, Finland, 2021.
2. Ondraf/Niras. *A Review of Corrosion and Material Selection Issues Pertinent to Underground Disposal of Highly Active Nuclear Waste in Belgium: A Report for ONDRAF/NIRAS Prepared by the Corrosion Study Panel*; Technical Report NIROND 2004-02; Ondraf-Niras: Brussels, Belgium, 2004.
3. Swedish Corrosion Institute. *Copper as Canister Material for Unreprocessed Nuclear Waste—Evaluation with Respect to Corrosion*; Technical Report KBS TR-90; Kärnbränslesäkerhet: Stockholm, Sweden, 1978.
4. Swedish Corrosion Institute. *Corrosion Resistance of a Copper Canister for Spent Fuel*; Technical Report KBS 83-24; Kärnbränsleförsörjning AB/Avdelning KBS: Stockholm, Sweden, 1983.
5. Marsh, G.P.; Taylor, K.J. An assessment of carbon steel containers for radioactive waste disposal. *Corros. Sci.* **1988**, *28*, 289–320. [CrossRef]
6. Marsh, G.P.; Harker, A.H.; Taylor, K.J. Corrosion of carbon steel nuclear waste containers in marine sediment. *Corrosion* **1989**, *45*, 579–589. [CrossRef]

7. Shoesmith, D.W.; Ikeda, B.M.; LeNeveu, D.M. Lifetime prediction for titanium nuclear waste containers. In *Life Prediction of Corrodible Structures*; Parkins, R.N., Ed.; NACE International: Houston, TX, USA, 1994; Volume I, pp. 484–496.

8. Shoesmith, D.W.; Ikeda, B.M.; LeNeveu, D.M. Modeling the failure of nuclear waste containers. *Corrosion* **1997**, *53*, 820–829. [CrossRef]

9. DOE (United States Department of Energy DOE). *Yucca Mountain Repository License Application*; Technical Report DOW/RW-0573; US Department of Energy: Washington, DC, USA, 2008.

10. JNC. *H-12: Project to Establish the Scientific and Technical Basis for HLW Disposal in Japan, Porting Report 2, Repository Design and Engineering Technology*; Technical Report JNC TN1410 2000-003; Japan Nuclear Cycle Development Institute: Tokyo, Japan, 2000.

11. Ogawa, Y.; Suzuki, S.; Kubota, S.; Deguchi, A. Re-evaluation of the required thickness of the carbon steel overpack for high-level radioactive waste disposal in Japan based on the latest scientific and engineering knowledge. *Corros. Eng. Sci. Technol.* **2017**, *52*, 204–209. [CrossRef]

12. Nakayama, G.; Nakamura, N.; Fukaya, Y.; Akashi, M.; Ueda, H. Assessment of crevice corrosion and hydrogen-induced stress-corrosion cracks in titanium-carbon steel composite overpack for geological disposal of high-level radioactive waste. In *Prediction of Long Term Corrosion Behaviour in Nuclear Waste Systems*; Féron, D., Macdonald, D.D., Eds.; European Federation of Corrosion, Number 36; Maney: London, UK, 2003; Chapter 25; pp. 373–394.

13. Nakayama, G.; Murakami, K.; Akashi, M. Assessment of crevice corrosion and hydrogen induced stress corrosion cracks of Ti-Pd alloys for HLW overpack in deep underground water environments. *Mat. Res. Soc. Symp. Proc.* **2003**, *757*, 771–778. [CrossRef]

14. Diomidis, N.; King, F. *Development of Copper Coated Canisters for the Disposal of SF and HLW in Switzerland*; Technical Report NTB 20-01; Nagra: Wettingen, Switzerland, 2022.

15. King, F.; Lilja, C.; Pedersen, K.; Pitkänen, P.; Vähänen, M. *An Update of the State-of-the-Art Report on the Corrosion of Copper under Expected Conditions in a Deep Geologic Repository*; Technical Report SKB TR-10-67; Svensk Kärnbränslehantering AB: Stockholm, Sweden, 2010.

16. King, F.; Lilja, C.; Vähänen, M. Progress in the understanding of the long-term corrosion behaviour of copper canisters. *J. Nucl. Mater.* **2013**, *438*, 228–237. [CrossRef]

17. Hall, D.S.; Behazin, M.; Binns, W.J.; Keech, P.G. An evaluation of corrosion processes affecting copper-coated nuclear waste containers in a deep geological repository. *Progr. Mater. Sci.* **2021**, *118*, 100766. [CrossRef]

18. SKB. *Corrosion Calculations Report for the Safety Assessment SR-Site*; Technical Report SKB TR-10-66; Svensk Kärnbränslehantering AB: Stockholm, Sweden, 2010.

19. Asano, H.; Nakamura, A.; Kobayashi, M. Long term integrity of overpack closure weld for HLW geological disposal. Part 1—Prediction and evaluation method for structural integrity of weld joint. *Corros. Eng. Sci. Technol.* **2011**, *46*, 165–170. [CrossRef]

20. King, F.; Burt, D.; Ganeshalingam, J.; Gardner, P.; Sanderson, D.; Watson, S.; Padovani, C. Coupled analysis of mechanical- and corrosion-related degradation of carbon steel spent fuel container. *Corros. Eng. Sci. Technol.* **2014**, *49*, 442–4591. [CrossRef]

21. Posiva, S.K.B. *The Integrated Sulfide Project—Summary Report. A Collaboration Project 2014–2018*; Technical Report 09; Posiva Oy: Eurajoki, Finland; Svensk Kärnbränslehantering AB: Stockholm, Sweden, 2021.

22. SRG (Scientific Review Group). *An Evaluation of the Environmental Impact Statement on Atomic Energy of Canada Limited's Concept for the Disposal of Canada's Nuclear Fuel Waste*; Report of the Scientific Review Group; Advisory to the Nuclear Fuel Waste Management and Disposal Concept Environmental Assessment Panel; Canadian Environmental Assessment Agency: Ottawa, ON, Canada, 1995.

23. Duquette, D.J.; Latanision, R.M.; Di Bella, C.A.W.; Kirstein, B.E. Corrosion issues related to disposal of high-level nuclear waste in the Yucca Mountain repository—Peer reviewers' perspective. *Corrosion* **2009**, *65*, 272–280. [CrossRef]

24. King, F. Predicting the lifetimes of nuclear waste containers. *JOM* **2014**, *66*, 526–537. [CrossRef]

25. King, F.; Kolář, M.; Briggs, S.; Behazin, M.; Keech, P.; Diomidis, N. Review of the modelling of corrosion processes and lifetime prediction for HLW/SF containers—Part 2. Performance assessment models. *Corros. Mater. Degrad.* **2024**, *to be published*.

26. King, F.; Wu, H.; Diomidis, N. *Probabilistic Canister Breaching Model (PBCM) for Carbon Steel Canisters in a Deep Geological Repository in Opalinus Clay*; Technical Report; Nagra: Wettingen, Switzerland, *to be published*.

27. Féron, D.; Macdonald, D.D. Prediction of long term corrosion behaviour in nuclear waste systems. *Mat. Res. Soc. Symp. Proc.* **2006**, *932*, 351. [CrossRef]

28. Macdonald, D.D. The Holy Grail: Deterministic prediction of corrosion damage thousands of years into the future. In *Prediction of Long Term Corrosion Behaviour in Nuclear Waste Systems*; Féron, D., Macdonald, D.D., Eds.; European Federation of Corrosion, Number 36; Maney: London, UK, 2003; Chapter 6; pp. 75–90.

29. Macdonald, D.D. The role of determinism in the prediction of corrosion damage. *Corros. Mater. Degrad.* **2023**, *4*, 212–273. [CrossRef]

30. Crusset, D.; Deydier, V.; Necib, S.; Gras, J.-M.; Combrade, P.; Féron, D.; Burger, E. Corrosion of carbon steel components in the French high-level waste programme: Evolution of disposal concept and selection of materials. *Corros. Eng. Sci. Technol.* **2017**, *52*, 17–24. [CrossRef]

31. Diomidis, N.; Johnson, L.H. Materials options and corrosion-related considerations in the design of spent fuel and high-level waste disposal canisters for a deep geological repository in Opalinus Clay. *JOM* **2014**, *66*, 461–470. [CrossRef]

32. Sandia. *General Corrosion and Localized Corrosion of Waste Package Outer Barrier*; Technical Report ANL-EBS-MD-000003 REV 03C; Sandia National Laboratories: Las Vegas, NV, USA, 2007.

33. Macdonald, D.D. The Point Defect Model for the passive state. *J. ElectroChem. Soc.* **1992**, *139*, 3434–3449. [CrossRef]

34. Macdonald, D.D. Passivity: The key to our metals-based civilization. *Pure Appl. Chem.* **1999**, *71*, 951–978. [CrossRef]

35. Macdonald, D.D. The history of the Point Defect Model for the passive state: A brief review of film growth aspects. *Electrochim. Acta* **2011**, *56*, 1761–1772. [CrossRef]

36. Bildstein, O.; Trotognon, L.; Perronnet, M.; Jullien, M. Modelling iron-clay interactions in deep geological disposal conditions. *Phys. Chem. Earth* **2006**, *31*, 618–625. [CrossRef]

37. Samper, J.; Lu, C.; Montenegro, L. Reactive transport model of interactions of corrosion products and bentonite. *Phys. Chem. Earth* **2008**, *33*, S306–S316. [CrossRef]

38. Marty, N.C.M.; Fritz, B.; Clément, A.; Michau, N. Modelling the long term alteration of the engineered bentonite barrier in an underground radioactive waste repository. *Appl. Clay Sci.* **2010**, *47*, 82–90. [CrossRef]

39. King, F.; Kolář, M. Prediction of the lifetimes of copper nuclear waste containers under restrictive mass-transport and evolving redox conditions. In *Proceedings of CORROSION95*; NACE International: Houston, TX, USA, 1995; paper 425.

40. King, F.; Kolář, M.; Maak, P. Reactive-transport model for the prediction of the uniform corrosion behaviour of copper used fuel containers. *J. Nucl. Mater.* **2008**, *379*, 133–141. [CrossRef]

41. Bataillon, C.; Bouchon, F.; Chainias-Hillairet, C.; Desgranges, C.; Hoareau, E.; Marin, F.; Perrin, S.; Tupin, M.; Talnadier, J. Corrosion modelling of iron based alloy in nuclear waste repository. *Electrochim. Acta* **2010**, *55*, 4451–4467. [CrossRef]

42. Shibata, T.; Watanabe, M.; Taniguchi, N.; Shimizu, A. Modelling of carbon steel corrosion under oxygen depleted environment. *Corros. Eng. Sci. Technol.* **2014**, *49*, 435–441. [CrossRef]

43. Hedin, A.; Johansson, A.J.; Lilja, C. Copper corrosion in pure water—Scientific and post-closure safety aspects. In Proceedings of the International High-Level Radioactive Waste Management Conference, Charlotte, NC, USA, 9–13 April 2017; American Nuclear Society: La Grange Park, IL, USA, 2017; pp. 559–567.

44. King, F.; Litke, C.D.; Quinn, M.J.; LeNeveu, D.M. The measurement and prediction of the corrosion potential of copper in chloride solutions as a function of oxygen concentration and mass-transfer coefficient. *Corros. Sci.* **1995**, *37*, 833–851. [CrossRef]

45. King, F.; Briggs, S. *Development and Validation of a COMSOL Version of the Copper Corrosion Model*; Technical Report NWMO-TR-2022-08; Nuclear Waste Management Organization: Toronto, ON, Canada, 2023.

46. Honda, A.; Taniguchi, N.; Ishikawa, H.; Hoch, A.R.; Porter, F.M.; Sharland, S.M. A modelling study for long-term life prediction of carbon steel overpack for geological isolation of high-level radioactive waste. In Proceedings of the International Symposium on Plant Aging and Life Prediction of Corrodible Structures, Sapporo, Japan, 15–18 May 1995; Shoji, T., Shibata, T., Eds.; NACE International: Houston, TX, USA, 1997; pp. 217–227.

47. Macdonald, D.D.; Sharifi-Asl, S. *Is Copper Immune to Corrosion When in Contact with Water and Aqueous Solutions?* Technical Report SSM 2011:09; Strålsäkerhetsmyndigheten: Stockholm, Sweden, 2011.

48. Macdonald, D.D.; Sharifi-Asl, S. Volt Equivalent diagrams as a means of displaying the electrochemical thermodynamics of the sulfur-water system. *Corros. Sci.* **2014**, *81*, 102–109. [CrossRef]

49. Lilja, C.; King, F.; Puigdomenech, I.; Pastina, B. Speciation of copper in high chloride concentrations, in the context of corrosion of copper canisters. *Mater. Corros.* **2021**, *72*, 293–299. [CrossRef]

50. Hesketh, J.; Haynes, H.; Reddy, B.; Rance, A.; Padovani, C.; Diomidis, N. Carbon steel corrosion in a bentonite buffer: A comparison between in-situ exposure and lab-based experiment. *Mater. Corros.* **2023**, *74*, 1728–1745. [CrossRef]

51. Diomidis, N.; King, F. The corrosion of radioactive waste disposal canisters based on in situ tests. In *Nuclear Corrosion: Research, Progress and Challenges*; Ritter, S., Ed.; European Federation of Corrosion, Number 69; Woodhead Publishing: Duxford, UK, 2020; Chapter 10; pp. 371–389.

52. Neff, D.; Dillmann, P.; Descostes, M.; Beranger, G. Corrosion of iron archaeological artefacts in soil: Estimation of the average corrosion rates involving analytical techniques and thermodynamic calculations. *Corros. Sci.* **2006**, *48*, 2947–2970. [CrossRef]

53. Hélie, M.; Desgranges, C.; Perrin, S. Prediction of corrosion behaviour of HLW containers in the framework of the French interim storage concept. *Nucl. Technol.* **2006**, *155*, 120–132. [CrossRef]

54. Ahn, T.; Jung, H.; He, X.; Pensado, O. Understanding long-term corrosion of Alloy 22 container in the potential Yucca Mountain repository for high-level nuclear waste disposal. *J. Nucl. Mater.* **2008**, *379*, 33–41. [CrossRef]

55. Kojima, Y.; Hioki, T.; Tsujikawa, S. Simulation of the state of carbon steel n years after disposal with n years of corrosion product on its surface in a bentonite environment. *Mat. Res. Soc. Symp. Proc.* **1995**, *353*, 711–718. [CrossRef]

56. Taniguchi, N. Effect of magnetite as a corrosion product on the corrosion of carbon steel overpack. In *Prediction of Long Term Corrosion Behaviour in Nuclear Waste Systems*; Féron, D., Macdonald, D.D., Eds.; European Federation of Corrosion, Number 36; Maney: London, UK, 2003; Chapter 28; pp. 424–438.

57. Macdonald, D.D. On the existence of our metals-based civilization. I. Phase-space analysis. *J. ElectroChem. Soc.* **2006**, *153*, B213–B224. [CrossRef]

58. Macdonald, D.D. On the tenuous nature of passivity and its role in the isolation of HLNW. *J. Nucl. Mater.* **2008**, *379*, 24–32. [CrossRef]

59. Macdonald, D.D.; Engelhardt, G.; Jayaweera, P.; Priyantha, N.; Davydov, A. The deterministic prediction of localised corrosion damage to Alloy C-22 HLNW canisters. In *Prediction of Long Term Corrosion Behaviour in Nuclear Waste Systems*; Féron, D., Macdonald, D.D., Eds.; European Federation of Corrosion, Number 36; Maney: London, UK, 2003; Chapter 8; pp. 104–117.

60. Lu, P.; Kursten, B.; Macdonald, D.D. Deconvolution of the partial anodic and cathodic processes during the corrosion of carbon steel in concrete pore solution under simulated anoxic conditions. *Electrochim. Acta.* **2014**, *143*, 312–323. [CrossRef]

61. McMillion, L.G.; Sun, A.; Macdonald, D.D.; Jones, D.A. General corrosion of Alloy 22: Experimental determination of model parameters from electrochemical impedance spectroscopy data. *Metall. Mater. Trans. A* **2005**, *36A*, 1129–1141. [CrossRef]

62. Urquidi-Macdonald, M.; Macdonald, D.D. Transients in the growth of passive films on high level nuclear waste canisters. In *Prediction of Long Term Corrosion Behaviour in Nuclear Waste Systems*; Féron, D., Macdonald, D.D., Eds.; European Federation of Corrosion, Number 36; Maney: London, UK, 2003; Chapter 12; pp. 165–178.

63. Lu, P.; Sharifi-Asl, S.; Kursten, B.; Macdonald, D.D. The irreversibility of the passive state of carbon steel in the alkaline concrete pore solution under simulated anoxic conditions. *J. ElectroChem. Soc.* **2015**, *162*, C572–C581. [CrossRef]

64. Macdonald, D.D.; Mao, F.; Dong, C.; Sharifi-Asl, S. *Measurements of Parameter Values for Predicting Corrosion Phenomena on Copper in Swedish HLNW Repositories. Phase IV: Impact of Chloride Ion on the Passivity and Pitting of Copper*; Technical Report SSM 2016:30; Strålsäkerhetsmyndigheten: Stockholm, Sweden, 2016.

65. Mao, F.; Dong, C.; Sharifi-Asl, S.; Lu, P.; Macdonald, D.D. Passivity breakdown on copper: Influence of chloride ion. *Electrochim. Acta.* **2014**, *144*, 391–399. [CrossRef]

66. Huttunen-Saarivirta, E.; Ghanbari, E.; Mao, F.; Rajala, P.; Carpén, L.; Macdonald, D.D. Kinetic properties of the passive film on copper in the presence of sulfate-reducing bacteria. *J. ElectroChem. Soc.* **2018**, *165*, C450–C460. [CrossRef]

67. Martino, T.; Chen, J.; Guo, M.; Ramamurthy, S.; Shoesmith, D.W.; Noël, J.J. Comments on E. Huttunen-Saarivirta et al. Kinetic Properties of the Passive Film on Copper in the Presence of Sulfate-Reducing Bacteria. *J. ElectroChem. Soc.* **2019**, *166*, Y13–Y16. [CrossRef]

68. Huttunen-Saarivirta, E.; Rajala, P.; Carpén, L.; Wang, J.; Liu, F.; Ghanbari, E.; Mao, F.; Dong, C.; Yang, J.; Sharifi-Asl, S.; et al. Response to "Comments on E. Huttunen-Saarivirta et al.; 'Kinetic Properties of the Passive Film on Copper in the Presence of Sulfate-Reducing Bacteria" by T. Martino, J. Chen, M. Guo, S. Ramamurthy, D.W. Shoesmith, and J.J. Noël. *J. ElectroChem. Soc.* **2019**, *166*, Y17–Y26. [CrossRef]

69. Bataillon, C. Application of the Point Defect Model to modelling the corrosion of iron based canisters in geological repository. In *Prediction of Long Term Corrosion Behaviour in Nuclear Waste Systems*; Féron, D., Macdonald, D.D., Eds.; European Federation of Corrosion, Number 36; Maney: London, UK, 2003; Chapter 11; pp. 154–164.

70. King, F.; Kolář, M.; Vähänen, M. Reactive-transport modelling of the sulphide-assisted corrosion of copper nuclear waste containers. In *Sulphur-Assisted Corrosion in Nuclear Disposal Systems*; Kursten, B., Féron, D., Druyts, F., Eds.; European Federation of Corrosion; Maney Publishing: Leeds, UK, 2011; Chapter 9; Volume 59, pp. 152–164.

71. King, F.; Kolář, M.; Vähänen, M.; Lilja, C. Modelling the long-term corrosion behaviour of copper canisters in a KBS-3 repository. *Corros. Eng. Sci. Technol.* **2011**, *46*, 217–222. [CrossRef]

72. King, F.; Kolář, M.; Puigdomenech, I.; Pitkänen, P.; Lilja, C. Modeling microbial sulfate reduction and the consequences for corrosion of copper canisters. *Mater. Corros.* **2021**, *72*, 339–347. [CrossRef]

73. King, F.; Kolář, M.; Keech, P.G. Simulations of long-term anaerobic corrosion of carbon steel containers in Canadian deep geological repository. *Corros. Eng. Sci. Technol.* **2014**, *49*, 455–460. [CrossRef]

74. Mohamed-Said, M.; Vuillemin, B.; Oltra, R.; Trenty, L.; Crusset, D. One-dimensional porous electrode model for predicting the corrosion rate under a conductive corrosion product layer. *J. ElectroChem. Soc.* **2017**, *164*, E3372–E3385. [CrossRef]

75. Mohamed-Said, M.; Vuillemin, B.; Oltra, R.; Trenty, L.; Crusset, D. Predictive modelling of the corrosion rate of carbon steel focusing on the effect of the precipitation of corrosion products. *Corros. Eng. Sci. Technol.* **2017**, *52*, 178–185. [CrossRef]

76. King, F. *Mixed-Potential Modelling of the Corrosion of Copper in the Presence of Sulphide*; Working Report, WR 2007-63; Posiva Oy: Eurajoki, Finland, 2008.

77. King, F.; Kolář, M. A numerical model for the corrosion of copper nuclear waste containers. *Mat. Res. Soc. Symp. Proc.* **1996**, *412*, 555–562. [CrossRef]

78. King, F.; Kolář, M. *The Copper Container Corrosion Model Used in AECL's Second Case Study*; Technical Report 06819-REP-01200-10041-R00; Ontario Power Generation Nuclear Waste Management Division: Toronto, ON, Canada, 2000.

79. King, F.; Kolář, M. *Copper Sulfide Model (CSM)—Model Improvements, Sensitivity Analyses, and Results from the Integrated Sulfide Project Inter-Model Comparison Exercise*; Technical Report TR-18-08; Swedish Nuclear Fuel and Waste Management Co.: Solna, Sweden, 2019.

80. King, F.; Kolář, M. Lifetime predictions for nuclear waste disposal containers. *Corrosion* **2019**, *75*, 309–323. [CrossRef]

81. King, F.; Kolář, M. *Theory Manual for the Steel Corrosion Model Version 1.0*; Technical Report NWMO-TR-2009-07; Nuclear Waste Management Organization: Toronto, ON, Canada, 2009.

82. King, F.; Chen, J.; Qin, Z.; Shoesmith, D.; Lilja, C. Sulphide-transport control of the corrosion of copper canisters. *Corros. Eng. Sci. Technol.* **2017**, *52*, 210–216. [CrossRef]

83. King, F.; Kolář, M.; Shoesmith, D.W. Modelling the effects of porous and semi-permeable layers on corrosion processes. In Proceedings of the CORROSION96, Denver, CO, USA, 24–29 March 1996; NACE International: Houston, TX, USA, 1996. paper 380.

84. Liu, M.; Kwon, B.; Kang, P.K. Machine learning to predict effective reaction rates in 3D porous media from pore structural features. *Sci. Rep.* **2022**, *12*, 5486. [CrossRef] [PubMed]

85. Le Traon, C.; Aquino, T.; Bouchez, C.; Maher, K.; Le Borgne, T. Effective kinetics driven by dynamic concentration gradients under coupled transport and reaction. *Geochim. Cosmochim. Acta* **2021**, *306*, 189–209. [CrossRef]

86. Manaka, M. Comparison of rates of pyrite oxidation by dissolved oxygen in aqueous solution and in compacted bentonite. *J. Mineral. Petrol. Sci.* **2009**, *104*, 59–68. [CrossRef]

87. Lu, C.; Samper, J.; Fritz, B.; Clement, A.; Montenegro, L. Interactions of corrosion products and bentonite: An extended multicomponent reactive transport model. *Phys. Chem. Earth* **2011**, *36*, 1661–1668. [CrossRef]

88. Ngo, V.V.; Delalande, M.; Clément, A.; Michau, N.; Fritz, B. Coupled transport-reaction modelling of the long-term interaction between iron, bentonite and Callovo-Oxfordian claystone in radioactive waste confinement systems. *Appl. Clay Sci.* **2014**, *101*, 430–443. [CrossRef]

89. Rashwan, T.L.; Asad, M.A.; Molnar, I.L.; Behazin, M.; Keech, P.G.; Krol, M.M. Exploring the governing transport mechanisms of corrosive agents in a Canadian deep geological repository. *Sci. Total Environ.* **2022**, *828*, 153944. [CrossRef] [PubMed]

90. Giroud, N.; Tomonaga, Y.; Wersin, P.; Briggs, S.; King, F.; Vogt, T.; Diomidis, N. On the fate of oxygen in a spent fuel emplacement drift in Opalinus Clay. *Appl. GeoChem.* **2018**, *97*, 370–378. [CrossRef]

91. Vokál, A.; Lukin, D.; Vopálka, D. Carbon steel canister performance assessment: Iron transfer study. *Mat. Res. Soc. Symp. Proc.* **2006**, *932*, 877–884. [CrossRef]

92. King, F.; Puigdomenech, I.; Lilja, C. *Effect of High Groundwater Chloride Concentration on the Corrosion of Copper Canisters*; Working Report WR-2021-10; Posiva Oy: Eurajoki, Finland, 2021.

93. Honda, A.; Taniguchi, N.; Ishikawa, H.; Kawasaki, M. A modelling study of general corrosion of copper overpack for geological isolation of high-level radioactive waste. *Mat. Res. Soc. Symp. Proc.* **1999**, *556*, 911–918. [CrossRef]

94. Qin, Z.; Daljeet, R.; Ai, M.; Farhangi, N.; Noël, J.J.; Ramamurthy, S.; Shoesmith, D.; King, F.; Keech, P. The active/passive conditions for copper corrosion under nuclear waste repository environment. *Corros. Eng. Sci. Technol.* **2017**, *52*, 45–49. [CrossRef]

95. Nakayama, G.; Fukaya, Y.; Akashi, M. The effects of carbonate-bicarbonate concentration on empirical corrosion diagrams of mild steel as a material of geological disposal package for high level nuclear wastes. *Mat. Res. Soc. Symp. Proc.* **1997**, *451*, 567–572. [CrossRef]

96. Taniguchi, N.; Honda, A.; Ishikawa, H. Experimental investigation of passivation behavior and corrosion rate of carbon steel in compacted bentonite. *Mat. Res. Soc. Symp. Proc.* **1998**, *506*, 495–501. [CrossRef]

97. Marsh, G.P.; Taylor, K.J.; Sharland, S.M.; Tasker, P.W. An approach for evaluation the general and localised corrosion of carbon-steel contains for nuclear waste disposal. *Mat. Res. Soc. Symp. Proc.* **1987**, *84*, 227–238. [CrossRef]

98. Briggs, S.; Lilja, C.; King, F. Probabilistic model for pitting of copper canisters. *Mater. Corros.* **2021**, *72*, 308–316. [CrossRef]

99. Féron, D.; Crusset, D.; Gras, J.-M. Corrosion issues in the French high-level nuclear waste program. *Corrosion* **2009**, *65*, 213–223. [CrossRef]

100. King, F.; LeNeveu, D. Prediction of the lifetimes of copper nuclear waste containers. In Proceedings of the Topical Meeting on Nuclear Waste Packaging. Focus 91, Las Vegas, NV, USA, 29 September–2 October 1991; American Nuclear Society: La Grange Park, IL, USA, 1992; pp. 253–261.

101. Akashi, M.; Fukuda, T.; Yoneyama, H. A corrosion localization assessment of the mild steel used for nuclear waste package. *Mat. Res. Soc. Symp. Proc.* **1990**, *176*, 525–532. [CrossRef]

102. Sharland, S.M.; Tasker, P.W. A mathematical model of crevice corrosion and pitting corrosion—I. The physical model. *Corros. Sci.* **1988**, *28*, 603–620. [CrossRef]

103. Watson, M.K.; Postlethwaite, J. Numerical simulation of crevice corrosion of stainless steels and nickel alloys in chloride solutions. *Corrosion* **1990**, *46*, 522–530. [CrossRef]

104. Taxén, C. *Pitting Corrosion of Copper. An Equilibrium—Mass Transport Study*; Technical Report SKB TR-02-22; Svensk Kärnbränslehantering AB: Stockholm, Sweden, 2002.

105. Taxén, C. *Pitting Corrosion of Copper. Further Model Studies*; Technical Report SKB TR-02-23; Svensk Kärnbränslehantering AB: Stockholm, Sweden, 2002.

106. Krouse, D.; Laycock, N.; Padovani, C. Modelling pitting corrosion of stainless steel in atmospheric exposure to chloride containing environments. *Corros. Eng. Sci. Technol.* **2014**, *49*, 521–528. [CrossRef]

107. Macdonald, D.D.; Qiu, J.; Sharifi-Asl, S.; Yang, J.; Engelhardt, G.R.; Xu, Y.; Ghanbari, E.; Xu, A.; Saatchi, A.; Kovalov, D. Pitting of carbon steel in the synthetic concrete pore solution. *Mater. Corros.* **2021**, *72*, 166–193. [CrossRef]

108. Dunn, D.S.; Cragnolino, G.A.; Sridhar, N. An electrochemical approach to predicting long-term localized corrosion of corrosion-resistant high-level waste container materials. *Corrosion* **2000**, *56*, 90–104. [CrossRef]

109. Henshall, G.A. Stochastic models for predicting pitting corrosion damage of HLRW containers. In Proceedings of the Topical Meeting on Nuclear Waste Packaging. Focus 91, Las Vegas, NV, USA, 29 September–2 October 1991; American Nuclear Society: La Grange Park, IL, USA, 1992; pp. 225–232.

110. Henshall, G.A. Stochastic modelling of the influence of environment on pitting corrosion damage of radioactive-waste containers. *Mat. Res. Soc. Symp. Proc.* **1995**, *353*, 679–686. [CrossRef]

111. Henshall, G.A. A phenomenological approach to simulating the evolution of radioactive-waste container damage due to pitting corrosion. *Mat. Res. Soc. Symp. Proc.* **1996**, *412*, 613–619. [CrossRef]

112. Apted, M.; King, F.; Langmuir, D.; Arthur, R.; Kessler, J. The unlikelihood of localized corrosion of nuclear waste packages arising from deliquescent brine formation. *JOM* **2005**, *57*, 43–48. [CrossRef]

113. Di Caprio, D.; Vautrin-Ul, C.; Stafiej, J.; Chaussé, A.; Féron, D.; Bidiali, J.P. Cellular automata approach for morphological evolution of localised corrosion. *Corros. Eng. Sci. Technol.* **2011**, *46*, 223–227. [CrossRef]

114. Briggs, S.; Lilja, C.; King, F. *Probabilistic Model for the Pitting of Copper Canisters under Aerobic, Saturated Conditions*; Technical Report SKB TR-20-01; Svensk Kärnbränslehantering AB: Stockholm, Sweden, 2020.

115. Wang, L. *Near-Field Chemistry of a HLW/SF Repository in Boom Clay—Scoping Calculations Relevant to the Ercontainer Design*; Technical Report SCK●CEN-ER-17; SCK●CEN: Boeretang, Belgium, 2006.

116. Foct, F.; Gras, J.-M. Semi-empirical model for carbon steel corrosion in long term geological nuclear waste disposal. In *Prediction of Long Term Corrosion Behaviour in Nuclear Waste Systems*; Féron, D., Macdonald, D.D., Eds.; European Federation of Corrosion, Number 36; Maney: London, UK, 2003; Chapter 7; pp. 91–102.

117. Dunn, D.S.; Pensado, O.; Pan, Y.-M.; Yang, L.T.; He, X. Modeling corrosion processes for Alloy 22 waste packages. *Mat. Res. Soc. Symp. Proc.* **2006**, *932*, 271. [CrossRef]

118. Bresle, A.; Saers, J.; Arrhenius, B. *Studies in Pitting Corrosion on Archaeological Bronzes. Copper*; Technical Report SKB TR-83-05; Svensk Kärnbränslehantering AB: Stockholm, Sweden, 1983.

119. Romanoff, M. *Underground Corrosion*; NACE International: Houston, TX, USA, 1989.

120. Fukuda, T.; Akashi, M. A Gumbel distribution model for assessing the general corrosion propagation of mild steel used for nuclear waste disposal package. In *Life Prediction of Corrodible Structures*; Parkins, R.N., Ed.; NACE International: Houston, TX, USA, 1994; Volume I, pp. 419–428.

121. Johnson, L.H.; King, F. The effect of the evolution of environmental conditions on the corrosion evolutionary path in a repository for spent fuel and high-level waste in Opalinus Clay. *J. Nucl. Mater.* **2008**, *379*, 9–15. [CrossRef]

122. SKB. *Post-Closure Safety for the Final Repository for Spent Nuclear Fuel at Forsmark. Fuel and Canister Process Report*, PSAR version; Technical Report SKB TR-21-02; Svensk Kärnbränslehantering AB: Stockholm, Sweden, 2022.

123. He, X.; Noël, J.J.; Shoesmith, D.W. Crevice corrosion damage function for grade-2 titanium of iron content 0.078 wt% at 95C. *Corros. Sci.* **2005**, *47*, 1177–1195. [CrossRef]

124. Payer, J.H.; Kelly, R.G. Perspectives on localized corrosion in thin layers of particulate. *Mat. Res. Soc. Symp. Proc.* **2007**, *985*, 801. [CrossRef]

125. Sharland, S.M. The theoretical evaluation of localised corrosion in radioactive waste canisters. *Mat. Res. Soc. Symp. Proc.* **1987**, *84*, 283–293. [CrossRef]

126. Sharland, S.M. A mathematical model of crevice corrosion and pitting corrosion—II. The mathematical solution. *Corros. Sci.* **1988**, *28*, 621–630. [CrossRef]

127. Sharland, S.M.; Jackson, C.P.; Diver, A.J. A finite-element model of the propagation of corrosion crevices and pits. *Corros. Sci.* **1989**, *29*, 1149–1166. [CrossRef]

128. Sharland, S.M.; Naish, C.C.; Taylor, K.J.; Marsh, G.P. An experimental and modelling study of the localized corrosion of carbon steel overpacks for the geological disposal of radioactive waste. In *Life Prediction of Corrodible Structures*; Parkins, R.N., Ed.; NACE International: Houston, TX, USA, 1994; Volume I, pp. 402–418.

129. Mousson, J.-L.; Vuillemin, B.; Oltra, R.; Crusset, D.; Santarini, G.; Combrade, P. Modelling of the propagation of crevice corrosion. In *Prediction of Long Term Corrosion Behaviour in Nuclear Waste Systems, Proceedings of the 2nd International Workshop, Nice, France, 14–15 September 2004*; Crusset, D., Féron, D., Gras, J.-M., Macdonald, D.D., Eds.; Andra Science and Technology Series: Châtenay-Malbry, France, 2004; pp. 180–186.

130. Sridhar, N.; Cragnolino, G.; Pennick, H.; Torng, T.Y. Application of a transient crevice corrosion model to the prediction of performance of high-level nuclear waste container materials. In *Life Prediction of Corrodible Structures*; Parkins, R.N., Ed.; NACE International: Houston, TX, USA, 1994; Volume I, pp. 429–453.

131. Farmer, J.C.; McCright, R.D.; Estill, J.C.; Gordon, S.R. Development of integrated mechanistically-based degradation-mode models for performance assessment of high-level waste containers. *Mat. Res. Soc. Symp. Proc.* **1999**, *556*, 855–862. [CrossRef]

132. Sharland, S.M. A mathematical model of the initiation of crevice corrosion in metals. *Corros. Sci.* **1992**, *33*, 183–201. [CrossRef]

133. Hoch, A.R.; Honda, A.; Porter, F.M.; Sharland, S.M.; Taniguchi, N. Development of mathematical models for long-term prediction of corrosion behaviour of carbon steel overpacks for radioactive waste disposal. *Mat. Res. Soc. Symp. Proc.* **1997**, *465*, 683–690. [CrossRef]

134. Taxén, C. Pitting corrosion of copper. Equilibrium-mass transport limitations. *Mat. Res. Soc. Symp. Proc.* **2000**, *608*, 103–108. [CrossRef]

135. Engelhardt, G.R.; McMillion, L.G.; Macdonald, D.D. A mathematical model for crevice corrosion under porous deposits. *J. Nucl. Mater.* **2008**, *379*, 48–53. [CrossRef]

136. Björck, M.; Taxen, C.; Vuoristo, T.; Elger, R.; Zavalis, T.; Wikström, L.; Sparr, M. *Embedded oxide particles in Friction Stir Welds*; Technical Report Posiva SKB Report 10; Posiva Oy: Eurajoki, Finland; Svensk Kärnbränslehantering AB: Stockholm, Sweden, 2019.

137. Engelhardt, G.; Macdonald, D.D. Monte-Carlo simulation of pitting corrosion with a deterministic model for repassivation. *J. ElectroChem. Soc.* **2020**, *167*, 013540. [CrossRef]

138. Qiu, J.; Zhu, Y.; Xu, Y.; Li, Y.; Mao, F.; Wu, A.; Macdonald, D.D. Effect of chloride on the pitting corrosion of carbon steel in alkaline solutions. *J. ElectroChem. Soc.* **2022**, *169*, 031501. [CrossRef]

139. Shoesmith, D.W.; Noël, J.J. Corrosion of titanium and its alloys. In *Shreir's Corrosion*, 4th ed.; Cottis, R.A., Graham, M.J., Lindsay, R., Lyon, S.B., Richardson, J.A., Scantlebury, J.D., Stott, F.H., Eds.; Elsevier: Amsterdam, The Netherlands, 2010; Volume 3, Chapter 3.10; pp. 2042–2052.

140. Chen, Z.Y.; Kelly, R.G. Computational modelling of bounding conditions for pit size on stainless steel in atmospheric environments. *J. ElectroChem. Soc.* **2010**, *157*, C69–C78. [CrossRef]

141. Chen, Z.Y.; Cui, F.; Kelly, R.G. Calculations of the cathodic current delivery capacity and stability of crevice corrosion under atmospheric conditions. *J. ElectroChem. Soc.* **2008**, *155*, C360–C368. [CrossRef]

142. Agarwal, A.S.; Landau, U.; Shan, X.; Payer, J.H. Modeling the effects of crevice former, particulates, and the evolving surface profile in crevice corrosion. *ECS Trans.* **2007**, *3*, 459–471. [CrossRef]

143. Payer, J.H.; Shan, X.; Agarwal, A.S.; Landau, U. Crevice corrosion damage evolution in high temperature brines. *ECS Trans.* **2008**, *11*, 39–53. [CrossRef]

144. Watson, M.K.; Postlethwaite, J. Numerical simulation of crevice corrosion: The effect of the crevice gap profile. *Corros. Sci.* **1991**, *32*, 1253–1262. [CrossRef]

145. Heppner, K.L.; Evitts, R.W.; Postlethwaite, J. Effect of the crevice gap on the initiation of crevice corrosion in passive metals. *Corrosion* **2004**, *60*, 718–728. [CrossRef]

146. Dunn, D.S.; Sridhar, N.; Cragnolino, G.A. Long-term prediction of localized corrosion of Alloy 825 in high-level nuclear waste repository environments. *Corrosion* **1996**, *52*, 115–124. [CrossRef]

147. Sridhar, N.; Dunn, D.; Cragnolino, G. The use of repassivation potential in predicting the p[performance of high-level nuclear waste container materials. *Mat. Res. Soc. Symp. Proc.* **1995**, *353*, 663–670. [CrossRef]

148. Dunn, D.S.; Pensado, O.; Brossia, C.S.; Cragnolino, G.A.; Sridhar, N.; Ahn, T.M. Modelling corrosion of Alloy 22 as a high-level radioactive waste canister material. In *Prediction of Long Term Corrosion Behaviour in Nuclear Waste Systems*; Féron, D., Macdonald, D.D., Eds.; European Federation of Corrosion, Number 36; Maney: London, UK, 2003; Chapter 15; pp. 208–224.

149. Bryan, C.; Jarek, R.; Wolery, T.; Shields, D.; Sutton, M.; Hardin, E.; Barr, D. Evaluation of the corrosivity of dust deposited on waste packages at Yuca Mountain, Nevada. *Mat. Res. Soc. Symp. Proc.* **2006**, *932*, 1061. [CrossRef]

150. Payer, J.H. The proposed Yucca Mountain repository from a corrosion perspective. *Mat. Res. Soc. Symp. Proc.* **2006**, *932*, 341. [CrossRef]

151. Pérez-Brokate, C.F.; di Caprio, D.; Féron, D.; de Lamare, J.; Chaussé, A. Probabilistic cellular automata model of generalised corrosion, transition to localised corrosion. *Corros. Eng. Sci. Technol.* **2017**, *52*, 186–193. [CrossRef]

152. Andra. *Dossier D'autorisation de Creation de L'installation Nucléaire de base (INB) Cigéo. Pièce 7. Version Préliminaire du Rapport de Sûreté. Partie III Démonstration de Sûreté*; Volume 8 La Demonstration de Sûreté après Fermeture; Technical Report CG-TE-D-NTE-AMOA-SR0-0000-21-0007/A; Agence nationale pour la gestion des déchets radioactifs: Châtenay-Malabry, France, 2022.

153. Bulidon, N.; Deydier, V.; Bumbieler, F.; Duret-Thual, C.; Mendibide, C.; Crusset, D. Stress corrosion cracking susceptibility pf P285NH and API 5L X65 steel grades in the high-level radioactive waste repository cell concept. *Mater. Corros.* **2021**, *72*, 154–165. [CrossRef]

154. Maak, P.; King, F. A model for predicting stress corrosion cracking of copper containers in a deep geological repository. *Mat. Res. Soc. Symp. Proc.* **2006**, *932*, 837–843. [CrossRef]

155. King, F. *Assessment of the Stress Corrosion Cracking of Copper Canisters*; Working Report, WR-2021-11; Posiva Oy: Eurajoki, Finland, 2021.

156. King, F.; Kolář, M. *Theory Manual for the Copper Corrosion Model for Stress Corrosion Cracking of Used Fuel Disposal Containers CCM-SCC.0*; Technical Report 06819-REP-01300-10095-R00; Ontario Power Generation Nuclear Waste Management Division: Toronto, ON, Canada, 2004.

157. King, F.; Kolář, M. *Preliminary Assessment of the Stress Corrosion Cracking of Used Fuel Disposal Containers Using the CCM-SCC.0 model*; Technical Report 06819-REP-01300-10103-R00; Ontario Power Generation Nuclear Waste Management Division: Toronto, ON, Canada, 2005.

158. Andresen, P.L.; Gordon, G.M.; Lu, S.C. The stress-corrosion-cracking model for high-level radioactive-waste packages. *JOM* **2005**, *57*, 27–30. [CrossRef]

159. King, F.; Litke, C.D.; Ikeda, B.M. The stress corrosion cracking of copper nuclear waste containers. *Mat. Res. Soc. Symp. Proc.* **1999**, *556*, 887–894. [CrossRef]

160. Shoesmith, D.W.; Noël, J.J.; Hardie, D.; Ikeda, B.M. *Hydrogen Absorption and the Lifetime Performance of Titanium Nuclear Waste Containers*; Technical Report AECL-11770, COG-97-035-I; Atomic Energy of Canada Limited: Pinawa, Manitoba, 1997.

161. Qin, Z.; Shoesmith, D.W. Failure model and Monte Carlo simulations for titanium (grade-7) drip shields under Yucca Mountain repository conditions. *J. Nucl. Mater.* **2008**, *379*, 169–173. [CrossRef]

162. Nakayama, G.; Fukaya, Y.; Akashi, M.; Sawa, S.; Kanno, T.; Owada, H.; Otsuki, A.; Asano, H. Hydrogen-induced stress corrosion crack initiation and propagation in titanium alloys in deep underground environments. In *Prediction of Long Term Corrosion Behaviour in Nuclear Waste Systems, Proceedings of the 2nd International Workshop, Nice, France, 14–15 September 2004*; Crusset, D., Féron, D., Gras, J.-M., Macdonald, D.D., Eds.; Andra Science and Technology Series: Châtenay-Malbry, France, 2004; pp. 35–44.

163. Sandia. *Stress Corrosion Cracking of Waste Package Outer Barrier and Drip Shield Materials*; Technical Report ANL-EBS-MD-000005 REV 04; Sandia National Laboratories: Las Vegas, NV, USA, 2007.

164. SKB. *Plementary Information on Canister Integrity Issues*; Technical Report SKB TR-19-15; Svensk Kärnbränslehantering AB: Stockholm, Sweden, 2019.

165. Hua, F.; Mon, K.; Paathi, P.; Gordon, G.; Shoesmith, D. A review of corrosion of titanium grade 7 and other titanium alloys in nuclear waste repository environments. *Corrosion* **2005**, *61*, 987–1003. [CrossRef]

166. Hua, F.; Mon, K.; Paathi, P.; Gordon, G.; Shoesmith, D. Modeling the hydrogen-induced cracking of titanium alloys in nuclear waste repository environments. *JOM* **2005**, *57*, 20–26. [CrossRef]

167. King, F. Microbiologically influenced corrosion of nuclear waste containers. *Corrosion* **2009**, *65*, 233–251. [CrossRef]

168. Marciales, A.; Peralta, Y.; Haile, T.; Crosby, T.; Wolodko, J. Mechanistic microbiologically influenced corrosion modelling—A review. *Corros. Sci.* **2019**, *146*, 99–111. [CrossRef]

169. Masurat, P.; Eriksson, S.; Pedersen, K. Microbial sulphide production in compacted Wyoming bentonite MX-80 under in situ conditions relevant to a repository for high-level radioactive waste. *Appl. Clay Sci.* **2010**, *47*, 58–64. [CrossRef]

170. Stroes-Gascoyne, S.; Hamon, C.J.; Maak, P.; Russell, S. The effects of the physical properties of highly compacted smectitic clay (bentonite) on the culturability of indigenous microorganisms. *Appl. Clay Sci.* **2010**, *47*, 155–162. [CrossRef]

171. Stroes-Gascoyne, S. *The Potential for Microbial Life in a Canadian High-Level Nuclear Fuel Waste Disposal Vault: A Nutrient and Energy Source Analysis*; Technical Report AECL-9574; Atomic Energy of Canada Limited: Pinawa, Manitoba, 1989.

172. King, F.; Kolář, M.; Stroes-Gascoyne, S. *Theory Manual for the Microbiological Copper Corrosion Model CCM-MIC.0*; Technical Report 06819-REP-01200-10091-R00; Ontario Power Generation Nuclear Waste Management Division: Toronto, ON, Canada, 2002.

173. King, F.; Kolář, M.; Stroes-Gascoyne, S. *Preliminary Simulations of the Long-Term Activity of Microbes in a Deep Geologic Repository Using CCM-MIC.0 and the Implications for Corrosion of Copper Containers*; Technical Report 06819-REP-01200-10104-R00; Ontario Power Generation Nuclear Waste Management Division: Toronto, ON, Canada, 2003.

174. King, F.; Kolář, M.; Stroes-Gascoyne, S.; Bellingham, P.; Chu, J.; Dawe, P.V. Modelling the activity of sulphate-reducing bacteria and the effects on container corrosion in an underground nuclear waste disposal vault. *Mat. Res. Soc. Symp. Proc.* **1999**, *556*, 1167–1174. [CrossRef]

175. Idiart, A.; Coene, E.; Bagaria, F.; Román-Ross Birgersson, M. *Reactive Transport Modelling Considering Transport in Interlayer Water. New Model, Sensitivity Analyses and Results from the Integrated Sulfide Project Inter-Model Comparison Exercise*; Technical Report SKB TR-18-07; Svensk Kärnbränslehantering AB: Stockholm, Sweden, 2019.

176. Pękala, M.; Alt-Epping, P.; Wersin, P. *3D and 1D Dual-Porosity Reactive Transport Simulations—Model Improvements, Sensitivity Analyses, and Results from the Integrated Sulfide Project Inter-Model Comparison Exercise*; Working Report, WR-2018-31; Posiva Oy: Eurajoki, Finland, 2019.

177. Pekala, M.; Wersin, P.; Cloet, V.; Diomidis, N. Reactive transport calculations to evaluate sulphide fluxes in the near-field of a SF/HLW repository in the Opalinus Clay. *Appl. GeoChem.* **2019**, *100*, 169–180. [CrossRef]

178. Hung, C.-C.; Briggs, S.; Yu, Y.-C.; Wu, Y.-C.; King, F. Reactive transport model for the production, transport, and consumption of sulfide in a spent nuclear fuel deep geological repository in crystalline rock. *Mater. Corros.* **2023**, *74*, 1848–1860. [CrossRef]

179. Briggs, S.; Krol, M. *Diffusive Transport Modelling of Corrosion Agents through the Engineered Barrier System in a Deep Geological Repository for Used Nuclear Fuel*; Technical Report NWMO-TR-2018-06; Nuclear Waste Management Organization: Toronto, ON, Canada, 2018.

180. Pedersen, K. Analysis of copper corrosion in compacted bentonite clay as a function of clay density and growth conditions for sulfate-reducing bacteria. *J. Appl. Microbiol.* **2010**, *108*, 1094–1104. [CrossRef]

181. Stroes-Gascoyne, S.; Hamon, C.J.; Maak, P. Limits to the use of highly compacted bentonite as a deterrent for microbiologically influenced corrosion in an nuclear fuel waste repository. *Phys. Chem. Earth* **2011**, *36*, 1630–1638. [CrossRef]

182. Aerts, S. *Effect of Geochemical Conditions on Bacterial Activity*; Technical Report SCK•CEN-ER-75; Belgian Nuclear Research Centre SCK•CEN: Boeretang, Belgium, 2009.

183. Haynes, H.M.; Bailey, M.T.; Lloyd, J.R. Bentonite barrier materials and the control of microbial processes: Safety case implications for the geological disposal of radioactive waste. *Chem. Geol.* **2021**, *581*, 120353. [CrossRef]

184. Taborowski, T.; Bengtsson, A.; Chukharkina, A.; Blom, A.; Pedersen, K. *Bacterial Presence and Activity in Compacted Bentonite*; Technical Report, Microbiology in Nuclear Waste Disposal (MIND); Deliverable D2.4, v2; European Commission: Brussels, Belgium, 2019.

185. King, F.; Kolář, M. *Consequences of Microbial Activity for Corrosion of Copper Used Fuel Containers—Analyses Using the CCM-MIC.0.1 Code*; Technical Report 06819-REP-01300-00120-R00; Ontario Power Generation Nuclear Waste Management Division: Toronto, ON, Canada, 2006.

186. Cloet, V.; Pekala, M.; Smith, P.; Wersin, P.; Diomidis, N. *An Evaluation of Sulphide Fluxes in the Near Field of a HLW Repository*; Technical Report NTB 17-04; Nagra: Wettingen, Switzerland, 2017.

187. Pekala, M.; Smith, P.; Wersin, P.; Diomidis, N.; Cloet, V. Comparison of models to evaluate microbial sulphide generation and transport in the near field of a SF/HLW repository in Opalinus Clay. *J. Contam. Hydrol.* **2020**, *228*, 103561. [CrossRef]

188. Ma, J.; Pekala, M.; Alt-Epping, P.; Pastina, B.; Maanoja, S.; Wersin, P. 3D modelling of long-term sulfide corrosion of copper canisters in a spent nuclear fuel repository. *Appl. GeoChem.* **2022**, *146*, 105439. [CrossRef]

189. Ma, J.; Alt-Epping, P.; Patina, B.; Niskanen, M.; Salonen, T.; Wersin, P. Development of a 2D model for rapid estimation of sulfide corrosion of copper canisters in a spent nuclear fuel repository. *Mater. Corros.* **2023**, *74*, 1823–1833. [CrossRef]

190. King, F.; Kolář, M. *Modelling the Long-Term Corrosion Behaviour of Copper Canisters in a KBS-3 Repository (Copper Sulfide Model Version 1.1)*; Working Report WR-2021-12; Posiva Oy: Eurajoki, Finland, 2021.

191. King, F.; Kolář, M. *Copper Sulfide Model for the Safety Case for the Operating Licence Application (CSM-SC-OLA)*; Working Report WR-2023-XX; Posiva Oy: Eurajoki, Finland, 2023.

192. King, F.; Ma, J.; Alt-Epping, P.; Wersin, P.; Kolář, M. *Benchmarking of University of Bern Sulfide Model (UBSM) and Copper Sulfide Model Used in the Safety Case SC-OLA*; Working Report, WR-2023-05; Posiva Oy: Eurajoki, Finland, 2023.

193. Posiva. *Sulfide Fluxes and Concentrations in the Spent Nuclear Fuel Repository at Olkiluoto—2021 Update*; Working Report WR-2021-07; Posiva Oy: Eurajoki, Finland, 2021.

194. Briggs, S.; McKelvie, J.; Keech, P.; Sleep, B.; Krol, M. Transient modelling of sulphide diffusion under conditions typical of a deep geological repository. *Corros. Eng. Sci. Technol.* **2017**, *521*, 200–203. [CrossRef]

195. Briggs, S.; McKelvie, J.; Sleep, B.; Krol, M. Multi-dimensional transport modelling of corrosive agents through a bentonite buffer in a Canadian deep geological repository. *Sci. Total Environ.* **2017**, *599–600*, 348–354. [CrossRef]

196. Briggs, S.; McKelvie, J.; Krol, M. Temperature dependent sulphide transport in highly compacted bentonite. In Proceedings of the International High-Level Radioactive Waste Management Conference, Charlotte, NC, USA, 9–13 April 2017; American Nuclear Society: La Grange Park, IL, USA, 2017; pp. 317–321.

197. Morco, R.P.; Jospeh, J.M.; Hall, D.S.; Medri, C.; Shoesmith, D.W.; Wren, J.C. Modelling of radiolytic production of HNO_3 relevant to corrosion of a used fuel container in deep geologic repository environments. *Corros. Eng. Sci. Technol.* **2017**, *52*, 141–147. [CrossRef]

198. Farnan, I.; King, F.; Roberts, D.; Smith, V.; Swanton, S.; Thetford, R. *Effects of Ionising Radiation of Engineered Barrier System Performance*; Technical Report; NDA Report no. RWM/Contr/19/041; Radioactive Waste Management: Oxfordshire, UK, 2019. Available online: https://webarchive.nationalarchives.gov.uk/ukgwa/20200401140306/https://rwm.nda.gov.uk/publication/effects-of-ionising-radiation-on-engineered-barrier-system-performance/ (accessed on 18 April 2023).

199. Westerman, R.E.; Nelson, J.L.; Pitman, S.G.; Kun, W.L.; Basham, S.J.; Moak, D.P. Evaluation of iron-base materials for waste package containers in a salt repository. *Mat. Res. Soc. Symp. Proc.* **1984**, *26*, 427–436. [CrossRef]

200. Shoesmith, D.W.; King, F. *The Effects of Gamma Radiation on the Corrosion of Candidate Materials for the Fabrication of Nuclear Waste Packages*; Technical Report AECL-11999; Atomic Energy of Canada Limited: Pinawa, Manitoba, 1999.

201. Kursten, B.; Macdonald, D.D.; Smart, N.R.; Gaggiano, R. Corrosion issues of carbon steel radioactive waste packages exposed to cementitious materials with respect to the Belgian ercontainer concept. *Corros. Eng. Sci. Technol.* **2017**, *52*, 11–16. [CrossRef]

202. King, F.; Behazin, M. A review of the effect of irradiation on the corrosion of copper-coated used fuel containers. *Corros. Mater. Degrad.* **2021**, *2*, 678–707. [CrossRef]

203. Macdonald, D.D.; Urquidi-Macdonald, M. Thin-layer mixed-potential model for the corrosion of high-level nuclear waste canisters. *Corrosion* **1990**, *46*, 380–390. [CrossRef]

204. Soroka, I.; Chae, N.; Jonsson, M. On the mechanism of γ-radiation-induced corrosion of copper in water. *Corros. Sci.* **2021**, *182*, 109279. [CrossRef]

205. Jonsson, M. Exploring the impact of groundwater constituents and irradiation conditions on radiation-induced corrosion of copper. *Radiat. Phys. Chem.* **2023**, *211*, 111048. [CrossRef]

206. Behazin, M.; Briggs, S.; King, F. Radiation-induced corrosion model for copper-coated used fuel containers. Part 1. Validation of the bulk radiolysis submodel. *Mater. Corros.* **2023**, *182*, 109279. [CrossRef]

207. Joseph, J.M.; Choi, B.S.; Yakabuskie, P.; Wren, J.C. A combined experimental and model analysis on the effect of pH and O_2(aq) on γ-radiolytically produced H_2 and H_2O_2. *Radiat. Phys. Chem.* **2008**, *77*, 1009–1020. [CrossRef]

208. Henshaw, J.; Spahiu, K. *Radiolysis Calculations of Air, Argon and Water Mixtures in a KBS-3 Canister*; Technical Report SKB TR-21-11; Svensk Kärnbränslehantering AB: Stockholm, Sweden, 2021.

209. Morco, R.P. Gamma-Radiolysis Kinetics and Its Role in the Overall Dynamics of Materials Degradation. Ph.D. Thesis, Western University, London, ON, Canada, 2020.

210. Wu, M.; Beahzin, M.; Nam, J.; Keech, P. *Internal Corrosion of Fused Fuel Container*; Technical Report NWMO-TR-2019-02; Nuclear Waste Management Organization: Toronto, ON, Canada, 2019.

211. Carver, M.B.; Hanley, D.V.; Chaplin, K.R. *MAKSIMA-CHEMIST. A Program for Mass Action Kinetics Simulation by Automatic Chemical Equation Manipulation and Integration Using Stiff Techniques*; Technical Report AECL-6413; Atomic Energy of Canada Limited: Chalk River, ON, Canada, 1979.

212. Hoch, A.R.; Sharland, S.M. *Assessment Study of the Stresses Induced by Corrosion in the Advanced Cold Process Canister*; Technical Report SKB TR-94-13; Svensk Kärnbränslehantering AB: Stockholm, Sweden, 1993.

213. Bond, A.E.; Hoch, A.R.; Jones, G.D.; Tomczyk, A.J.; Wiggin, R.M.; Worraker, W.J. *Assessment of a Spent Fuel Disposal Canister. Assessment Studies for a Copper Canister with Cast Steel Inner Component*; Technical Report SKB TR-97-19; Svensk Kärnbränslehantering AB: Stockholm, Sweden, 1997.

214. Smart, N.R.; Rance, A.P.; Fennell, P.A.H. *Expansion Due to the Anaerobic Corrosion of Iron*; Technical Report SKB TR-06-41; Svensk Kärnbränslehantering AB: Stockholm, Sweden, 2006.

215. Engelhardt, G.R.; Kursten, B.; Macdonald, D.D. Corrosion of carbon steel in physically constrained locations in high level nuclear waste isolation systems. *Corros. Sci.* **2020**, *177*, 108974. [CrossRef]

216. Patel, R.; Punshon, C.; Nicholas, J.; Bastid, P.; Zhou, R.; Schneider, C.; Bagshaw, N.; Howse, D.; Hutchinson, E.; Asano, R.; et al. *Canister Design Concepts for Disposal of Spent Fuel and High Level Waste*; Technical Report NTB 124-06; Nagra: Wettingen, Switzerland, 2012.

217. *BS 7910:2019*; Guide to Methods for Assessing the Acceptability of Flaws in Metallic Structures. British Standards Institute: London, UK, 2019.

218. Korzhavyi, P.A.; Abrikosov, I.A.; Johansson, B. Theoretical investigation of the defect interactions in dilute copper alloys intended for nuclear waste containers. *Mat. Res. Soc. Symp. Proc.* **1999**, *556*, 895–902. [CrossRef]

219. Korzhavyi, P.A.; Abrikosov, I.A.; Johansson, B. Theoretical study of bulk and surface properties of digenite Cu$_{2-\delta}$S. *Mat. Res. Soc. Symp. Proc.* **2000**, *608*, 115–120. [CrossRef]

220. Korzhavyi, P.A.; Johansson, B. *Thermodynamic Properties of Copper Compounds with Oxygen and Hydrogen from First Principles*; Technical Report SKB TR-10-30; Svensk Kärnbränslehantering AB: Stockholm, Sweden, 2010.

221. Stenlid, J.H.; Johansson, A.J.; Leygraf, C.; Brinck, T. Computational analysis of the early stage of cuprous oxide sulphidation: A top-down process. *Corros. Eng. Sci. Technol.* **2017**, *52*, 50–53. [CrossRef]

222. Stenlid, J.H.; dos Santos, E.C.; Arán-Ais, R.M.; Bagger, A.; Johansson, A.J.; Cuenya, B.R.; Rossmeisl, J.; Pettersson, L.G.M. Uncovering the electrochemical interface of low-index copper surfaces in deep groundwater environments. *Electrochim. Acta* **2020**, *362*, 137111. [CrossRef]

223. Stenlid, J.H.; dos Santos, E.G.; Johansson, A.J.; Pettersson, L.G.M. Properties of interfaces between copper and copper sulphide/oxide films. *Corros. Sci.* **2021**, *183*, 109313. [CrossRef]

224. Kong, D.; Xu, A.; Dong, C.; Mao, F.; Xiao, K.; Li, X.; Macdonald, D.D. Electrochemical investigation and ab initio computation of passive film properties on copper in anaerobic sulphide solutions. *Corros. Sci.* **2017**, *116*, 34–43. [CrossRef]

225. Turchi, P.E.A.; Kaufman, L.; Liu, Z.-K. Stability and aging of candidate alloys for the Yucca Mountain Project: CALPHAD results. *Mat. Res. Soc. Symp. Proc.* **2003**, *757*, paper II4.3. [CrossRef]

226. Hall, D.; Walton, J. Conceptual model for low separation processes affecting waste package environment, Yucca Mountain, Nevada. *Appl. GeoChem.* **2006**, *21*, 859–869. [CrossRef]

227. Turnbull, A. *A Review of the Possible Effects of Hydrogen on Lifetime of Carbon Steel Nuclear Waste Canisters*; Technical Report NTB 09-04; Nagra: Wettingen, Switzerland, 2009.

228. Yu, Y.-C.; Chen, C.-J.; Chung, C.-C.; Ni, C.-F.; Lee, I.-H.; Wu, Y.-C.; Lin, T.-Y. A multimodel framework for quantifying flow and advective transport controlled by earthquake-induced canister failures in a reference case for radioactive waste geological disposal. *Energies* **2023**, *16*, 5081. [CrossRef]

229. Birgersson, M.; Karnland, O. Ion equilibrium between montmorillonite interlayer space and an external solution—Consequences for diffusional transport. *Geochim. Cosmochim. Acta* **2009**, *73*, 1908–1923. [CrossRef]

230. Bradbury, M.H.; Baeyens, B. Porewater chemistry in compacted re-saturated MX-80 bentonite. *J. Contam. Hydrol.* **2003**, *61*, 329–338. [CrossRef] [PubMed]

231. Wersin, P. Geochemical modelling of bentonite porewater in high-level waste repositories. *J. Contam. Hydrol.* **2003**, *61*, 405–422. [CrossRef]

232. Wersin, P.; Curti, E.; Appelo, C.A.J. Modelling bentonite-water interactions at high solid/liquid ratios: Swelling and diffuse double layer effects. *Appl. Clay Sci.* **2004**, *26*, 249–257. [CrossRef]

233. Berner, U.R. Evolution of pore water chemistry during degradation of cement in a radioactive waste repository environment. *Waste Manage.* **1992**, *12*, 201–219. [CrossRef]

234. BSC (Bechtel SAIC Company). *In-Drift Precipitates/Salts Model*; Technical Report for U.S. Department of Energy; NV, USA, ANL-EBS-MD-000045 REV 02; Bechtel SAIC Company: Las Vegas, NV, USA, 2004.

235. BSC (Bechtel SAIC Company). *Analysis of Dust Deliquescence for FEP Screening*; Technical Report for U.S. Department of Energy; ANL-EBS-MD-000074 REV 01; Bechtel SAIC Company: Las Vegas, NV, USA, 2005.

236. Sandia. *Engineered Barrier System: Physical and Chemical Environment*; Technical Report ANL-EBS-MD-000033 REV 06; Sandia National Laboratories: Las Vegas, NV, USA, 2007.

237. Guo, R. *Coupled Thermal-Mechanical Modelling of a Deep Geological Repository Using the Horizontal Tunnel Placement Method in Sedimentary Rock Using CODE_BRIGHT*; Technical Report NWMO-TR-2010-22; Nuclear Waste Management Organization: Toronto, ON, Canada, 2010.

238. Guo, R. *Thermal Modelling of a Mark II Container*; Technical Report NWMO-TR-2015-06; Nuclear Waste Management Organization: Toronto, ON, Canada, 2015.

239. Guo, R. *Thermal Response of a Mark II Conceptual Deep Geological Repository in Crystalline Rock*; Technical Report NWMO-TR-2016-03; Nuclear Waste Management Organization: Toronto, ON, Canada, 2016.

240. Samper, J.; Zheng, L.; Montenegro, L.; Fernández, A.M.; Rivas, P. Coupled thermo-hydro-chemical models of compacted bentonite after FEBEX in situ test. *Appl. GeoChem.* **2008**, *23*, 1186–1201. [CrossRef]

241. Åkesson, M.; Kristensson, O.; Börgesson, L.; Dueck, A.; Hernelind, J. *THM Modelling of Buffer, Backfill and Other System Components*; Technical Report SKB TR-10-11; Svensk Kärnbränslehantering AB: Stockholm, Sweden, 2010.

242. Ariani, I. *Dose Rate Analysis to Port Radiolysis Assessment of Used CANDU Fuel*; Technical Report NWMO-TR-2022-02; Nuclear Waste Management Organization: Toronto, ON, Canada, 2022.

243. Gutiérrez, M.M.; Caruso, S.; Diomidis, N. Effects of materials and design on the criticality and shielding assessment of canister concepts for the disposal of spent nuclear fuel. *Appl. Radiat. Isotopes* **2018**, *139*, 201–208. [CrossRef]

244. Sidborn, M.; Neretniks, I. Modelling of biochemical processes in rocks: Oxygen depletion by pyrite oxidation—Model development and exploratory simulations. *Mat. Res. Soc. Symp. Proc.* **2003**, *757*, II11.5. [CrossRef]

245. Yang, C.; Samper, J.; Molinero, J.; Bonilla, M. Modelling geochemical and microbial consumption of dissolved oxygen after backfilling a high level radioactive waste repository. *J. Contam. Hydrol.* **2007**, *93*, 130–148. [CrossRef]

246. Jonsson, M.; Emilsson, G.; Emilsson, L. *Mechanical Design Analysis for the Canister*; Technical Report Posiva SKB Report 04; Posiva Oy: Eurajoki, Finland; Svensk Kärnbränslehantering AB: Stockholm, Sweden, 2018.

247. Pourbaix, M. *Atlas of Electrochemical Equilibria in Aqueous Solutions*, 2nd ed.; NACE International: Houston, TX, USA, 1974.

248. Puigdomenech, I.; Taxén, C. *Thermodynamic Data for Copper. Implications for the Corrosion of Copper under Repository Conditions*; Technical Report SKB TR-00-13; Svensk Kärnbränslehantering AB: Stockholm, Sweden, 2000.

249. Protopopoff, E.; Marcus, P. Potential-pH diagrams for sulfur and hydroxyl adsorbed on copper surfaces in water containing sulfides, sulfites or thiosulfates. *Corros. Sci.* **2003**, *45*, 1191–1201. [CrossRef]

250. Protopopoff, E.; Marcus, P. Potential-pH diagrams for hydroxyl and hydrogen adsorbed on copper surfaces. *Electrochim. Acta* **2005**, *51*, 408–417. [CrossRef]

251. Frankel, G.S.; Sridhar, N. Understanding localized corrosion. *Mater. Today* **2008**, *11*, 38–44. [CrossRef]

252. Liu, C.; Kelly, R.G. A review of the application of finite element method (FEM) to localized corrosion modelling. *Corrosion* **2019**, *75*, 1285–1299. [CrossRef] [PubMed]

253. Macdonald, D.D.; Engelhardt, G.R. A brief review of determinism in the prediction of localized corrosion damage. *Zeit. Phys. Chem.* **2012**, *226*, 871–888. [CrossRef]

254. Pospiskova, I.; Dobrev, D.; Kouril, M.; Stoulil, J.; Novikova, D.; Kotnour, P.; Matal, O. Czech national programme and disposal concept. *Corros. Eng. Sci. Technol.* **2017**, *52*, 6–10. [CrossRef]

255. Walton, J.C.; Sagar, B. A corrosion model for nuclear waste containers. *Mat. Res. Soc. Symp. Proc.* **1987**, *84*, 271–282. [CrossRef]

256. Worgan, K.; Apted, M.; Sjöblom, R. Performance analysis of copper canister corrosion under oxidizing or reducing conditions. *Mat. Res. Soc. Symp. Proc.* **1995**, *353*, 695–702. [CrossRef]

257. Lee, J.H.; Atkins, J.E.; Dunlap, B. Incorporating of "corrosion-time" and effects of corrosion-product spalling in waste package degradation simulation in the potential repository at Yucca Mountain. *Mat. Res. Soc. Symp. Proc.* **1997**, *465*, 1075–1082. [CrossRef]

258. Trotignon, L.; Faure, M.-H.; Cranga, M.; Peycelon, H. Numerical simulation of the interaction between granitic groundwater, engineered clay barrier and iron canister. *Mat. Res. Soc. Symp. Proc.* **1999**, *556*, 599–606. [CrossRef]

259. Gondolli, J.; Dobrev, D.; Klajmon, M.; Mendoza, A.; Černoušek, T.; Kouřil, M.; Stoulil, J. *Corrosion Products—Final Report*; Technical Report 329/2018/ENG; SÚRAO: Prague, Czech Republic, 2018.

260. Pensado, O.; Dunn, D.S.; Cragnolino, G.A. Long-term extrapolation of passive behavior of Alloy 22. *Mat. Res. Soc. Symp. Proc.* **2003**, *757*, 42. [CrossRef]

261. Hœrlé, S.; Mazaudier, F. A contribution to the modelling of atmospheric corrosion of iron. In *Prediction of Long Term Corrosion Behaviour in Nuclear Waste Systems*; Féron, D., Macdonald, D.D., Eds.; European Federation of Corrosion, Number 36; Maney: London, UK, 2003; Chapter 13; pp. 179–193.

262. Bataillon, C.; Bouchon, F.; Chainais-Hillairet, C.; Fuhrman, J.; Hoaru, E.; Touzani, R. Numerical methods for the simulation of a corrosion model with moving oxide layer. *J. Comput. Phys.* **2012**, *231*, 6213–6231. [CrossRef]

263. Chainais-Hillairet, C.; Bataillon, C. Mathematical and numerical study of a corrosion model. *Numer. Math.* **2008**, *110*, 1–25. [CrossRef]

264. Martin, F.A.; Bataillon, C. Modelling of the evolution of iron passivity: Solving the moving boundary problem. *Mat. Res. Soc. Symp. Proc.* **2012**, *1475*, 275–280. [CrossRef]

265. Desgranges, C.; Abbas, A.; Terlain, A. Model for low temperature oxidation during long term interim storage. In *Prediction of Long Term Corrosion Behaviour in Nuclear Waste Systems*; Féron, D., Macdonald, D.D., Eds.; European Federation of Corrosion, Number 36; Maney: London, UK, 2003; Chapter 14; pp. 194–207.

266. Desgranges, C.; Bertrand, N.; Gauvain, D.; Terlain, A.; Poquillon, D.; Monceau, D. Model for low temperature oxidation during long term interim storage. In *Prediction of Long Term Corrosion Behaviour in Nuclear Waste Systems, Proceedings of the 2nd International Workshop, Nice, France, 14–15 September 2004*; Crusset, D., Féron, D., Gras, J.-M., Macdonald, D.D., Eds.; Andra Science and Technology Series: Châtenay-Malabry, France, 2004; pp. 170–179.

267. Kim, S.S.; Chun, K.S.; Kang, K.C.; Baik, M.H.; Kwon, S.H.; Choi, J.W. Estimation of the corrosion thickness of a disposal container for high-level radioactive wastes in a wet bentonite. *J. Ind. Eng. Chem.* **2007**, *13*, 959–964.

268. Peña, J.; Torres, E.; Turrero, M.J.; Escribano, A.; Martín, P.L. Kinetic modelling of the attenuation of carbon steel canister corrosion due to diffusive transport through corrosion product layers. *Corros. Sci.* **2008**, *50*, 2197–2204. [CrossRef]

269. Macdonald, D.D.; Urquidi-Macdonald, M.; Engelhardt, G.R.; Azizi, O.; Saleh, A.; Almazooqi, A.; Rosas-Camacho, O. Some important issues in electrochemistry of carbon steel in simulated concrete pore water. Part I—Theoretical issues. *Corros. Eng. Sci. Technol.* **2011**, *46*, 98–103. [CrossRef]

270. Macdonald, D.D.; Sharifi-Asl, S.; Engelhardt, G.R.; Urquidi-Macdonald, M. *Issues in the Corrosion of Copper in a Swedish High Level Nuclear Waste Repository*; Technical Report SSM 2012:11; Strålsäkerhetsmyndigheten: Stockholm, Sweden, 2012.

271. Macdonald, D.D.; Sharifi-Asl, S.; Engelhardt, G.R. *Issues in the Corrosion of Copper in a Swedish High Level Nuclear Waste Repository. Phase III. Role of Sulphide Ion in Anodic and Cathodic Processes—Research Report*; Technical Report SSM 2014:57; Strålsäkerhetsmyndigheten: Stockholm, Sweden, 2014.

272. King, F.; Kolář, M. *Simulation of the Anaerobic Corrosion of Carbon Steel Used Fuel Containers Using the Steel Corrosion Model Version 1.0 (SCM V1.0)*; Technical Report NWMO-TR-2012-07; Nuclear Waste Management Organization: Toronto, ON, Canada, 2012.

273. King, F.; Kolář, M.; Maak, P.; Keech, P. Simulation of the anaerobic corrosion of carbon steel used fuel containers and the impact of corrosion products on other barriers in the repository. In Proceedings of the CORROSION2013, Orlando, FL, USA, 17 March 2013; NACE International: Houston, TX, USA, 2013. paper 2735.

274. Björck, M. *Estimation of Oxide Growth on Joint Surfaces during FSW*; Technical Memo, skb.1402837.doc; Svensk Kärnbränslehantering AB: Stockholm, Sweden, 2015. Available online: https://skb.se/wp-content/uploads/2015/05/1402837-Estimation-of-oxide-growth-on-joint-surfaces-during-FSW_2.pdf (accessed on 12 August 2019).

275. Johansson, A.J.; Lilja, C.; Hedin, A. Corrosion of copper in repository-like field tests: Compilation and analysis of data. In Proceedings of the International High-Level Radioactive Waste Management, Knoxville, TN, USA, 14–18 April 2019; American Nuclear Society: La Grange Park, IL, USA, 2019; pp. 316–327.

276. Leupin, O.X.; Smart, N.R.; Zhang, Z.; Stefanoni, M.; Angst, U.; Papafotiou, A.; Diomidis, N. Anaerobic corrosion of carbon steel in bentonite: An evolving interface. *Corros. Sci.* **2021**, *187*, 109523. [CrossRef]

277. Marsh, G.P.; Taylor, K.J.; Bland, I.D.; Westcott, C.; Tasker, P.W.; Sharland, S.M. Evaluation of the localised corrosion of carbon steel overpacks for nuclear waste disposal in granite environments. *Mat. Res. Soc. Symp. Proc.* **1985**, *50*, 421–428. [CrossRef]

278. Marsh, G.P. Predicting the long term corrosion of metal containers for nuclear waste disposal. *Mat. Res. Soc. Symp. Proc.* **1988**, *112*, 85–97. [CrossRef]

279. Marsh, G.P.; Taylor, K.J.; Harker, A.H. *The Kinetics of Pitting Corrosion of Carbon Steel Applied to Evaluating Containers for Nuclear Waste Disposal*; Technical Report TR-91-62; Swedish Nuclear Fuel and Waste Management Co.: Solna, Sweden, 1991.

280. Walton, J.C. Mathematical modelling of large-scale nonuniform corrosion: Coupling of corrosion, transport, and geochemical processes in nuclear waste isolation. *Nucl. Chem. Waste Manag.* **1988**, *8*, 143–156. [CrossRef]

281. Walton, J.C. Theoretical modelling of crevice and pitting corrosion processes in relation to corrosion of radioactive waste containers. *Mat. Res. Soc. Symp. Proc.* **1990**, *176*, 509–516. [CrossRef]

282. Macdonald, D.D.; Urquidi-Macdonald, M. Corrosion damage function—Interface between corrosion science and engineering. *Corrosion* **1992**, *48*, 354–367. [CrossRef]

283. Engelhardt, G.; Macdonald, D.D. Deterministic prediction of pit depth distribution. *Corrosion* **1998**, *54*, 469–479. [CrossRef]

284. Roux, F.; Stafiej, J.; Chaussé, A.; Badiali, J.P. Numerical simulations of simple processes associated with corrosion, diffusion and formation of a passive layer. In *Prediction of Long Term Corrosion Behaviour in Nuclear Waste Systems*; Féron, D., Macdonald, D.D., Eds.; European Federation of Corrosion, Number 36; Maney: London, UK, 2003; Chapter 9; pp. 118–128.

285. Lee, J.H.; Mon, K.G.; Longsine, D.E.; Bullard, B.E. An integrated stochastic model for long term performance of waste package for high level nuclear waste disposal. In *Prediction of Long Term Corrosion Behaviour in Nuclear Waste Systems*; Féron, D., Macdonald, D.D., Eds.; European Federation of Corrosion, Number 36; Maney: London, UK, 2003; Chapter 10; pp. 129–153.

286. Taniguchi, N.; Suzuki, H.; Kawasaki, M.; Naito, M.; Kobayashi, M.; Takahashi, R.; Asano, H. Propagation behaviour of general and localised corrosion of carbon steel in simulated groundwater under aerobic condition. *Corros. Eng. Sci. Technol.* **2011**, *46*, 117–123. [CrossRef]

287. Shukla, P.; Pabalan, R.; He, X. *In-Crevice Chemistry Model Development for Nickel-Based Alloys and Analysis of Model Results in View of Literature Information*; Technical Report Contract NRC-02-07-006; Center for Nuclear Waste Regulatory Analyses: San Antonio, TX, USA, 2011. Available online: https://www.nrc.gov/docs/ML1126/ML112640376.pdf (accessed on 9 March 2012).

288. King, F.; Lilja, C. *Localised Corrosion of Copper Canisters in Bentonite Pore Water*; Technical Report TR-13-27; Swedish Nuclear Fuel and Waste Management Co.: Solna, Sweden, 2013.

289. King, F.; Lilja, C. Localised corrosion of copper canisters. *Corros. Eng. Sci. Technol.* **2014**, *49*, 420–424. [CrossRef]

290. King, F. *Overview of a Carbon Steel Container Corrosion Model for a Deep Geological Repository in Sedimentary Rock*; Technical Report NWMO-TR-2007-01; Nuclear Waste Management Organization: Toronto, ON, Canada, 2007.

291. Martinsson, Å.; Sandström, R. Hydrogen depth profile in phosphorus-doped, oxygen-free copper after cathodic charging. *J. Mater. Sci.* **2012**, *47*, 6768–6776. [CrossRef]

292. Sandström, R. *Analysis of a MODEL for Hydrogen Bubble Nucleation and Growth in Copper*; Technical memo, skb.1337317.doc; Svensk Kärnbränslehantering AB: Stockholm, Sweden, 2014. Available online: https://skb.se/wp-content/uploads/2015/05/1337317.pdf (accessed on 10 December 2017).

293. King, F.; Stroes-Gascoyne, S. Microbially influenced corrosion of nuclear fuel waste disposal containers. In Proceedings of the International Conference of Microbially Influenced Corrosion, New Orleans, LO, USA, 8–10 May 1995; NACE International: Houston, TX, USA, 1995; pp. 35/1–35/14.

294. King, F.; Kolář, M.; Stroes-Gascoyne, S.; Maak, P. Model for the microbiological corrosion of copper containers in a deep geologic repository. *Mat. Res. Soc. Symp. Proc.* **2004**, *807*, 811–816. [CrossRef]

295. Sidborn, M.; Neretnieks, I. Corrosion of copper canisters through microbially mediated sulphate reduction. *Mat. Res. Soc. Symp. Proc.* **2006**, *932*, 261. [CrossRef]

296. Dou, W.; Jia, R.; Jin, P.; Liu, J.; Chen, S.; Gu, T. Investigation of the mechanism and characteristics of copper corrosion by sulfate reducing bacteria. *Corros. Sci.* **2018**, *144*, 237–248. [CrossRef]

297. Garcia-Hernandez, J.A.; Ponnambalam, K.; Sivaraman, M. Lifetime of used nuclear fuel containers affected by sulphate-reducing bacteria reactions inside the Canadian deep geological repository. *Appl. Sci.* **2021**, *11*, 7806. [CrossRef]

298. King, F. *The Effect of Discontinuities on the Corrosion Behaviour of Copper Canisters*; Technical Report SKB TR-04-05; Svensk Kärnbränslehantering AB: Stockholm, Sweden, 2004.

299. Williford, R.E. Uncertainties in container failure time predictions. *Mat. Res. Soc. Symp. Proc.* **1991**, *212*, 335–342. [CrossRef]

300. Blackwood, D.J.; Hoch, A.R.; Naish, C.C.; Rance, A.; Sharland, S.M. *Research on Corrosion Aspects of the Advanced Cold Process Canister*; Technical Report SKB TR-94-12; Svensk Kärnbränslehantering AB: Stockholm, Sweden, 1994.